EDGEWOOD

CHEMICAL BIOLOGICAL CENTER

U.S. ARMY RESEARCH, DEVELOPMENT AND ENGINEERING COMMAND

ECBC-CR-084

INVESTIGATION OF EMISSIVE SMOKE

Robert E. Turner

SCIENCE APPLICATIONS
INTERNATIONAL CORPORATION
Abingdon, MD 21009

20061107282

June 2006

ABERDEEN PROVING GROUND, MD 21010-5424

Disclaimer

The findings in this report are not to be construed as an official Department of the Army position unless so designated by other authorizing documents.

REPORT DOCUMENTATION PAGE

Public reporting burden for this collection of information is estimated to average 1 hour per response, including the time for reviewing instructions, searching existing data sources, gathering and maintaining the data needed, and completing and reviewing this collection of information. Send comments regarding this burden estimate or any other aspect of this collection of information, including suggestions for reducing this burden to Department of Defense, Washington Headquarters Services, Directorate for Information Operations and Reports (0704-0188), 1215 Jefferson Davis Highway, Suite 1204, Arlington, VA 22202-4302. Respondents should be aware that notwithstanding any other provision of law, no person shall be subject to any penalty for failing to comply with a collection of information if it does not display a currently valid OMB control number. **PLEASE DO NOT RETURN YOUR FORM TO THE ABOVE ADDRESS.**

1. REPORT DATE (DD-MM-YYYY) XX-06-2006	2. REPORT TYPE Final	3. DATES COVERED (From - To) Oct 2002 - Oct 2004
4. TITLE AND SUBTITLE Investigation of Emissive Smoke		**5a. CONTRACT NUMBER** DAAD13-01-D-0007
		5b. GRANT NUMBER
		5c. PROGRAM ELEMENT NUMBER
6. AUTHOR(S) Turner, Robert E.		**5d. PROJECT NUMBER** A552
		5e. TASK NUMBER T-03-SBCCOM-004
		5f. WORK UNIT NUMBER
7. PERFORMING ORGANIZATION NAME(S) AND ADDRESS(ES) AND ADDRESS(ES) SAIC, 3465A Box Hill Corporate Center Drive, Abingdon, MD 21009		**8. PERFORMING ORGANIZATION REPORT NUMBER** ECBC-CR-084
9. SPONSORING / MONITORING AGENCY NAME(S) AND ADDRESS(ES) DIR, ECBC, ATTN: AMSRD-ECB-RT-TD, APG, MD 21010-5424		**10. SPONSOR/MONITOR'S ACRONYM(S)**
		11. SPONSOR/MONITOR'S REPORT NUMBER(S)

12. DISTRIBUTION / AVAILABILITY STATEMENT
Approved for public release; distribution is unlimited.

13. SUPPLEMENTARY NOTES
COR: D. Jeffrey Hale, AMSRD-ECB-RT-TD, (410) 436-2607

14. ABSTRACT
This report describes the procedure for creating a model for the description of radiation in and released from emissive smoke clouds, that is, clouds in which sources of radiation consist of the internal thermal radiation from an ambient medium as well as from isolated flares. The distribution of the flares in the cloud is in a regular, three-dimensional lattice and is uniform throughout. The model is applicable to the spectral region from the near ultraviolet to the microwave. This smoke cloud model can be used in realistic scenes using external atmospheric conditions and the optical and geometric properties of clouds, flares, targets, and a background. The model is designed to allow a wide range of parameter values to be used to quantify the physical, optical, and geometric properties of clouds, flares and targets, and backgrounds. The model contains simple input and output files, and is user friendly in that all parameters are explained with explicit units given for all constants and variables. However, the user of this model has to have some degree of familiarity with the basic concepts of radiometry and thermal physics.

15. SUBJECT TERMS

Emissive smoke clouds	Radiative transfer	Targets and background	Flares	Contrast

16. SECURITY CLASSIFICATION OF:			17. LIMITATION OF ABSTRACT	18. NUMBER OF PAGES	19a. NAME OF RESPONSIBLE PERSON Sandra J. Johnson
a. REPORT U	**b. ABSTRACT** U	**c. THIS PAGE** U	UL	127	**19b. TELEPHONE NUMBER (include area code)** (410) 436-2914

Standard Form 298 (Rev. 8-98)
Prescribed by ANSI Std. Z39.18

Blank

FOREWORD

This report describes the analysis on a two-year project to produce radiation models that can be used to account for the multiply-scattered radiation that is scattered and absorbed by a smoke cloud that lies between a target and a sensor. The final mathematical model developed herein is applicable for the spectral region from the near ultraviolet to the microwave. It is well known that smoke can be an effective screening agent in that the radiation from a target is absorbed and scattered by the smoke that lies between the target and some detector. What is not so well known is that a smoke medium that contains isolated, heated, point-like sources called flares can be a more effective screening agent. In previous interim reports, we went into considerable detail regarding the optical and thermal properties of the smoke and the flare sources of radiation. In this report, we present the results on the final radiative-transfer model that is to be used for the analysis of the thermal radiation in a smoke cloud. This radiative-transfer model, called FlareW actually encompasses several submodels. This factor is important for this investigation in that there is the question as to which radiation field is dominant, the flare source radiation field or the thermal radiation field that arises from the internal thermal component as well as the external thermal component. The analysis presented here is concerned with the development of a model for the computation of the radiation field at the surface of a heated cloud. In the course of this investigation, we performed a number of mathematical calculations to determine the radiance from a cloud. One method was the use of an expansion of the radiance function in terms of spherical harmonics. We then found a solution for the radiance for the P1, P3, and the P5 approximations for a plane-parallel medium, where Pl is the designation for the l-th term in the Legendre polynomial expansion. These calculations were quite involved mathematically but we did examine the radiance as a function of the zenith angle. It appears as though many higher-order approximations would have to be done for an adequate analysis of the angular effects of the radiation field. Significant oscillations occur in the lower-order approximations. To perform the actual calculations for higher-order terms in the expansion would be well beyond the scope of this investigation so we decided to try more elementary angular averaging techniques. This seems quite reasonable because a realistic smoke cloud would be spatially inhomogeneous anyway.

After trying the spherical harmonic method, the modified diffusion method, and a method based on angular moments, we decided to use a mathematically exact calculation for the single-scattering component and then use this scattering integral in conjunction with a photon statistical counting method (Monte Carlo) to account for all higher orders of scattering. This seemed to be reasonable approach considering the fact that we are dealing with a smoke cloud of intermediate optical thickness. For an optically thick medium, the diffusion method may give reasonable results far from the boundaries and for an optically thin case, the single-scattering technique would be applicable. However, for the intermediate optical thickness case neither approximation will suffice.

The smoke cloud model that we produced is not to be considered in the abstract, but rather in the context of realistic scenes incorporating thermal radiation produced in the cloud by normal heating due to the ambient conditions as well as radiation that is external to the cloud. Thus, the user can model external atmospheric conditions and the radiation from a target and a background. Since we essentially have a Monte Carlo photon model the computational run time is dictated by the selection of random numbers by a pseudorandom number generator. The user

can easily gain experience to determine run time versus computational accuracy. The other radiative processes such as the calculation of the internal and external radiation fields are performed using a two-stream approximation and these calculations in the computer program run very quickly.

We also present a general description of the various metrics for the analysis of the radiation for the discrimination of a target and a background. Some of these are the target-background contrast, the signal-to-noise ratio, and the signal-to-noise ratio transmittance. One can clearly see the effect on the contrast and the signal-to-noise ratio of additional internal point sources of radiation in a cloud.

Finally, the model is designed so that a wide range of parameter values can be used to quantify the physical, optical, and geometric properties of the cloud, the flares, and the targets and backgrounds. Many possible physical and geometric conditions can be represented by using various combinations of the parameters. The model contains a simple input file and an output file and is user friendly in that all the parameters are explained with explicit units given for all the constants and variables. It is assumed, however, that the user of this model has some degree of familiarity with the basic concepts of radiometry and thermal physics. We also present some advice to the community of users on how this model can be used to simulate actual field tests. Thus, by running the model a number of times for various conditions, one can determine what radiance, contrast, and signal-to-noise values one can expect in a specific field test.

PREFACE

The work described in this report was authorized under Contract No. DAAD13-01-D-0007. This work was started in October 2002 and completed in October 2004.

The use of either trade or manufacturers' names in this report does not constitute an official endorsement of any commercial products. This report may not be cited for purposes of advertisement.

The text of this contractor report is published as received and was not edited by the Technical Releases Office, U.S. Army Edgewood Chemical Biological Center.

This report has been approved for public release. Registered users should request additional copies from the Defense Technical Information Center; unregistered users should direct such requests to the National Technical Information Service.

Blank

CONTENTS

FIGURES

TABLES

Blank

INVESTIGATION OF EMISSIVE SMOKE

1.   INTRODUCTION

1.1   <u>Background</u>.

The problem of accounting for the scattered radiation in a medium with an internal, uniform thermal source is one that has been dealt with many times. Indeed this is one of the first problems that was investigated in the analysis of the radiation from stars. For astrophysics problems, however, one usually deals with a large optical thickness. In addition, one also does not have to consider external radiation fields at the top or the bottom of the medium. In our situation, however, we must consider a finite three-dimensional medium with external as well as internal radiation fields. Approximations to the three-dimensional, time-independent, radiative-transfer equation can be used to find solutions for the radiation field within and on the surface of the smoke cloud. This solution is usually characterized by a radiometric quantity called the radiance, that is, the power per unit surface area on a detector element normal to the line of sight along the path between the detector and the target per unit solid angle. The major technical difficulty in solving this problem lies in the details of the mathematical representation of the scattered radiation field for a particular geometry. Radiative-transfer is a notoriously complicated problem from a mathematical point of view. It has a long history and is associated with the corresponding problem in neutron transport theory [1]. There are very few mathematically exact solutions so it is usually necessary to find approximations that provide reasonable results.

1.2   <u>Objective</u>.

The objective of this work is to find solutions of various forms of the radiative-transfer equation or approximate formulations for the radiance on the surface of the scattering-absorbing medium. We want to determine a reasonable mathematical representation of the radiance and to develop a corresponding computer model for the computation of radiance and irradiance. This is to be done for the multiply-scattered radiation from both the internal thermal radiation field as well as for the radiation fields external to the cloud that have an effect on the radiance that emerges at the face of the cloud in between the target and an observer along some designated line of sight. Certain assumptions must be introduced. We assume a uniform temperature throughout the interior of the cloud and a homogeneous smoke particle medium. It will also be assumed that the number density of the flares is much smaller than the number density of the smoke particles themselves. This means that we may neglect the interaction of the thermal radiation with the flares in the cloud and consider only the interaction of the thermal radiation with the much higher density of the smoke particles. We also assume that the external sources of radiation are reasonably isotropic and that they can be characterized by a Planck radiation function with some emissivity. For our purposes here we consider greybody radiation instead of a spectral emissivity for the external radiation. Whether one is justified in using a Planck radiation function to describe either the internal or the external radiation is open to question. This is an assumption that has been used for many years in the infrared community but this author has never seen a theoretical justification for it. The assumption is also used frequently in stellar physics but in those cases one deals with massive objects with a very large optical thickness. We know for example, that the Sun cannot be characterized by a true blackbody because it is radiating an enormous amount of radiation into space. The Sun is not inside of a hohlraum!

1

Nevertheless, the spectrum from the Sun is, to a good approximation, represented as a blackbody with an effective temperature of about 5800 K. This is because there is such a large mass relative to the amount of radiation that is lost to space. This is probably also true for a massive object such as a military tank in relationship to the thermal radiation that it loses. Whether this assumption is a valid one for a relatively small, finite cloud of smoke is questionable, at least to this author. Nevertheless, to consider non-thermal radiation in a smoke cloud is beyond the scope of this effort for the present time. In order to obtain useful results that can be tested in a laboratory or in the field we will indeed make the assumption that all the radiation fields that we deal with here are the result of a medium being in local thermodynamic equilibrium. One must keep in mind, however, the possibility that thermal radiation fields that are not in local thermodynamic equilibrium can exist in the situation that we are attempting to simulate.

2. PHYSICAL PROPERTIES OF THE MEDIUM

In this section we present the basic optical, physical, and thermal properties of the smoke cloud particles as well as the corresponding properties of the flare particles that serve as the source of radiation in the medium. The material contained in this section has been changed slightly as a result of technical discussions with Dr. Janon Embury but the general treatment is quite similar to that dealt with in the first three interim progress reports. It is included here because the data will be of use in the application of the specific computational models described in this final report.

2.1 Smoke and Flare Structure.

The most significant property of the particles is their shape and size. The shape of the smoke particles is in the form of disks and the flares are considered to be spheres. Typical values for the properties of these particles are listed in table 1.

Table 1. Physical Properties of Smoke and Flare Particles.

Property	Smoke	Flare
Diameter	1.0 μm	200 to 2000 μm
Thickness	0.1 μm	-----
Aspect Ratio	10	-----
Concentration	10^{-8}	10^{-8}
Drop Time	∞	10 s
Optical Thickness	1.0	TBD
Temperature	300 K	TBD

In table 1, TBD means that this quantity is to be determined by analysis. The aspect ratio is defined as the ratio of the diameter of a particle to its thickness. The concentration is the ratio of the volume occupied by the particles in some arbitrary volume to that total volume. It is, of course, dimensionless. The drop time is the time that it takes for the particle to drop some distance in the cloud. Table 1 indicates a drop time for the smoke particles as infinity. In reality, it is not true but for our purposes we shall make that assumption since this time is much greater than the drop time of the larger and heavier flares, and, in any case, these times are far greater than the photon transport times. The optical thickness is a dimensionless quantity that is indicative of the number of photon mean free paths in the medium. It is defined mathematically as

$$\tau = \int_0^L \kappa(s)\,ds \tag{1}$$

where $\kappa(s)$ is the volume extinction coefficient along path s up to the maximum path length L. By extinction we are referring to the combination of both the scattering and absorptive characteristics of the medium. Both these processes remove photons from the beam of radiation that is directed to the observer. If the extinction coefficient is constant along the path, then the optical thickness is just equal to the product of the extinction coefficient and the total path length L. As a result, we then see that for an optical thickness of 1 and a total path of 10 meters, the volume extinction coefficient of the smoke is 0.1 m^{-1}. From the definition of concentration we have the following relation

$$C_S = n_S v_S = n_S \pi r_S^2 t_S = n_S \pi \frac{f_S^2 t_S^3}{4} \tag{2}$$

where n_S, v_S, r_S, f_S, and t_S are the number density, volume, radii, aspect ratio, and the thickness of the disk-shaped smoke particles respectively. A relation similar to that given in equation (2) is also given in equation (3) for the spherical flare particles. It is

$$C_F = n_F v_F = n_F \frac{4}{3}\pi r_F^3 \tag{3}$$

using the values from table 1, we can calculate the number density of the flare particles, nF in the cloud and the ratio of the total number of smoke particles, NS to the total number of flare particles, NF. This is given in table 2.

Table 2. Flare Number Densities.

r_F (µm)	n_F (m^{-3})	N_F	N_X	Δx (cm)	N_S/N_F
100	2.387324×10^3	2.387324×10^6	133.6500	7.48223	5.333333×10^7
200	2.984155×10^2	2.984155×10^5	66.8252	14.96440	4.266667×10^8
500	1.909859×10^1	1.909859×10^4	26.7301	37.41100	6.666667×10^9
1000	2.387324×10^0	2.387324×10^3	13.3650	74.82230	5.333333×10^{10}

In table 2, we also list the value of N_X, which is the cube root of the total number of flares as given in the third column. It represents the number of flares in one dimension of the cloud. The quantity Δx is the inter-flare spacing, that is, the average distance between flares in one dimension. The last column is the ratio of the total number of smoke particles to the total number of flare particles in the cloud. One can easily see that the number of smoke particles is far greater than the number of flares.

2.2   Optical Properties.

It is of some interest to calculate the optical thickness of the flares to determine if this value needs to be considered in the radiative-transfer calculations. The optical thickness of the flares is given by

$$\tau_F = n_F Q_F \pi r_F^2 L \tag{4}$$

where Q_F is the ratio of the total interaction cross section to the geometric cross section and L is the geometric path length through the cloud. The corresponding optical thickness of the smoke is given by

$$\tau_S = n_S Q_S \pi r_S^2 L \tag{5}$$

Now, using equations (2) and (3) to relate the number densities to the radii of the particles we can get the ratio of the flare optical thickness to the smoke optical thickness. Because of the disk-like shape of the smoke particles, however, Embury [2] has determined that the efficiency factor of the disk-like smoke particle be modified. Thus, the ratio of the flare optical thickness to the smoke optical thickness should be given by

$$\frac{\tau_F}{\tau_S} = \frac{3 Q_F t_S}{2 Q_S r_F} \tag{6}$$

There exist computer programs for the actual computation of this quantity for particles of specific shapes, sizes, and wavelengths of the radiation. These optical properties can be calculated. Values for the ratio of the flare optical thickness to the smoke optical thickness are given in table 3.

Table 3. Ratio of the Flare Optical Thickness to the Smoke Optical Thickness.

r_F (μm)	τ_F/τ_S	τ_F
100	0.00150	0.00150
200	0.00075	0.00075
500	0.00030	0.00030
1000	0.00015	0.00015

The third column in table 3 gives the total optical thickness of the flares as being equal to the ratio in column 2 only because we have stipulated that the smoke optical thickness be 1. It is clear that the flare optical thickness is much less than the smoke optical thickness and therefore it can be neglected in our radiation calculations. We will see later that only optical thickness values greater than 0.1 are of significance in the radiation calculations.

2.3   Thermal Properties.

It is also of interest to consider the thermal properties of the smoke and flares. One can calculate the change in temperature of the flares as a result of the chemical reactions that occur when the flares are burning in the smoke cloud. The change in the temperature can be calculated by using an energy balance equation as in equation (7).

$$\frac{4\pi h r_F^3}{3\tau_t} + 4\pi r_F^2 \sigma T_0^4 = 4\pi r_F^2 \sigma (T_0 + \Delta T)^4 \tag{7}$$

where h is the heat of reaction, r_F is the flare particle radius, τ_t is the flare drop time, σ is the Stefan-Boltzmann constant (5.67040×10^{-8} W-m^{-2}-K^{-4}), T_0 is the ambient temperature of the cloud, and ΔT is the increase in the flare temperature. One can easily solve equation (7) for the temperature increase. It is given by

$$\Delta T = T_0 \left\{ \left[\frac{h r_F}{3\sigma \tau_t T_0^4} + 1 \right]^{1/4} - 1 \right\} \tag{8}$$

For example, given a value of 20,000 Joules per cubic centimeter for h, a flare drop time of 10 seconds, and an ambient temperature of 300 K, one can find a simple equation for the increase in temperature to be

$$\Delta T = T_0 \left[\left(1 + 1.175696012 x 10^{10} \frac{r_F(\mu m)}{T_0^4} \right)^{1/4} - 1 \right] \tag{9}$$

5

For an ambient temperature of 300 K one can use equation (9) to arrive at the temperature increase as well as the final temperature of the flares. The results of our calculations are given in table 4.

Given the final temperature of the flares from the third column of table 4, one can then calculate the output power from the flares. The power is just the product of the surface area of the flare and the thermal flux. Knowing the flare surface area and the final temperature, one can calculate the total power output of all the flares from equation (10).

$$p_F = A_F \sigma T_F^4 \tag{10}$$

Table 4. Temperatures in Flares vs. Flare Particle Radius.

r_F (μm)	ΔT (K)	$T_0 + \Delta T$ (K)
100	743.0838424	1043.083842
200	939.3804132	1239.380413
500	1257.635239	1557.635239
1000	1552.032219	1852.032219

and from equation (7) we have

$$T_F^4 = (T_0 + \Delta T)^4 = T_0^4 + \frac{h r_F}{3\sigma \tau_t} \tag{11}$$

When the example numerical values are put into equation (11) it becomes

$$p_F = T_0^4 r_F^2(\mu m)\left[7.125634793 + \frac{8.37758041 \; x10^{10} \, r_F \, (\mu m)}{T_0^4}\right]10^{-19} \tag{12}$$

Once again, if we use an ambient temperature of 300 K we get a simple equation for the power output of a flare in terms of its radius as

$$p_F = [5.771764182 + 8.37758041 \; r_F \, (\mu m)] r_F^2(\mu m) x10^{-9} \tag{13}$$

From equation (13) the output power per flare and the total output power of all the flares in the cloud were calculated and are given in table 5.

6

Table 5. Flare Output Power.

r_F (μm)	N_F	Flare Power p_F (watts)	Total Flare Power P_F (watts)
100	2.3873242×10^6	0.008435298	20137.7907
200	2.9841552×10^5	0.067251514	20068.8954
500	1.9098593×10^4	1.048640492	20027.5581
1000	2.3873242×10^3	8.383352174	20013.7791

The average (mean) power of all the flares is 20,062.0058 watts.

Finally, it must be noted that all these calculations were based on the total number of particles given in table 2. We cannot use these numbers in the radiation programs, however, because there would be a non-integer number of particles in any given x, y, or z direction in the cube. As a result, it is necessary to go back to table 2 and choose even integers nearest to the ones given there and then re-compute the new flare power output quantities. The results of this analysis are given in table 6.

One can see from table 6 that the flares now have new radius values. It is the power per flare value in column 6 that will be used in the radiation computer models.

Table 6. Power Output for an Integer Number of Flares in One Dimension.

N_X	N_X'	N'	n_X' (m^{-3})	r_F' (μm)	p_F (watts)	P_F (watts)
133.650	134	2.406104×10^6	2406.10	99.7392	0.00836962	20138.176
66.8252	66	2.874960×10^5	287.496	202.501	0.06980318	20068.135
26.7301	26	1.757600×10^4	17.5760	514.040	1.13943888	20026.778
13.3650	14	2.744000×10^3	2.74400	954.646	7.29388627	20014.424

The average (mean) total power output from table 6 is 20,061.878 watts.

3. RADIATIVE-TRANSFER THEORY

3.1 The Radiative-Transfer Equation.

In a previous technical report we described in some detail the P-N method as well as other methods for solving the radiative-transfer equation for point sources distributed throughout the medium. However, it was decided that many of these methods were mathematically too complicated for the type of spatial configuration we are dealing with and also the optical thickness of the medium is such that these methods would lead to very approximate solutions. Therefore, we adopt a simple and more direct approach although it takes greater computer time. We will consider a mathematically exact solution in quadrature form for the single-scattering component and then use the scattering integral in conjunction with a

photon-counting technique using a pseudorandom number generator to evaluate the higher order scattering terms.

We now consider a solution of the radiative-transfer equation for a three-dimensional, cubic-shaped medium with internal and external thermal radiation sources that are characterized by Planck radiation functions. The integro-differential equation is given by

$$\xi \frac{\partial L}{\partial x} + \eta \frac{\partial L}{\partial y} + \mu \frac{\partial L}{\partial z} + \kappa(x, y, z)L(x, y, z, \mu, \phi) = \alpha(x, y, z)B(x, y, z)$$

$$+ \frac{P}{4\pi} \delta(x - x_0, y - y_0, z - z_0)$$

$$+ \frac{\beta(x, y, z)}{4\pi} \int_0^{2\pi} \int_{-1}^{1} p(\mu, \phi, \mu', \phi')L(x, y, z, \mu', \phi')d\mu'd\phi' \qquad (14)$$

where $\alpha(x, y, z)$ and $\beta(x, y, z)$ are the volume absorption and volume scattering coefficients respectively of the medium, $B(x, y, z)$ is the isotropic Planck radiance, and P is the power output of the isotropic point source located at x_0, y_0, z_0. The single-scattering phase function is given by $p(\mu, \phi, \mu'\phi')$ and the direction cosines are ξ, η, μ. We consider a situation in which the observer is located at the center of the square on the bottom of the cube and is looking directly up toward the top of the cube along the positive z axis. The isotropic point source of radiation can be at any position inside the cube. To find an exact solution let us first define the two-dimensional Fourier transform of the radiance function, that is,

$$\widetilde{L}(k, l, z, \mu, \phi) = \int_{-\infty}^{\infty} \int_{-\infty}^{\infty} e^{-i(kx+ly)} L(x, y, z, \mu, \phi)dxdy \qquad (15)$$

with a corresponding inverse transform, that is,

$$L(x, y, z, \mu, \phi) = \frac{1}{(2\pi)^2} \int_{-\infty}^{\infty} \int_{-\infty}^{\infty} e^{i(kx+ly)} \widetilde{L}(k, l, z, \mu, \phi)dkdl \qquad (16)$$

8

Applying these transforms to the radiative-transfer equation transforms it into a one-dimensional equation with a complex attenuation coefficient, that is,

$$\frac{d\widetilde{L}}{dz} + \frac{\Lambda}{\mu}\widetilde{L} = (2\pi)^2\frac{\alpha B}{\mu}\delta(k)\delta(l) + \frac{P}{4\pi\mu}e^{-i(kx_0+ly_0)}\delta(z-z_0)$$

$$+ \frac{\beta}{4\pi}\int_0^{2\pi}\int_{-1}^1 p(\mu,\phi,\mu',\phi')\widetilde{L}(k,l,z,\mu',\phi')d\mu'd\phi' \qquad (17)$$

where $\Lambda = \kappa + i(k\xi + l\eta)$.

3.2 The General Solution.

Integrating equation (17) over the vertical distance z from 0 to z provides a formal solution for the upwelling radiation and integrating the equation from z = c (top of the cube) down to z = z with $\mu\rightarrow$ -μ gives us the downwelling radiation field. Performing these integrations over z and then taking the inverse two-dimensional Fourier transform produces the radiation solution. The upwelling radiation field is given by

$$L(x,y,z,\mu,\phi) = \frac{\alpha B}{\kappa}\left[1 - e^{-\kappa z/\mu}\right]$$

$$+ \frac{Pe^{\frac{-\kappa}{\mu}(z-z_0)}H(z-z_0)}{4\pi\mu}\delta\left[(x-x_0) - \frac{\xi}{\mu}(z-z_0)\right]\delta\left[(y-y_0) - \frac{\eta}{\mu}(z-z_0)\right]$$

$$+ \frac{\beta}{4\pi\mu}\int_0^z\int_0^{2\pi}\int_{-1}^1 e^{-\frac{\kappa}{\mu}(z-z')}p(\mu,\phi,\mu',\phi')x$$

$$L(x-\frac{z-z'}{\mu}\xi, y - \frac{z-z'}{\mu}\eta, z',\mu',\phi')d\mu'd\phi'dz' \qquad (18)$$

9

The first term on the right-hand side of equation (18) represents the attenuated thermal radiation, the second term represents the directly attenuated radiation from the point source where H (z − z_0) is the Heaviside function. The last term involving the triple integral represents the summation of all scattered radiation at some arbitrary point and in some direction $\theta'(= \cos^{-1} \mu'), \phi'$ into the field point at x, y, z. This scattering process is illustrated in figure 1.

Likewise, we can give a similar equation for the downwelling radiation. It is given by equation (19). It should be noted that at this point in the discussion these two equations can be used to describe the entire internal radiation field. The problem is not restricted to single scattering.

$$L(x,y,z,-\mu,\phi) = \frac{\alpha B}{\kappa}\left[1 - e^{-\kappa(c-z)/\mu}\right]$$

$$+\frac{Pe^{\frac{\kappa}{\mu}(z-z_0)}H(z_0-z)}{4\pi\mu}\delta\left[(x-x_0)-\frac{\xi}{\mu}(z_0-z)\right]\delta\left[(y-y_0)-\frac{\eta}{\mu}(z_0-z)\right]$$

$$+\frac{\beta}{4\pi\mu}\int_0^z\int_0^{2\pi}\int_{-1}^1 e^{-\frac{\kappa}{\mu}(z'-z)}\,p(-\mu,\phi,\mu',\phi')x$$

$$L(x-\frac{z'-z}{\mu}\xi, y-\frac{z'-z}{\mu}\eta, z', \mu', \phi')d\mu'd\phi'dz' \tag{19}$$
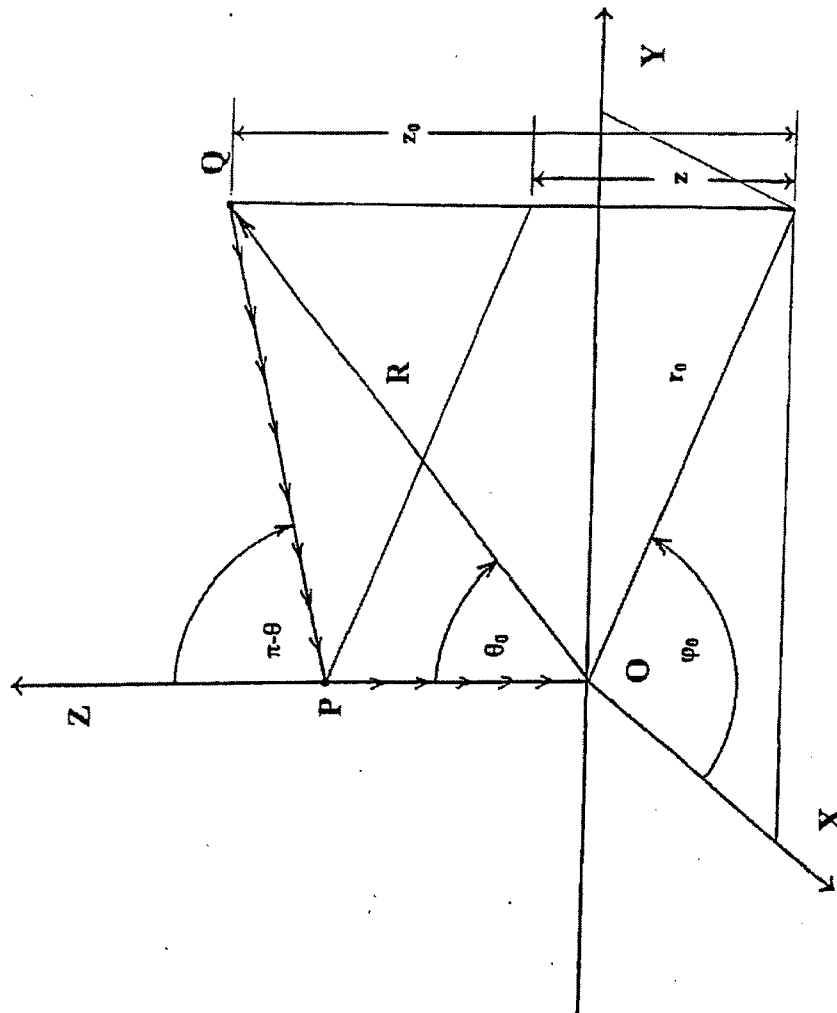
Figure 1. Representation of Singly-Scattered Radiation from a Single Point Source Q to an Arbitrary Point P to the Observer at Point O.

3.3   The Particular Solution.

In order to find a practical solution to the problem with an isolated point source in the medium we will perform the integrations so that there is a quadrature form for the solution of single scattering. One should note that the radiance from a point source is given by

$$L(x - \frac{z'-z}{\mu}\xi, y - \frac{z'-z}{\mu}\eta, z', \mu', \phi')$$

$$= \frac{P}{4\pi r^2} e^{-\kappa r} \delta(\mu' - \mu_S) \delta(\phi' - \phi_S) \qquad (20)$$

where the distance r is given by

$$r = \sqrt{(x'-x_0)^2 + (y'-y_0)^2 + (z'-z_0)^2} \qquad (21)$$

and where μ_S and ϕ_S are given by

$$\mu_S = \frac{z'-z}{r} \qquad (22)$$

$$\phi_S = \tan^{-1}\left[\frac{y'-y_0}{x'-x_0}\right] \qquad (23)$$

Now, inserting equation (20) into equation (19) allows us to find the solution for the singly-scattered radiation from a single point source. It is given by equation (24), that is

$$L(x, y, z, -\mu, \phi) =$$

$$\frac{\beta P}{(4\pi)^2 \mu} \int_0^c p(-\mu, \phi, \mu_S, \phi_S) \frac{e^{-\{\kappa[r+(z'-z)/\mu]\}}}{r^2} dz' \qquad (24)$$

where the distance r can be given explicitly in terms of the variable z' as the following:

$$r = \sqrt{R^2 - 2R(z' - z)\tan\theta\cos(\psi - \phi) + (z' - z)^2 \tan^2\theta + (z' - z_0)^2} \quad (25)$$

with the radial distance R in the x-y plane and the angle ψ given by

$$R = \sqrt{(x - x_0)^2 + (y - y_0)^2} \quad (26)$$

$$\psi = \tan^{-1}\left[\frac{y - y_0}{x - x_0}\right] \quad (27)$$

3.4   Phase Functions.

The actual scattering phase function, or, as it is sometimes called, the differential scattering cross section can be computed using Mie scattering equations. For our purposes, however, we will use a good analytical approximation, that is, the Henyey-Greenstein phase function, given by

$$p(v) = \frac{1 - g^2}{(1 + g^2 - 2gv)^{3/2}} \quad (28)$$

where the quantity v is the cosine of the angle between the incoming and scattered radiation directions. That is,

$$v = \mu\mu' + \sqrt{(1 - \mu^2)(1 - \mu'^2)}\cos(\phi - \phi') \quad (29)$$

The quantity g is called the asymmetry parameter and is used to describe the asymmetry of the scattered radiation. For example, if g = -1 the scattering is all in the backward direction, but if g = +1 the scattering is all in the forward direction. For g = 0 the scattering is isotropic. For most cases involving smoke clouds g is a small positive number.

13

3.5   <u>Single Point Source Solution.</u>

From all the analysis in the previous sections we can now find the solution for singly-scattered radiation from a single point isotropic source. The solution is given by

$$L = \frac{\beta P (1 - g^2) e^{-\kappa z_0}}{(4\pi)^2 r_0 (1 + g^2)^{3/2}} \int_{\theta_m}^{\theta_M} \frac{e^{-\kappa r_0 (\csc\theta + \cot\theta)}}{[1 + G\cos\theta]^{3/2}} d\theta \tag{30}$$

where the radial distance r_0 is given by

$$r_0 = \sqrt{x_0^2 + y_0^2} \tag{31}$$

and the factor G is given by

$$G = \frac{2g}{1 + g^2} \tag{32}$$

The upper and lower limits on the integral are given by

$$\theta_M = \pi - \tan^{-1}\left(\frac{r_0}{z_0}\right) \tag{33}$$

and

$$\theta_m = \tan^{-1}\left(\frac{r_0}{c - z_0}\right) \tag{34}$$

The single-scattering integral of equation (30) is in quadrature form and can be evaluated using a two-point Gaussian quadrature method. We performed this computation in Fortran code and also using the software Mathematica® and got the same results. This is the basic integral that is to be evaluated many times for all the point sources in the medium so it is necessary that it be done with high accuracy and with a minimum of computer time. To this extent we performed the integration using various segments along the path and determined that 30 was the optimum number in order to obtain at least six significant figures in the final result.

Figure 2 illustrates radiation from a single point source in the medium that originates from the point source and then is scattered at some arbitrary point source to all points along the line of sight. The dashed lines indicate the evaluation of the integral in equation (30) many times for various angles along the line of sight. In a previous interim report on this project we showed numerous examples of the radiance as a function of the parameters in the problem.

14
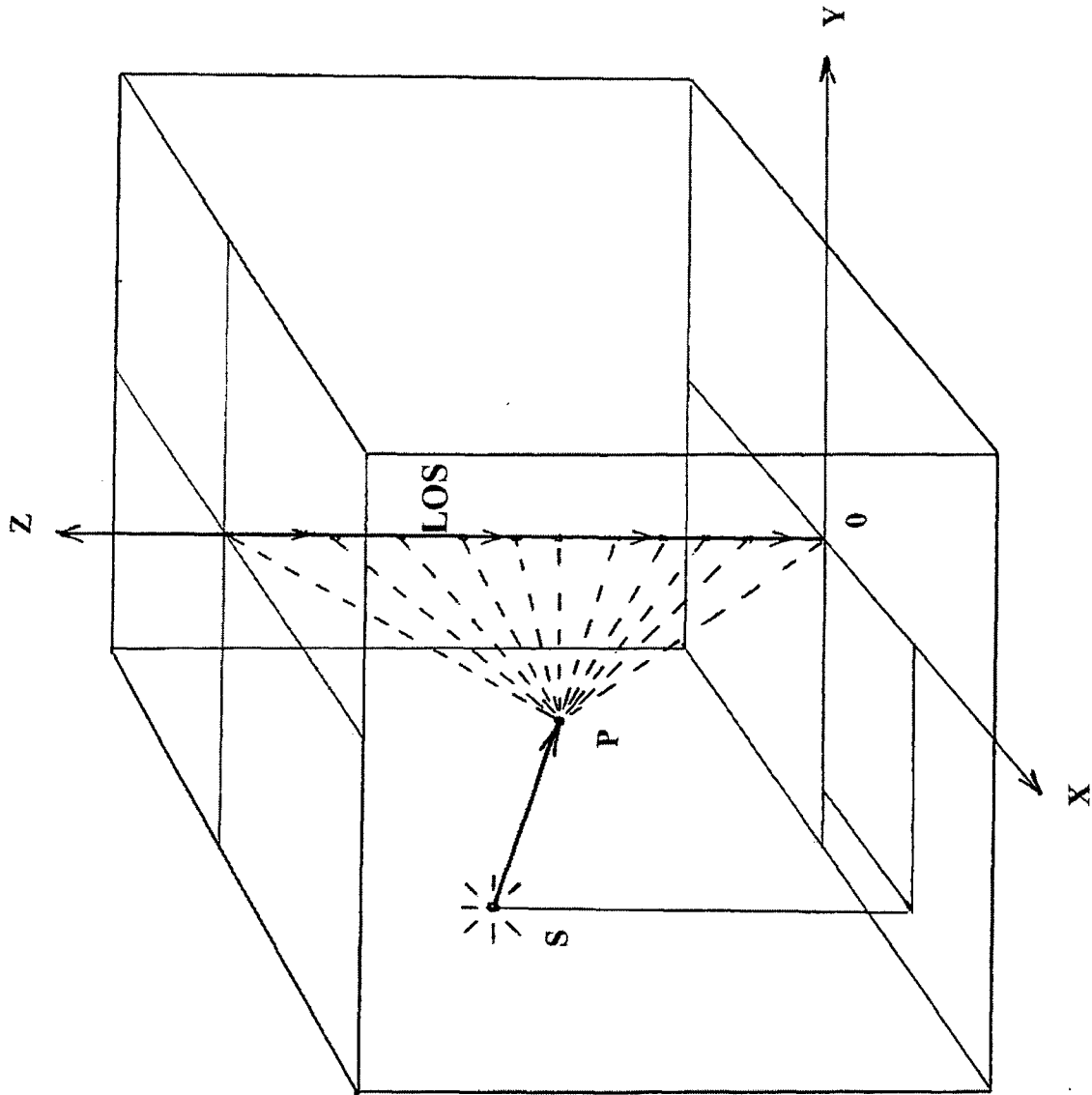
Figure 2. Illustration of Single Scattering from an Arbitrary Point in the Medium to the Line of Sight.

15

3.6   Multiple Point Source Solution.

Our problem is concerned with not just one, but many isotropic point sources in the medium designated as heated flares. To understand the significance of the problem we can let the array of sources be specified for a Cartesian lattice. As we will see later the number of sources is not that important in the computation of the radiance at the exit point of the cloud. Also, having a regular lattice arrangement of the sources allows the use of symmetry in the calculations, thereby greatly reducing the amount of computer time. The observer is always located at the origin of coordinates at the center of the bottom face of the cube looking directly upward along the positive z axis. The lattice is specified so that the observer never looks directly at any source. To do so would render the computations meaningless for a point source since the result would be infinite. In actual fact, of course, the flares are not points but small spheres with a finite but very large radiance. A sensor that has one of the flares in its field of view would register a temporary sharp signal in a manner similar to that when one momentarily looks at the daytime sky with a telescope and then accidentally scans through the Sun. The computer model automatically prevents such an occurrence. This fact is illustrated in figure 3 where we show the number of flares as a function of the distance in the x-direction. One can see that for N points in one dimension the distance between flares is $L/(N+1)$ where L is the length of a side of the cube. Thus, the model allows only for the computation of radiation that is scattered and absorbed by the smoke in the medium. This is referred to as the path radiance. Figure 4 illustrates one quadrant of the three-dimensional lattice of point sources for a user selection of four point sources along any one dimension of the medium. It is also of importance to note that at no time will any source be on a face of the medium. Thus, when a user selects any number of sources they will all be located inside the medium. In figure 4 we depict only one quadrant for the sake of visibility of the lattice arrangement. Therefore, in this case of four sources in one dimension the computer program automatically sets up the lattice with a total of $4^3 = 64$ points. Because of the symmetry, however, it is only necessary to compute the results for one quadrant and then multiply the result by 4 to obtain the total path radiance for all 64 points. This results in a saving of computer time by a factor of four. We have run the computer program for up to 100 point sources in one dimension or for one million total points in the medium. As was shown in a previous report the number of sources makes little difference in the final result.
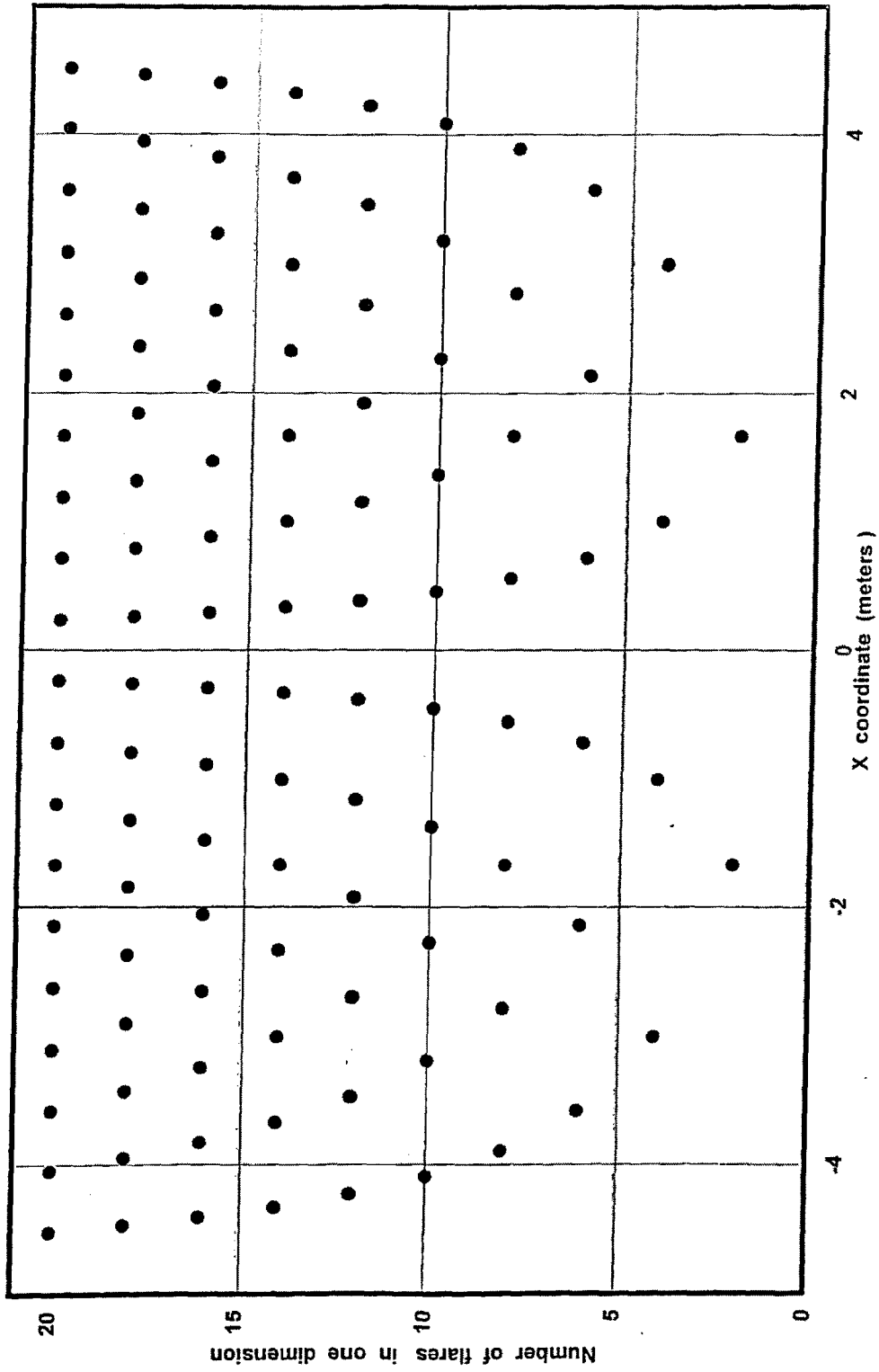
Figure 3. Placement of Flares along One Dimension in the X-Y Plane in a Cubic Medium with a Side of Length 10 Meters.

17
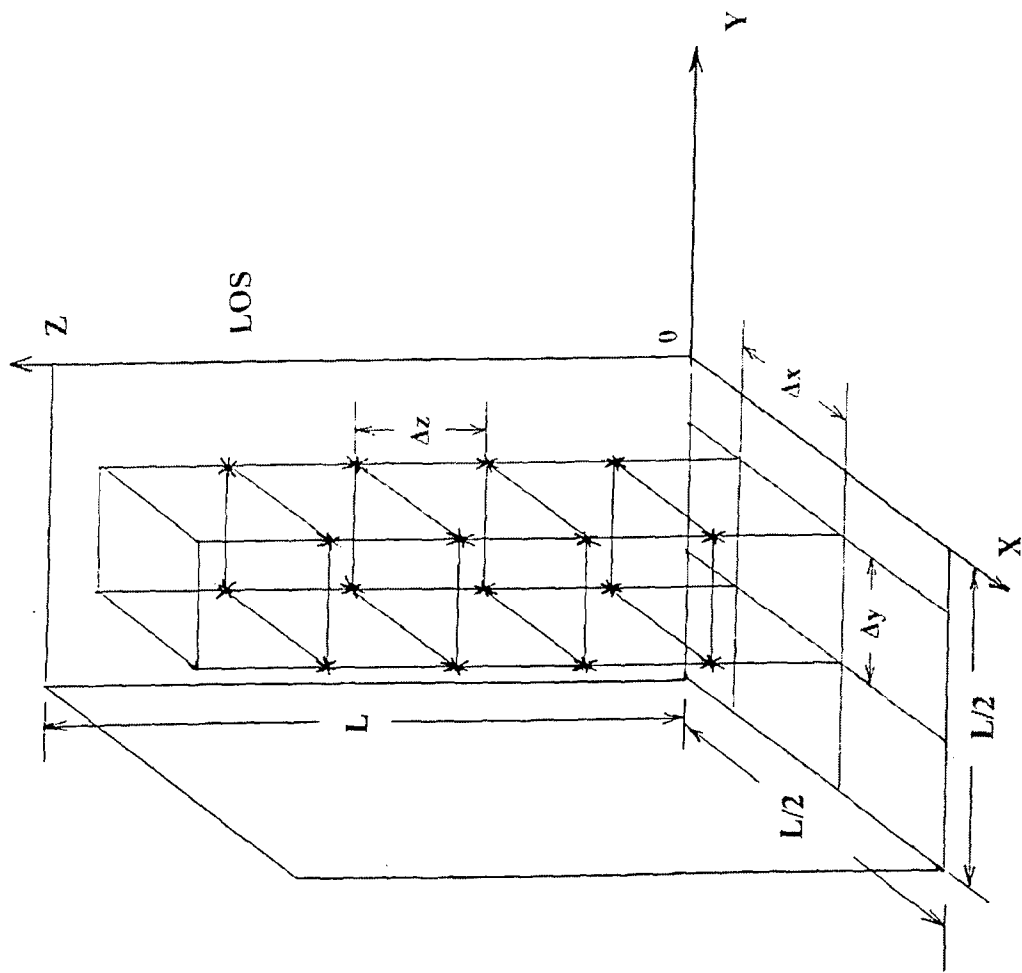
Figure 4. Lattice Arrangement of Flares in One Quadrant of a Cube for N (number of flares in one dimension) = 4.

3.7 The Two-Stream Method.

In a previous interim technical report we have shown the mathematics of a general P-N method and in particular, the P-1, P-3, and P-5 approximations. In general if one could solve the system for an infinite number of equations then one would have an exact solution to the problem. Clearly, this is not possible. In the early days of radiative-transfer a simple solution was found by performing an average of the radiance over an upward and a downward hemisphere in a one-dimensional medium. Hence, the description "two-stream." We shall now use this approximation to derive expressions for the albedo, the transmission, and the emissivity of a cloud. First, we look at the radiative-transfer equation in a one-dimensional medium with azimuthal independence. It is given by

$$\mu \frac{dL}{dz} + \kappa L = \alpha B + \frac{\beta}{2} \int_{-1}^{1} p(\mu, \mu') L(z, \mu') d\mu' \tag{35}$$

We can now define the scalar irradiance in the upward and downward hemispheres as

$$L_+(z) = 2\pi \int_0^1 L(z, \mu) d\mu \tag{36}$$

$$L_-(z) = 2\pi \int_0^1 L(z, -\mu) d\mu \tag{37}$$

and the corresponding vector irradiances as

$$E_+(z) = 2\pi \int_0^1 \mu L(z, \mu) d\mu \tag{38}$$

$$E_-(z) = 2\pi \int_0^1 \mu L(z, -\mu) d\mu \tag{39}$$

After carrying out the appropriate integrations over the two hemispheres we get two-coupled linear differential equations, that is

$$\frac{dM}{d\tau} + 2[1 + \varpi_0(1 - 2F)]N = 0 \tag{40}$$

$$\frac{dN}{d\tau} + 2(1 - \varpi_0)M = 4\pi(1 - \varpi_0)B \tag{41}$$

where ϖ_0 is the single-scattering albedo and the optical depth τ is given as the product of the volume extinction coefficient κ and the distance from the base of the cloud to some altitude z. The parameter F is a function of the asymmetry parameter g, that is

$$F = \frac{(1+g)}{2g}\left[1 - \frac{1-g}{\sqrt{1+g^2}}\right] \tag{42}$$

and the dependent variables M and N are the following combinations of the irradiances:

$$M(\tau) = E_+(\tau) + E_-(\tau) \tag{43}$$

$$N(\tau) = E_+(\tau) - E_-(\tau) \tag{44}$$

It should be noted that if the scattering is isotropic then F = ½, whereas if the scattering is entirely in the forward direction then F = 1. If the scattering is entirely in the backward direction then F = -1. For all other cases F lies between 0 and 1.

We can now use the following boundary conditions:

$$E_+(0) = \pi B_1 \tag{45}$$

$$E_-(\tau_0) = \pi B_2 \tag{46}$$

where B_1 is the input Planck radiance at the bottom of the cloud and B_2 is the input Planck radiance at the top of the cloud. Thus, we assume that the input radiances are isotropic exterior to the cloud. The two, coupled differential equations (40) and (41) can easily be solved in terms of the boundary conditions, equations (45) and (46). This we have done but it is more useful for our purpose to consider the solutions at the boundaries of the cloud. Therefore the upward and downward radiant exitances at the top and bottom of the cloud are given by

$$E_+(\tau_0) = \pi B + \pi\left[\frac{4k(B_1 - B) + (1 - k^2)(B_2 - B)\left\{e^{\lambda \tau_0} - e^{-\lambda \tau_0}\right\}}{(1+k)^2 e^{\lambda \tau_0} - (1-k)^2 e^{-\lambda \tau_0}}\right] \tag{47}$$

$$E_-(0) = \pi B + \pi\left[\frac{4k(B_2 - B) + (1 - k^2)(B_1 - B)\left\{e^{\lambda \tau_0} - e^{-\lambda \tau_0}\right\}}{(1+k)^2 e^{\lambda \tau_0} - (1-k)^2 e^{-\lambda \tau_0}}\right] \tag{48}$$

20

where the parameter λ is given by

$$\lambda = 2\sqrt{(1-\varpi_0)[1-\varpi_0(2F-1)]} \tag{49}$$

and the parameter k is

$$k = \frac{2(1-\varpi_0)}{\lambda} \tag{50}$$

It is significant to note that the only difference between equations (47) and (48) is in the interchange of the input radiances B_1 and B_2. It is also of interest to note that the top exitance is related to the bottom exitance independent of the internal radiance! Thus, eliminating the internal Planck function we have

$$E_+(\tau_0) = E_-(0) + \pi(B_1 - B_2)\left[\frac{4k - (1-k^2)\left\{e^{\lambda\tau_0} - e^{-\lambda\tau_0}\right\}}{(1+k)^2 e^{\lambda\tau_0} - (1-k)^2 e^{-\lambda\tau_0}} \right] \tag{51}$$

From equation (51) we see that if the external radiances are the same then the top and bottom exitances are equal as well.

4.   CLOUD THERMAL PARAMETERS

In this section we present the basic cloud quantities associated with the reflection, transmission, and emission of thermal radiation in and through a cloud. A detailed derivation and analysis of this work appeared in the previous interim technical report.

4.1   Albedo.

Using equations (47) and (48) of the two-stream model of section 3 we can easily determine the albedo of the cloud. It is just the ratio of the exitance divided by the incoming, external irradiance. Thus,

$$A = \left(\frac{1-k}{1+k}\right)\left[\frac{1 - e^{-2\lambda\tau_0}}{1 - \left(\frac{1-k}{1+k}\right)^2 e^{-2\lambda\tau_0}} \right] \tag{52}$$

The albedo is just a function of the optical thickness of the medium, the single-scattering albedo, and the asymmetry parameter. For isotropic radiation the albedo is

$$A \to \frac{2[1 - \sqrt{1 - \varpi_0}]}{\varpi_0} - 1 \; ; \; \varpi_0 \neq 0 \tag{53}$$

which approaches 1 for the case when $\varpi_0 = 1$. This is more easily seen when we write the actual expression for the albedo in the special case of a pure scattering medium for isotropic scattering. It is given by

$$A = \frac{\tau_0}{1 + \tau_0} \tag{54}$$

From equation (54) one can easily see the asymptotic nature of the albedo. It is clear that it is always less than or equal to 1 and that it approaches the value of 1 as the optical thickness increases without bound.

4.2   Transmission.

Now we investigate the diffuse transmission of radiation through the cloud. As in the case of albedo we use the basic equations of (47) and (48) of section 3.7 to get the transmission. The diffuse transmission of the cloud is given by

$$T_D = \frac{4k}{(1+k)^2} \left[\frac{e^{-\lambda \tau_0}}{1 - \left(\frac{1-k}{1+k}\right)^2 e^{-2\lambda \tau_0}} \right] \tag{55}$$

For the special case when there is no absorption in the cloud we have

$$T_D = \frac{1}{1 + 2(1 - F)\tau_0} \; ; \; \varpi_0 = 1 \tag{56}$$

which indicates that the diffuse transmission is always less than or equal to 1.

22

4.3 Emissivity.

The last term to be considered in the analysis of the radiation in clouds is the emissivity. Again, using equations (47) and (48) of section 3.7 we have

$$\varepsilon = 1 - \left[\frac{4k + (1-k^2)\left\{e^{\lambda\tau_0} - e^{-\lambda\tau_0}\right\}}{(1+k)^2 e^{\lambda\tau_0} - (1-k)^2 e^{-\lambda\tau_0}} \right] \tag{57}$$

For the special case when there is no absorption in the cloud then we have

$$\varepsilon = 0, \; \varpi_0 = 1 \tag{58}$$

which simply means that the cloud reflects and transmits radiation but none is absorbed.

4.4 Beam Transmittance.

So far we have shown the dependence of the albedo, the diffuse transmission, and the emissivity as functions of the cloud parameters such as the optical thickness, the single-scattering albedo, and the asymmetry parameter. However, it is perhaps more meaningful to describe the cloud albedo, transmission, and the emissivity in terms of a measurable quantity such as the line-of-sight or beam transmittance. The beam transmittance describes the attenuation of a beam of radiation of infinitesimal thickness as the radiation propagates from one point in the medium to another. It is given by

$$T_B = e^{-\tau_0} \tag{59}$$

where τ_0 is the optical thickness along the path through the cloud. It is a quantity that can more easily be measured with a detector than the other quantities that depend on the cloud geometric extent. For example, one can use a laser to shine a beam through the cloud and simply measure the light attenuation at the other side of the cloud. Therefore, we present in this section a series of plots of the cloud albedo, the cloud diffuse transmission, and the cloud emissivity in terms of the beam transmittance. First, we present the formulas for the albedo, the diffuse transmission, and the emissivity of a cloud in a more compact form in terms of the optical thickness and in terms of the beam transmittance.

$$A = \rho\left[\frac{1 - e^{-2\lambda\tau_0}}{1 - \rho^2 e^{-2\lambda\tau_0}} \right] = \rho\left[\frac{1 - T_B^{2\lambda}}{1 - \rho^2 T_B^{2\lambda}} \right] \tag{60}$$

$$T_D = (1 - \rho^2)\left[\frac{e^{-\lambda\tau_0}}{1 - \rho^2 e^{-2\lambda\tau_0}}\right] = (1 - \rho^2)\left[\frac{T_B^\lambda}{1 - \rho^2 T_B^{2\lambda}}\right] \tag{61}$$

$$\varepsilon = (1 - \rho)\left[\frac{1 - e^{-\lambda\tau_0}}{1 + \rho e^{-\lambda\tau_0}}\right] = (1 - \rho)\left[\frac{1 - T_B^\lambda}{1 + \rho T_B^\lambda}\right] \tag{62}$$

where

$$\rho = \frac{1 - k}{1 + k} \tag{63}$$

$$k = \sqrt{\frac{1 - \varpi_0}{1 - \varpi_0(2F - 1)}} \tag{64}$$

$$\lambda = 2\sqrt{(1 - \varpi_0)[1 - \varpi_0(2F - 1)]} \tag{65}$$

$$F = \frac{1 + g}{2g}\left[1 - \frac{1 - g}{\sqrt{1 + g^2}}\right] \tag{66}$$

5.   IMAGE METRICS

Various measures exist to discriminate a target from the background. In our case we will explore these measures for application to an imaging system with an attenuating, flare-emitting cloud in between the target and a sensor.

5.1   Contrast Function.

Contrast can be defined in several ways. It can be defined as simply the difference between the target radiance and the background radiance. Thus, one can write the target and the background radiances at the sensor aperture as

$$L_t = L_{t0}T + P \tag{67}$$

$$L_b = L_{b0}T + P \tag{68}$$

where T is the beam transmittance, P is the path radiance, and L_{t0} and L_{b0} are the target and background radiances at the target position. The contrast is

$$C = L_t - L_b = (L_{t0} - L_{b0})T \tag{69}$$

One can also define the contrast ratio as

$$C_R = \frac{L_t}{L_b} = \frac{L_{t0}T + P}{L_{b0}T + P} \tag{70}$$

but this definition does not take into account the difference between the target and background radiances. The most common definition of contrast is the following:

$$C = \frac{L_t - L_b}{L_b} = \frac{(L_{t0} - L_{b0})T}{L_{b0}T + P} \tag{71}$$

If we define the intrinsic contrast as the target-background contrast at the target position, that is, as

$$C_0 = \frac{L_{t0} - L_{b0}}{L_{b0}} \tag{72}$$

then the contrast transmittance, defined as the ratio of the contrast and the intrinsic contrast, is given by

$$T_C = \frac{1}{1 + \dfrac{P}{L_{b0}T}}$$

(73)

It should be noted that the physics of scattering and emission into the line of sight is contained in the path radiance term P. The beam transmittance T just accounts for the radiation that is attenuated by scattering and absorption along the line of sight. It must also be kept in mind that for all these definitions we assume that the target and background are infinitesimally close to the same line of sight. One can also say that the observer is looking at a target element very close to the background boundary.

The path radiance can be written as

$$P = B_F T_D + B_N A + \varepsilon B$$

(74)

where B_F is the effective Planck radiance that enters the far side of the cloud, that is, the side closest to the target. Likewise, B_N is the effective Planck radiance that leaves the near side of the cloud, that is, the side closest to the sensor. B is just the Planck radiance inside the cloud that is characteristic of the temperature in the cloud. The other terms in equation (74) are the quantities we explored at great length in section 4. T_D is the cloud diffuse transmission, A is the cloud albedo, and ε is the cloud emissivity.

Let us now look at plots of the contrast transmittance as a function of the cloud parameters. Figure 5 depicts the contrast transmittance versus the beam transmittance for a "cool" cloud with three single-scattering albedos. The contrast transmittance for a scattering cloud is lower than the contrast transmittance for an absorbing cloud. As in the previous sections however, if we have a "warm" cloud we see the reverse as is indicated in figure 6 for a cloud that has a temperature higher than that of the exterior environment. For a cloud with the internal and external temperatures the same there is no dependence on the single-scattering albedo.

We can also examine the dependence of the contrast transmittance on the single-scattering albedo. Figure 7 illustrates this for the "cool" cloud for four values of the optical thickness and figure 8 shows a similar effect in reverse for the "warm" cloud. One can easily see that there is very little dependence on the single-scattering albedo.

It is important for our analysis that we look at the wavelength dependence of the contrast transmittance. Figure 9 shows the variation in the contrast transmittance versus the wavelength of the radiation for a "warm" cloud with no scattering. It is a blackbody cloud emitting thermal radiation along its line-of-sight (LOS) path. As one might expect, the contrast transmittance is less for an optically thick cloud because of the greater amount of thermal emission inside the

26
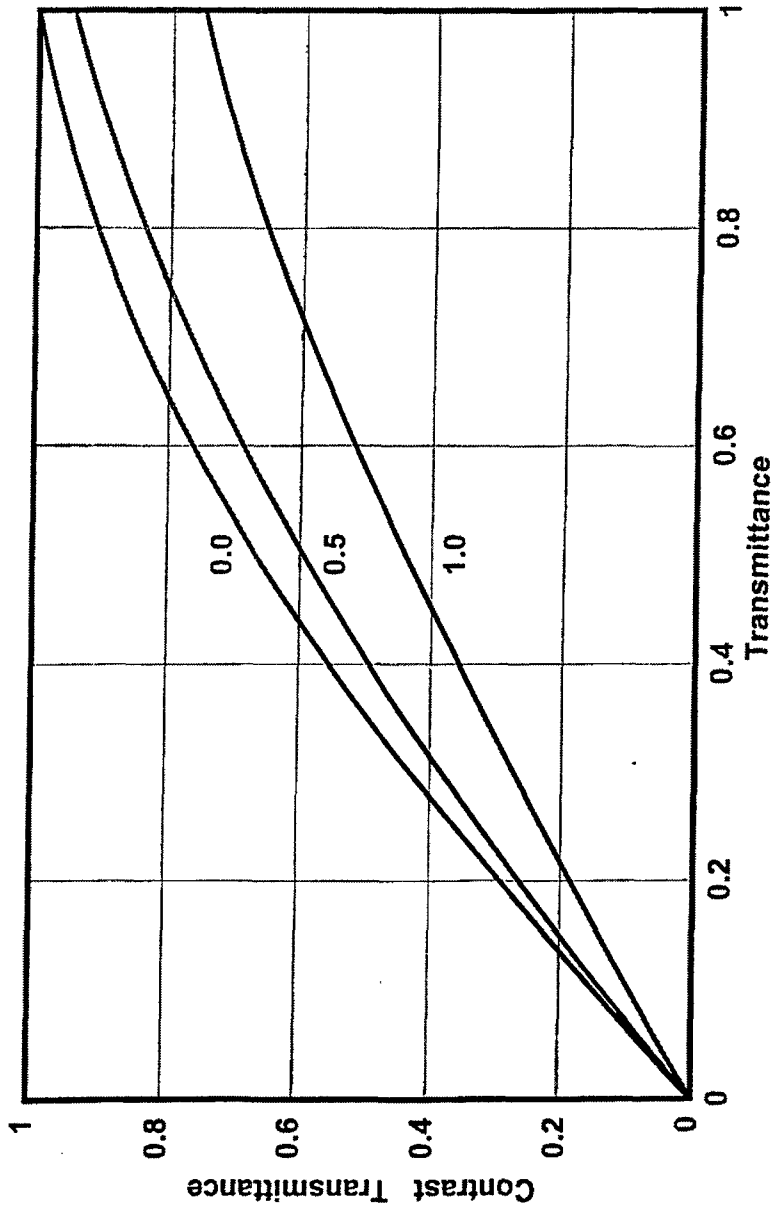
Figure 5. Variation of the Contrast Transmittance at a Wavelength of 10 μm for a Plane-Parallel Cloud *vs.* the Beam Transmittance for Three Values of the Single-Scattering Albedo. Cloud Temperature = 30°F, External Temperature = 70°F.

27
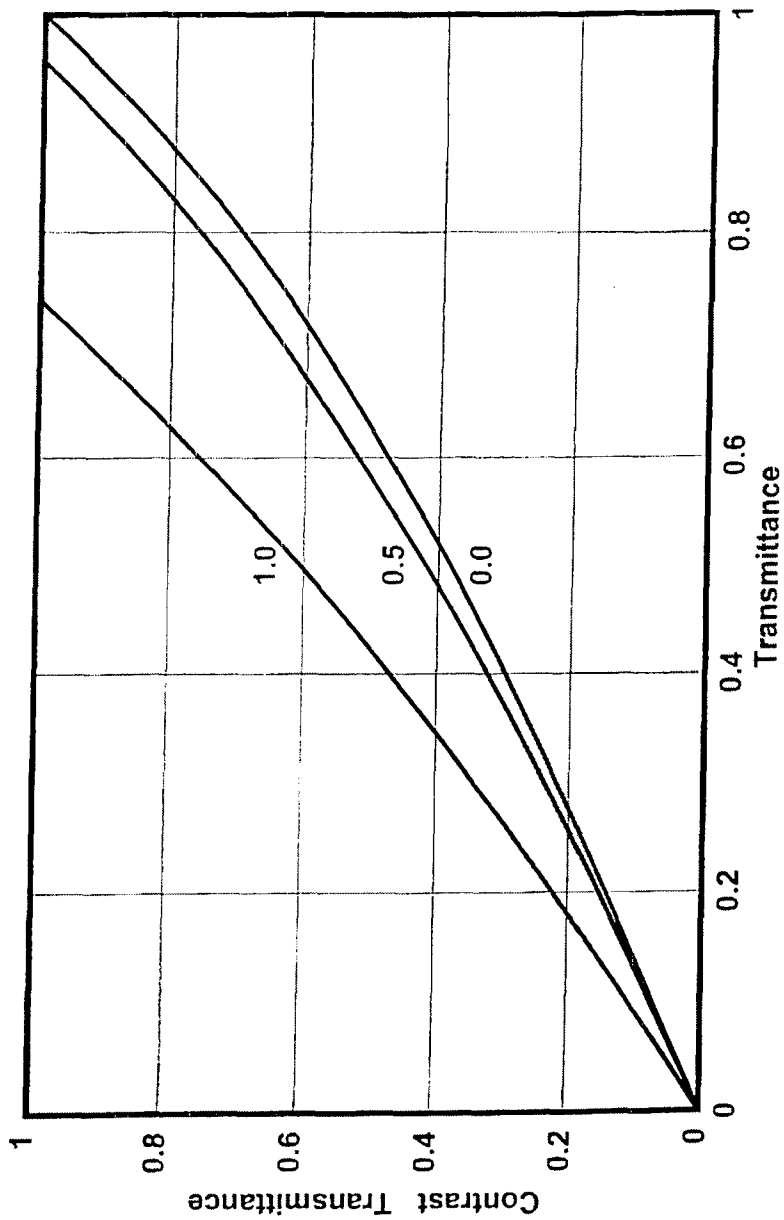
Figure 6. Variation of the Contrast Transmittance at a Wavelength of 10 μm for a Plane-Parallel Cloud vs. the Beam Transmittance for Three Values of the Single-Scattering Albedo. Cloud Temperature = 110°F, External Temperature = 70°F.

28
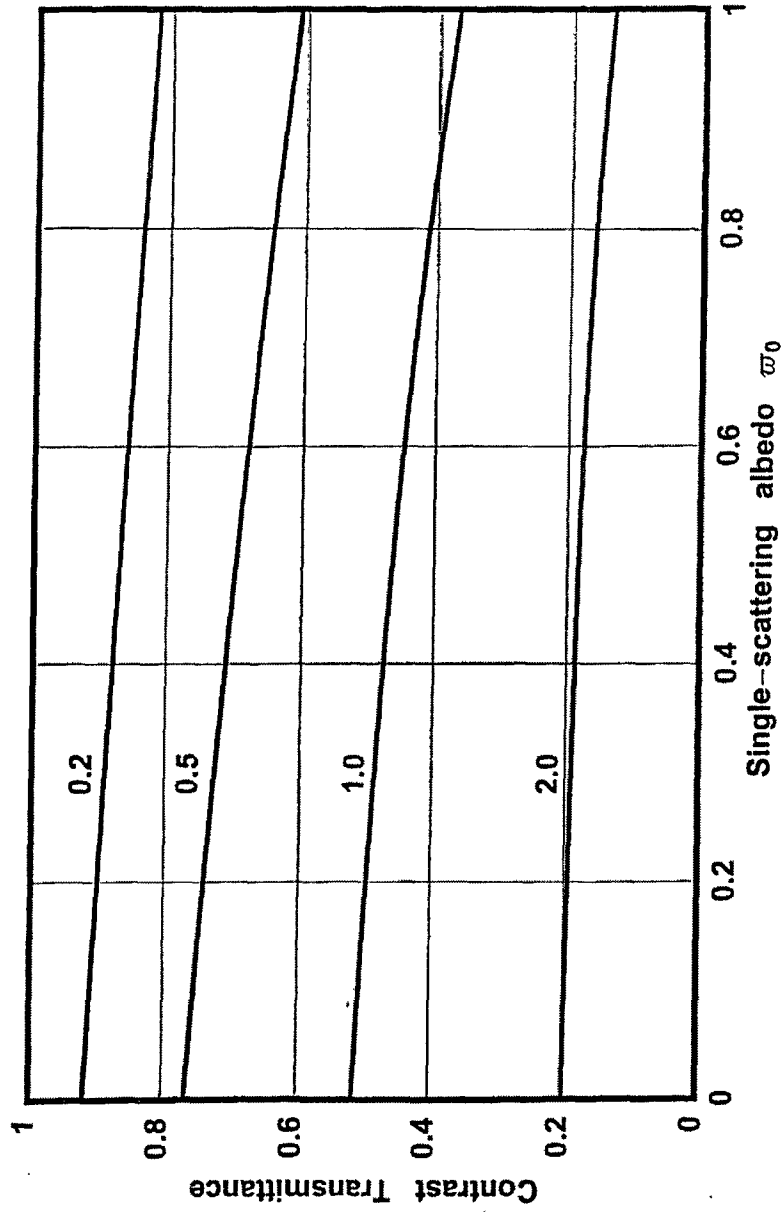
Figure 7. Variation of the Contrast Transmittance at a Wavelength of 10 μm for a Plane-Parallel Cloud vs. the Single-Scattering Albedo for Four Values of the Optical Thickness. Cloud Temperature = 30°F, External Temperature = 70°F.
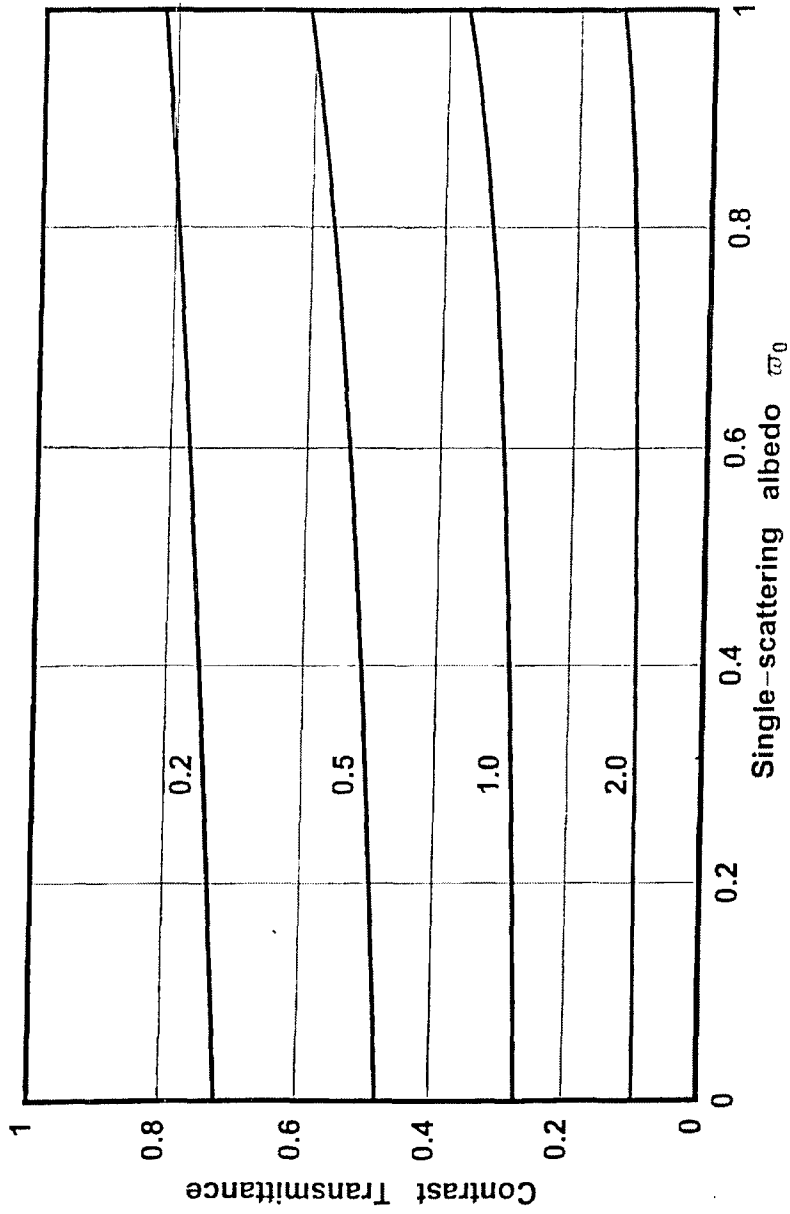
Figure 8. Variation of the Contrast Transmittance at a Wavelength of 10 μm for a Plane-Parallel Cloud vs. the Single-Scattering Albedo for Four Values of the Optical Thickness. Cloud Temperature = 110°F, External Temperature = 70°F.
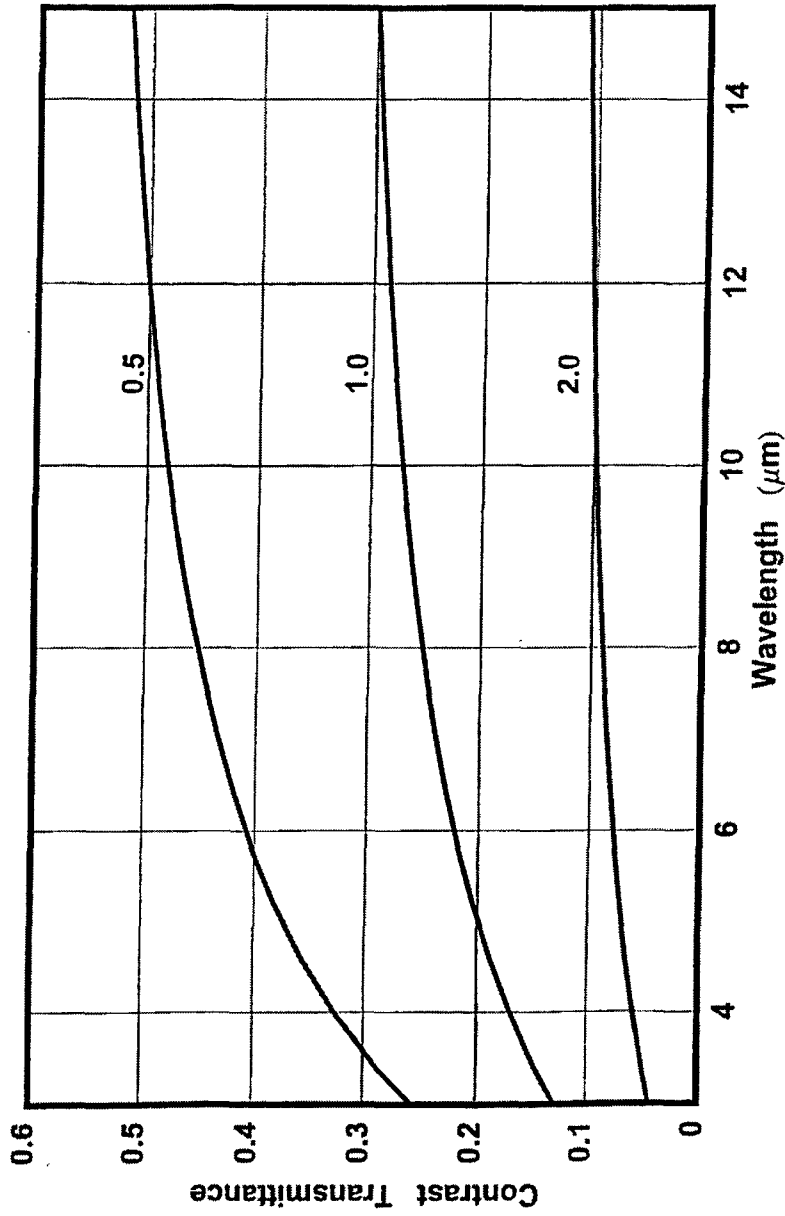
Figure 9. Variation of the Contrast Transmittance *vs.* Wavelength for a Plane-Parallel Cloud for Three Values of the Optical Thickness and a Single-Scattering Albedo = 0.0. Cloud Temperature = 110°F, External Temperature = 70°F.

31

cloud. For a "cool" cloud the effect is the reverse as can be seen in figure 10. If the cloud temperature is the same as the external temperature then there is no dependence of the contrast transmittance on wavelength. It is interesting to note that for clouds with scattering the contrast transmittance is greater than for an absorbing cloud and that there is very little dependence on the wavelength. This is clear from figures 11 and 12. These plots show a set of curves similar to those of figures 9 and 10 except that they represent cloud with a single-scattering albedo = 0.9.

Finally, we can look at the explicit dependence of the contrast transmittance as a function of wavelength for several single-scattering albedos. Figure 13 shows the variation of the contrast transmittance versus wavelength for four single-scattering albedos for a "cool" cloud with an optical thickness = 1.0. One can see that the contrast transmittance is almost independent of the wavelength for highly scattering clouds. In the case of a "warm" cloud the effect is the same except that the curves are reversed. This is indicated in figure 14.

Everything that we have dealt with up to this point has been with thermal sources of radiation in the interior of the cloud. The important part of this entire effort, however, is to demonstrate the change in the image metrics with and without point flare sources of radiation in the cloud. We now examine the effect of the presence of the radiance due to the point sources of radiation in the cloud known as flares. Let us re-write the contrast
transmittance as

$$T_C' = \cfrac{1}{1 + \cfrac{P + P'}{L_{b0}T}}$$

(75)

where P' represents the path radiance due exclusively to the flare particles in the cloud. The beam transmittance T remains unaffected by the flares. If we now let f be the ratio of the flare path radiance to the normal thermal cloud path radiance, then we can express

the "total" contrast transmittance T_C' in terms of the thermal contrast transmittance T_C. Thus,

$$T_C' = \frac{T_C}{1 + f(1 - T_C)}$$

(76)

Figure 15 depicts the variation in the total contrast transmittance versus the thermal contrast transmittance for five values of f, the ratio of the flare path radiance to the thermal path radiance. This shows the diminution in the total contrast transmittance when flares are present in the cloud. For example, if the thermal contrast transmittance is 0.6 and the flare path radiance is twice the thermal path radiance, then the total contrast transmittance is 0.25. One can also look at this with respect to the inverse of f, that is, with respect to the ratio of the thermal path radiance to the
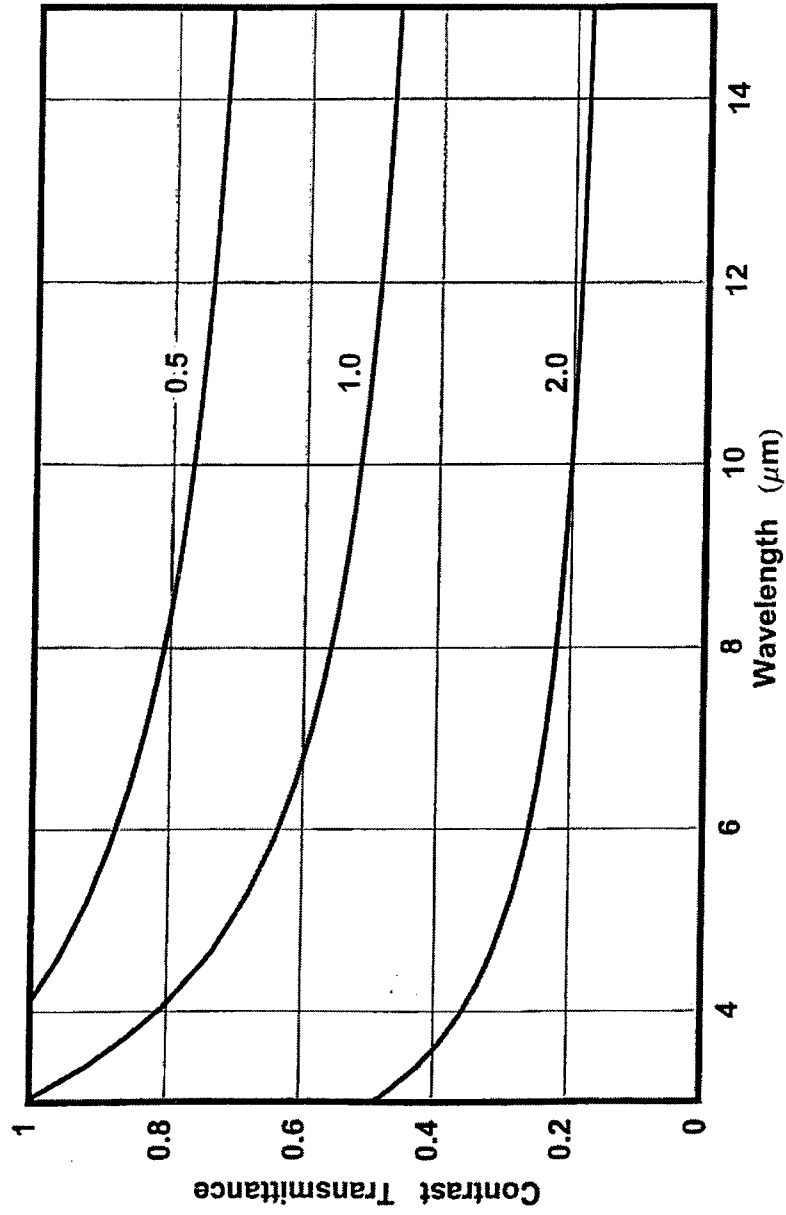
Figure 10. Variation of the Contrast Transmittance vs. Wavelength for a Plane-Parallel Cloud for Three Values of the Optical Thickness and a Single-Scattering Albedo = 0.0. Cloud Temperature = 30°F, External Temperature = 70°F.

33
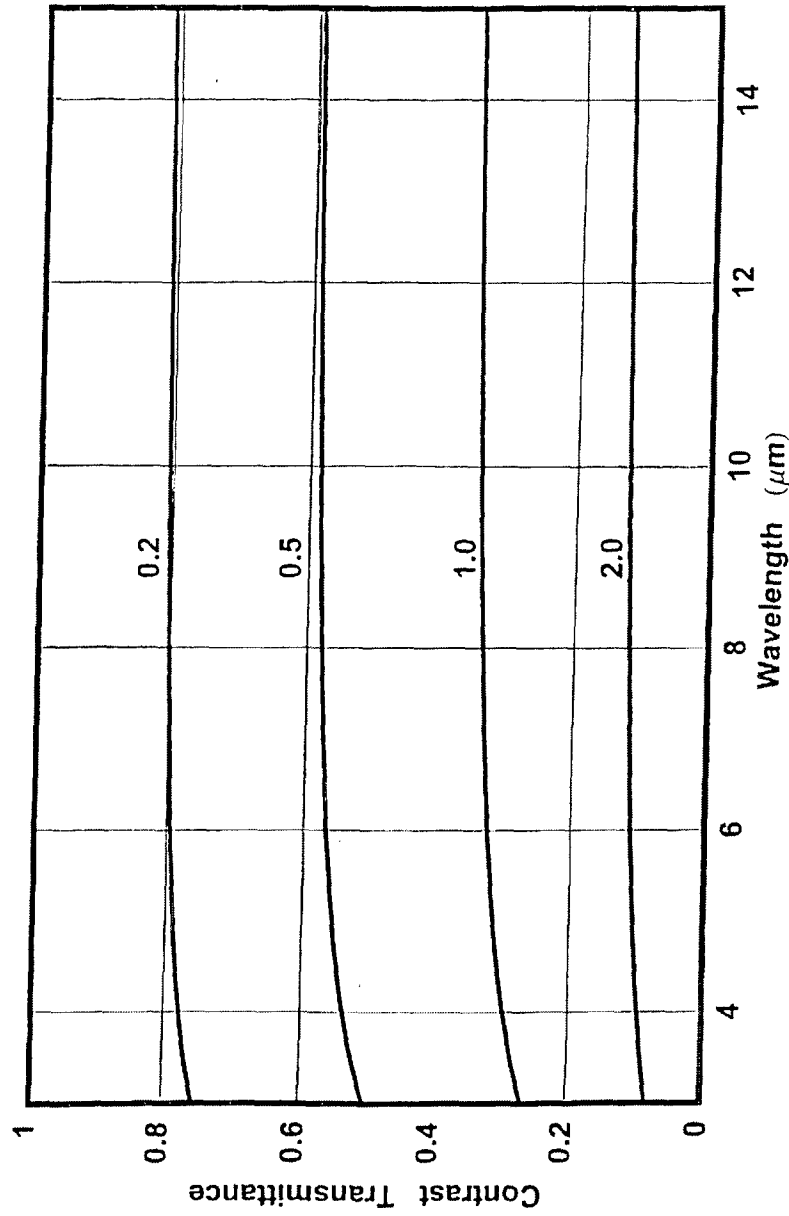
Figure 11. Variation of the Contrast Transmittance vs. Wavelength for a Plane-Parallel Cloud for Four Values of the Optical Thickness and a Single-Scattering Albedo = 0.9. Cloud Temperature = 110°F, External Temperature = 70°F.

34
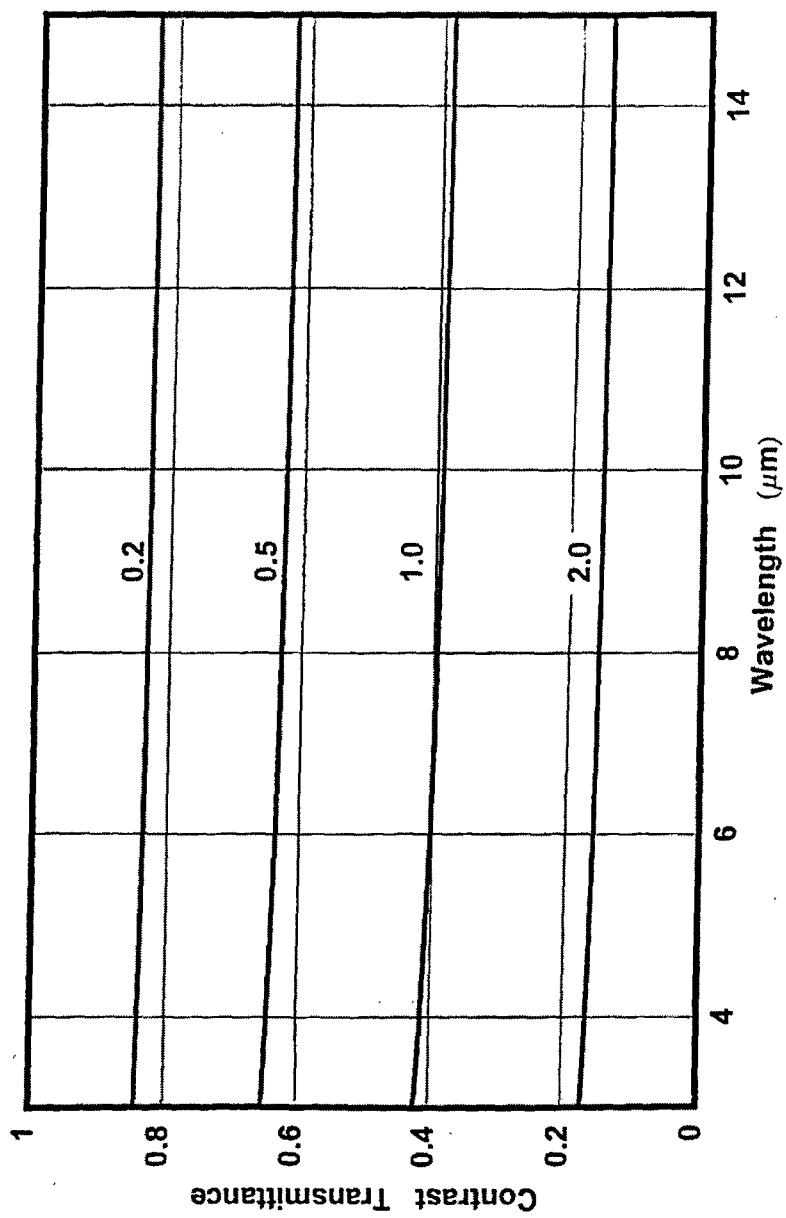
Figure 12. Variation of the Contrast Transmittance vs. Wavelength for a Plane-Parallel Cloud for Four Values of the Optical Thickness and a Single-Scattering Albedo = 0.9. Cloud Temperature = 30°F, External Temperature = 70°F.

35
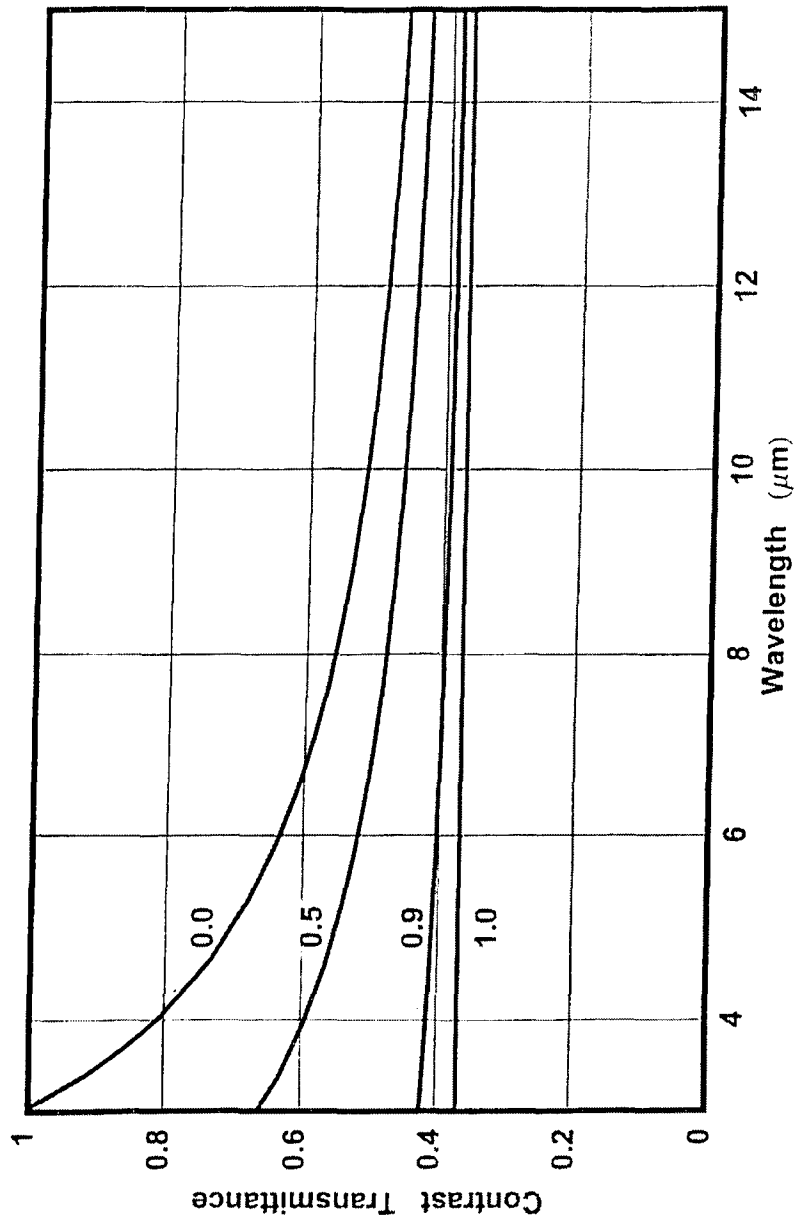
Figure 13. Variation of the Contrast Transmittance *vs.* Wavelength for a Plane-Parallel Cloud for Four Values of the Single-Scattering Albedo and an Optical Thickness = 1.0. Cloud Temperature = 30°F, External Temperature = 70°F.

36
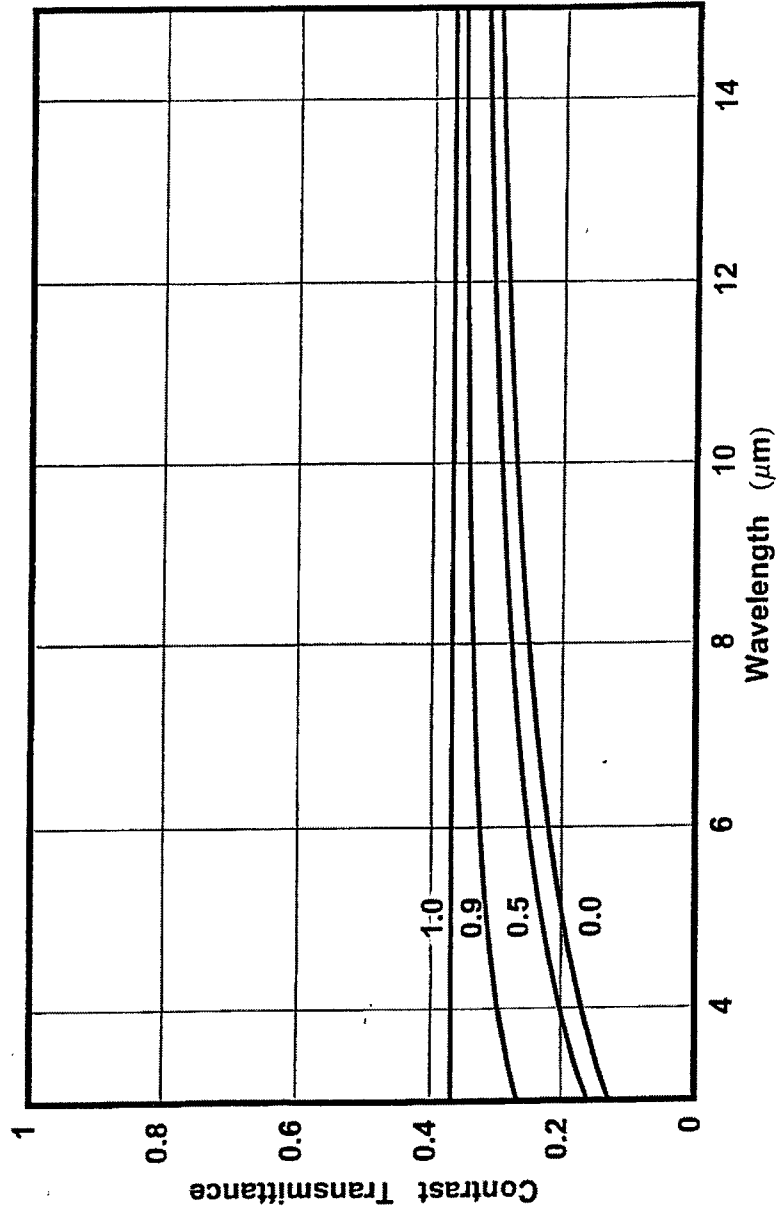
Figure 14. Variation of the Contrast Transmittance vs. Wavelength for a Plane-Parallel Cloud for Four Values of the Single-Scattering Albedo and an Optical Thickness = 1.0. Cloud Temperature = 110°F, External Temperature = 70°F.

37
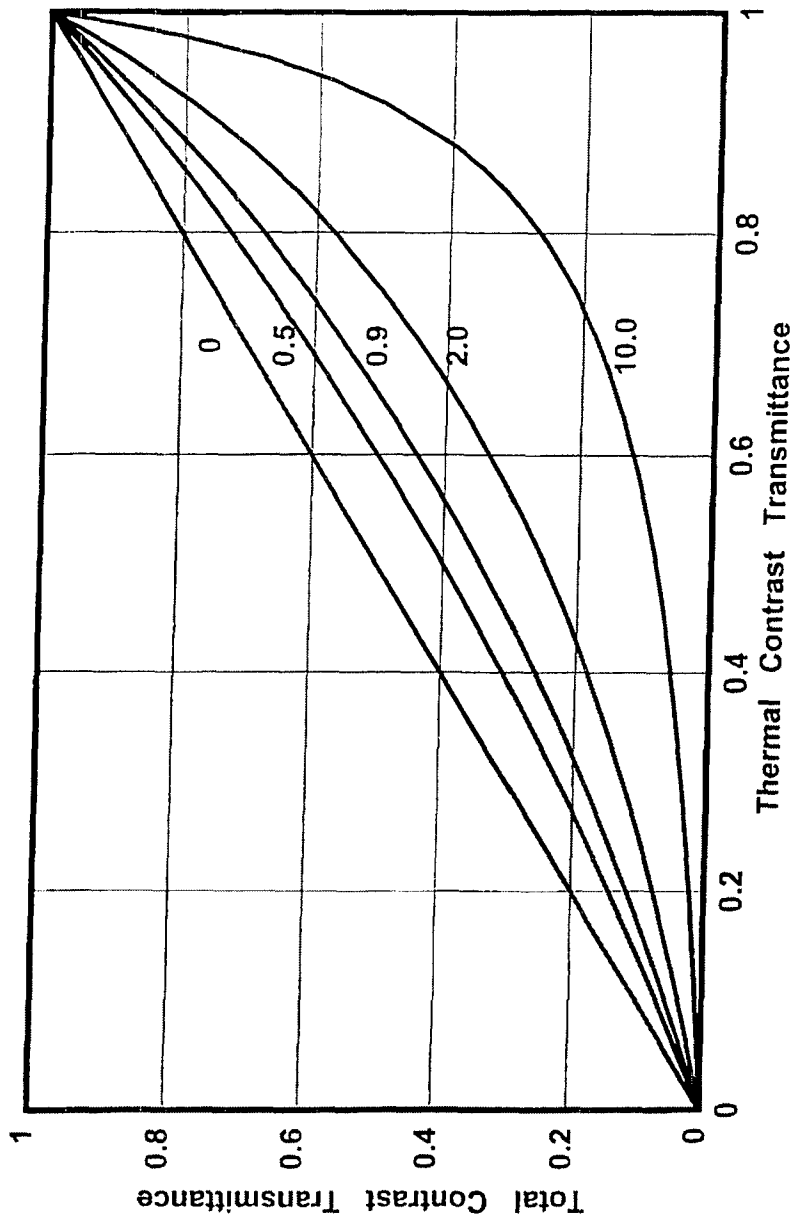
Figure 15. Variation of the Total Contrast Transmittance vs. the Thermal Contrast Transmittance for Five Values of the Ratio of the Flare Path Radiance to the Thermal Path Radiance.

38

flare path radiance. Let us call this ratio R. Figure 16 illustrates this effect, which we see is the inverse of figure 15 with respect to the path radiance ratios.

Finally, we can examine the variation of the total contrast transmittance as a function of the ratio R for several values of the thermal contrast transmittance. This is shown in figure 17. This is a very interesting plot. It indicates that for a large flare path radiance, (small R) relative to the thermal path radiance, the total contrast transmittance changes rapidly, but as the flare path radiance decreases there is very little change in the total contrast transmittance.

5.2   Modulation Function.

Sometimes another function is used for contrast analysis. It is the modulation function defined as

$$M = \frac{L_t - L_b}{L_t + L_b} = \frac{(L_{t0} - L_{b0})T}{(L_{t0} + L_{b0})T + 2P} \qquad (77)$$

As in the case with the contrast transmittance we can construct the modulation transmittance. It is given by

$$T_M = \frac{1}{1 + \dfrac{2P}{(L_{t0} + L_{b0})T}} \qquad (78)$$

a function that is quite similar to the contrast transmittance function of equation (73). We can express the contrast transmittance in terms of the modulation transmittance as follows:

$$T_C = \frac{2T_M}{(1 - R_0)T_M + (1 + R_0)} \qquad (79)$$

where the quantity R_0 is the ratio of the intrinsic target radiance to the intrinsic background radiance. In our case we will just use the Planck radiances for these functions. The question is how similar are these two representations of the contrast between a target and a background? In figure 18 we show the contrast transmittance as a function of the modulation transmittance for a target with a temperature of 120°F and several background temperatures. One can see that although we used a rather large range in background temperatures there is very little difference between the two representations. Likewise, we can take the difference between the modulation

39
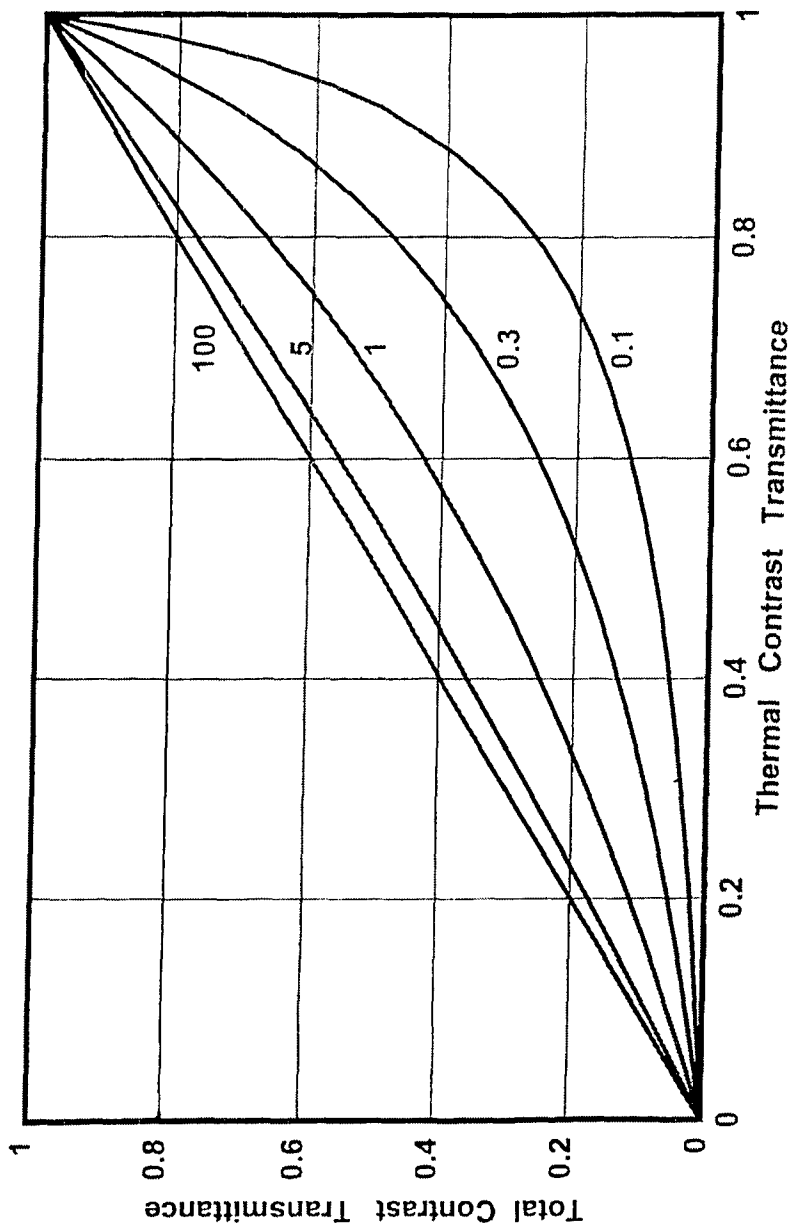
Figure 16. Variation of the Total Contrast Transmittance vs. the Thermal Contrast Transmittance for Five Values of the Ratio of the Thermal Path Radiance to the Flare Path Radiance.
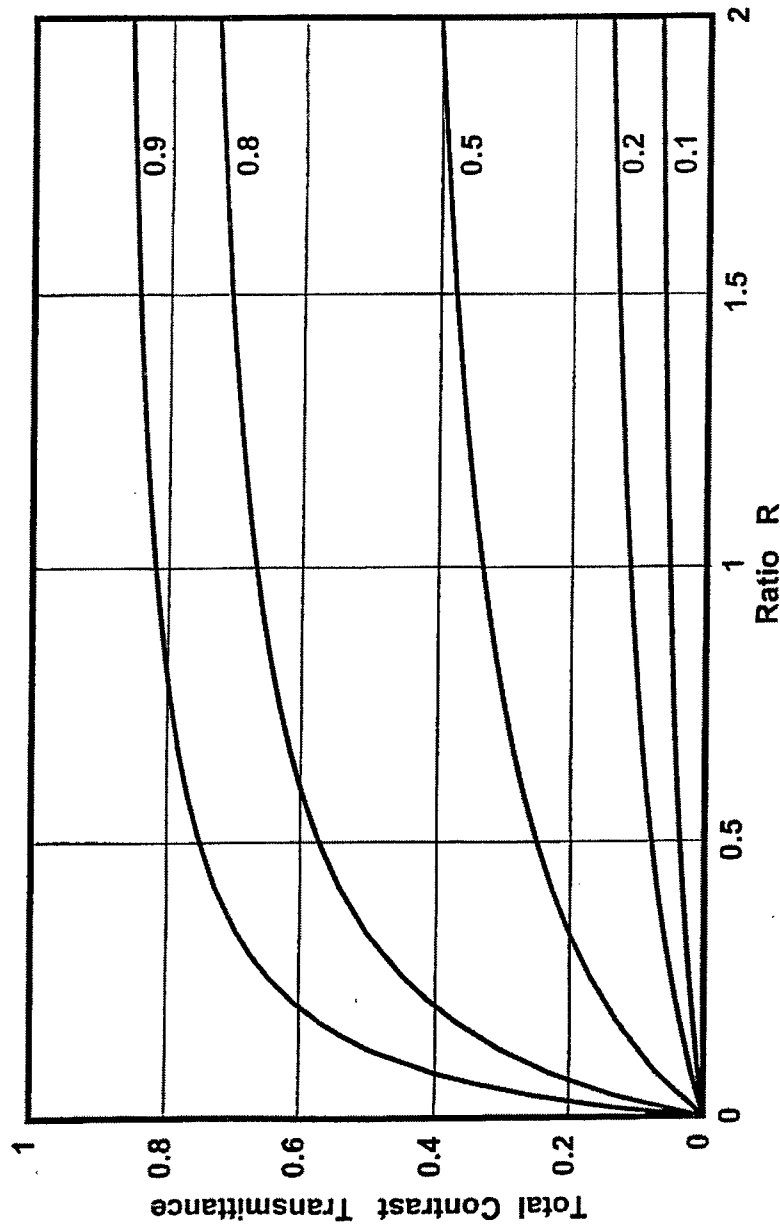
Figure 17. Variation of the Total Contrast Transmittance vs. the Ratio of the Thermal Path Radiance to the Flare Path Radiance for Five Values of the Thermal Contrast Transmittance.

41
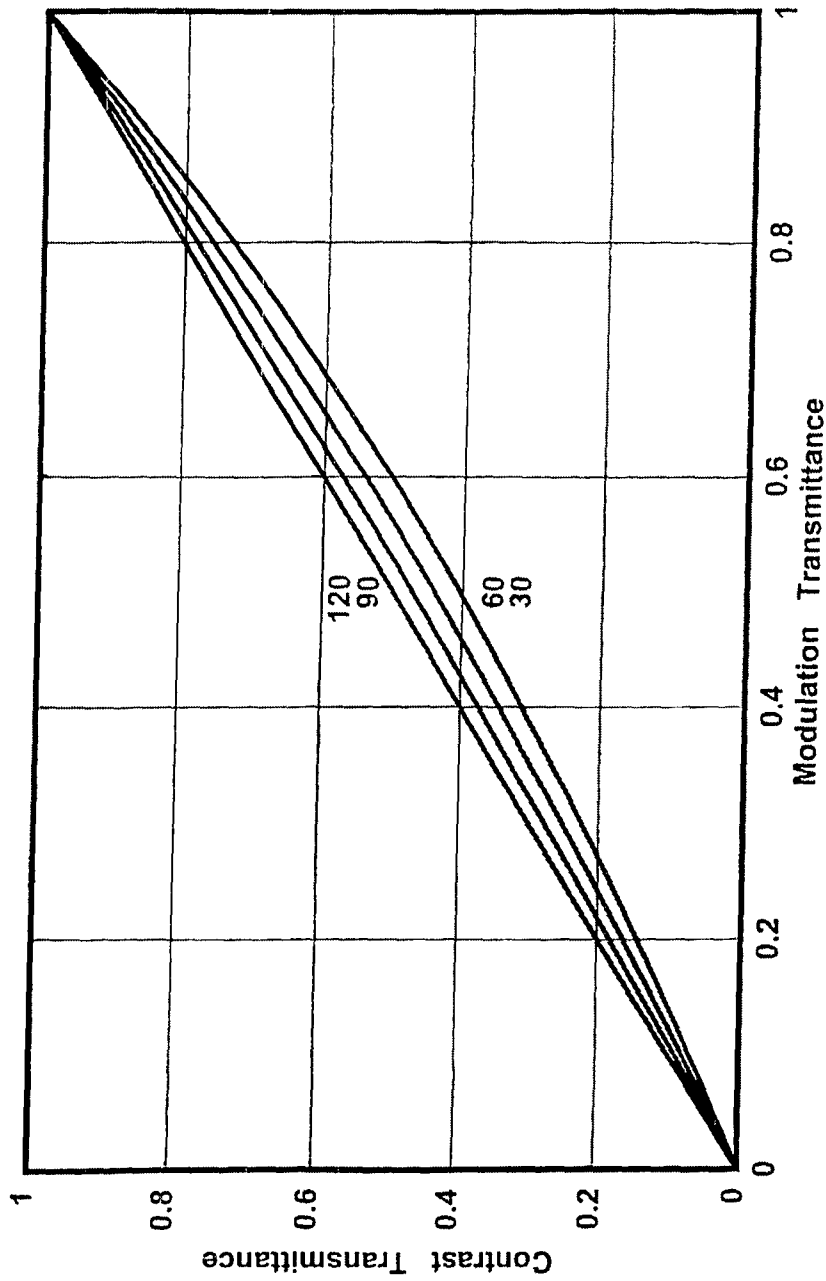
Figure 18. Variation of the Contrast Transmittance vs. the Modulation Transmittance for Four Background Temperatures and a Target Temperature = 120°F.

42

transmittance and the contrast transmittance and divide by the modulation transmittance. This is shown in figure 19. Again, we see very little difference between the functions. Nevertheless, under extreme environmental conditions, for example, in the case of a hot generator on an ice pack there would be some differences to be taken under consideration.

5.3 Signal-to-Noise Ratio.

In a final analysis of target-background discrimination functions we consider the so-called signal-to-noise ratio, SN. Using the definition of the SN given by Embury [1] we have

$$SN = \frac{L_t - L_b}{\sqrt{L_t^2 + L_b^2}} \tag{80}$$

with a similar expression for the intrinsic signal-to-noise ratio SN_0, that is, for the case when there is no atmosphere. The signal-to-noise transmittance, SN_T is then defined as the ratio of SN to SN_0, that is

$$SN_T = \frac{SN}{SN_0} \tag{81}$$

If we use the usual terms for the path radiance and the beam transmittance we get for the signal-to-noise transmittance the following:

$$SN_T \frac{1}{\sqrt{1 + \dfrac{2P(L_{t0} + L_{b0})}{(L_{t0}^2 + L_{b0}^2)T} + \dfrac{2P^2}{(L_{t0}^2 + L_{b0}^2)T^2}}} \tag{82}$$

At this point it is instructive to examine the change in the SN as a function of the target-background temperature difference. The intrinsic SN is illustrated in figure 20 for several target temperatures. Likewise, in figure 21 we show the SN for an atmosphere with a beam transmittance of 0.1. One should note that there is a factor of ten difference in the SN with an atmosphere and the SN without an atmosphere.

43
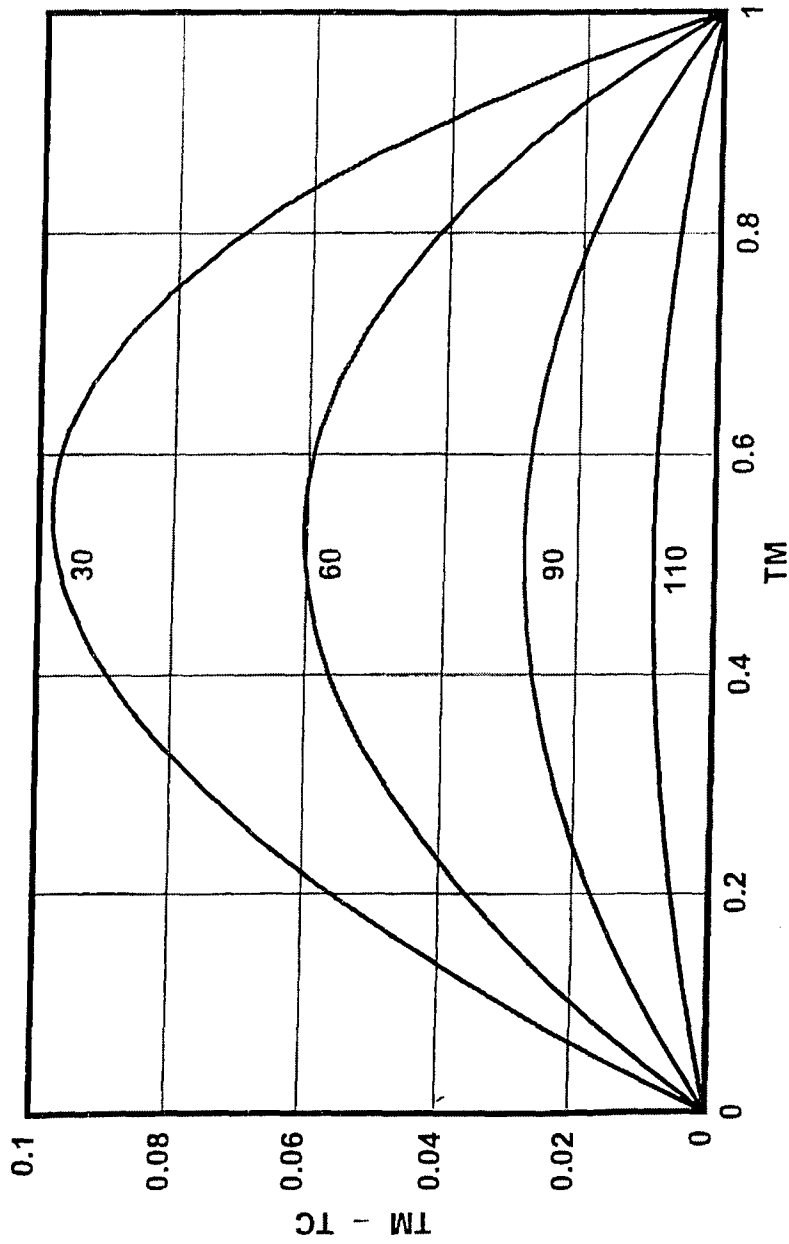
Figure 19. Variation of the Difference Between the Modulation Transmittance and the Contrast Transmittance vs. the Modulation Transmittance for Four Background Temperatures and a Target Temperature = 120°F.
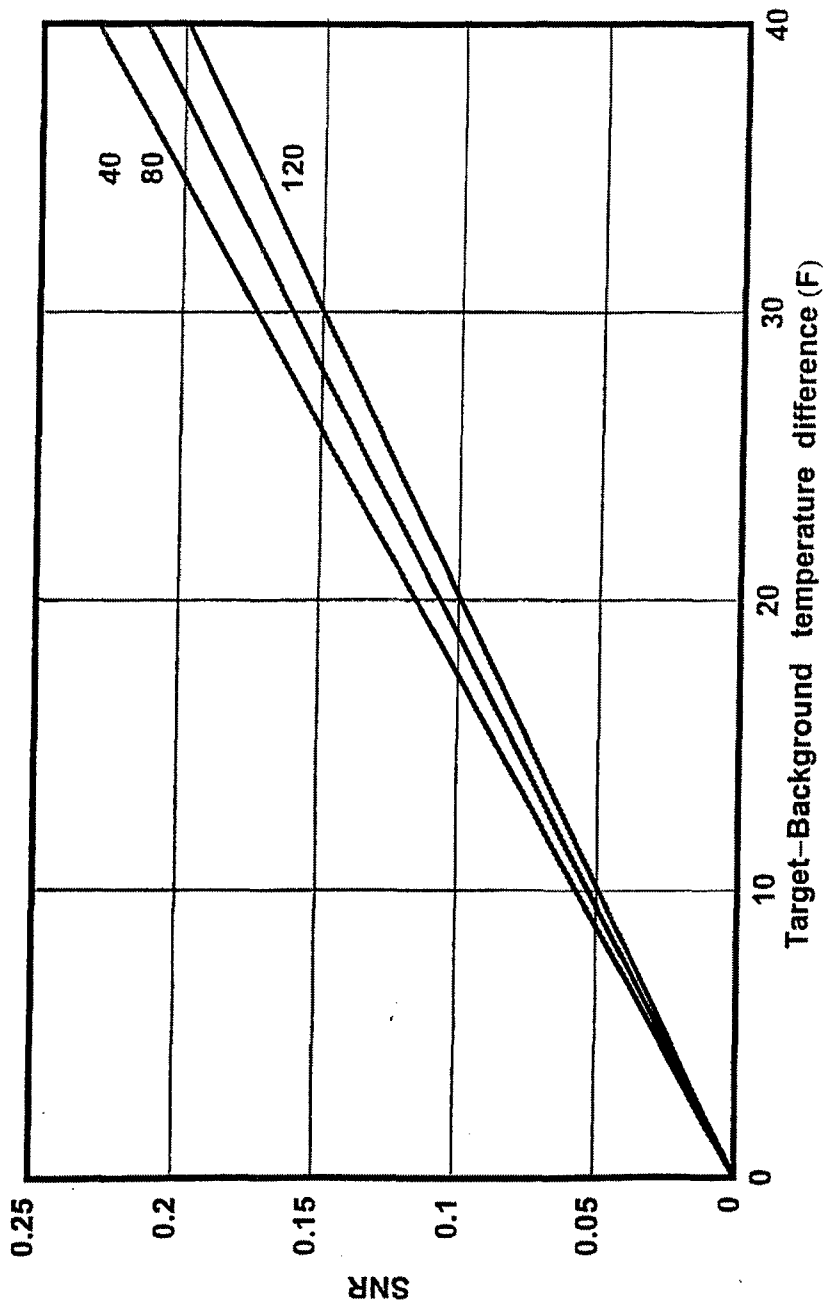
Figure 20. Variation in the Signal-to-Noise Ratio vs. the Target-Background Temperature Difference for Three Target Temperatures with No Atmosphere.

45
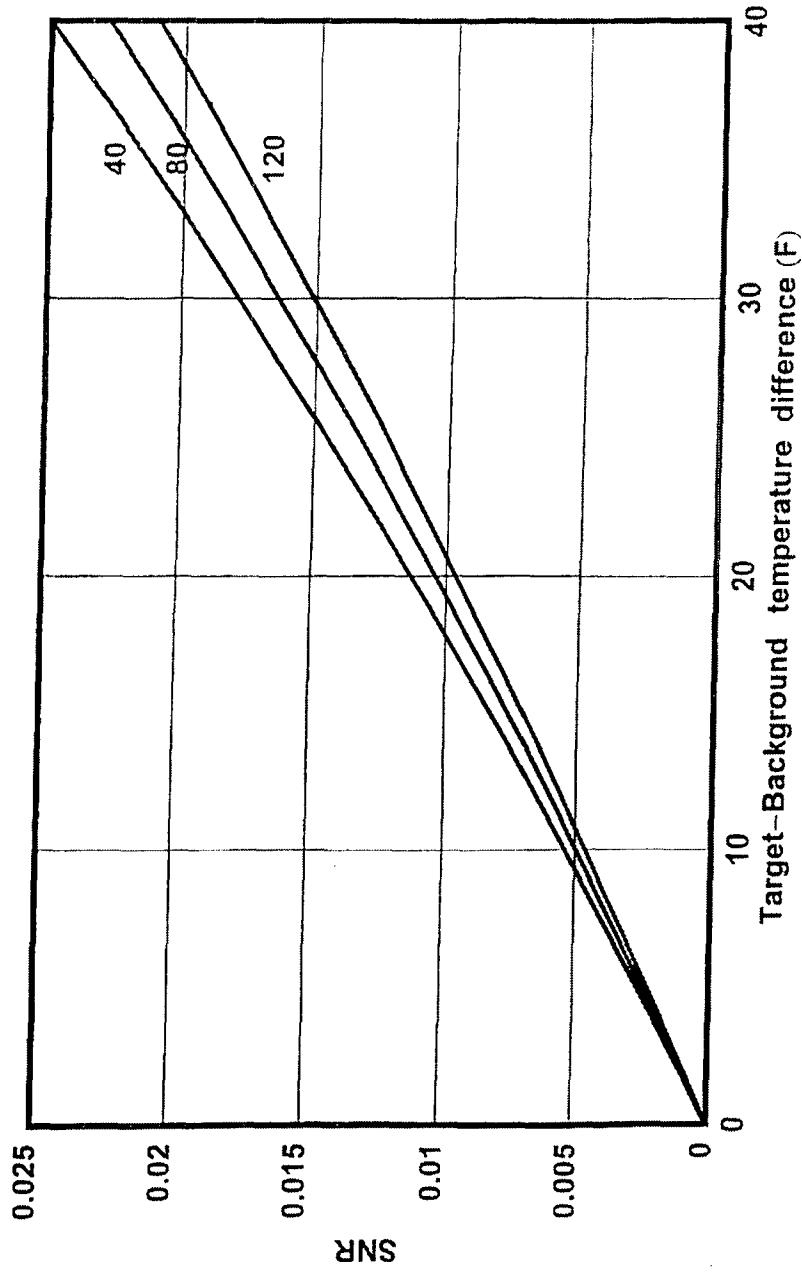
Figure 21. Variation in the Signal-to-Noise Ratio vs. the Target-Background Temperature Difference for Three Target Temperatures with a Cloud with a Beam Transmittance = 0.1.

46

As in the case of the contrast transmittance we can now examine the signal-to-noise transmittance with and without the flare sources. After considerable algebraic manipulation we get the following expression for the general signal-to-noise transmittance SN_T for a cloud with flares and the signal-to-noise transmittance SN_{T0} without the flares. It is given by the following:

$$SN_T = \frac{SN_{T0}}{\sqrt{\left(\dfrac{a\sigma^2}{2} - 1\right)f(f+1)SN_{T0}^2 + (f+1)^2 - \dfrac{\sigma f(f+1)SN_{T0}}{2}\sqrt{a[(a\sigma^2 - 4)SN_{T0}^2 + 4]}}} \tag{83}$$

where f has the same meaning as in the case of the contrast transmittance. The quantities a and σ are given by

$$a = \frac{2}{L_{t0}^2 + L_{bo}^2} \tag{84}$$

$$\sigma = L_{t0} + L_{b0} \tag{85}$$

Now we can look at the signal-to-noise transmittance for a cloud with flare sources versus the corresponding signal-to-noise transmittance for the same cloud with no flares sources present. Figure 22 illustrates this for five values of the flare path radiance to thermal path radiance ratio. We can see that even for a rather small ratio the signal-to-noise transmittance for a "flare" cloud is less than the signal-to-noise transmittance for a purely "thermal" cloud. Therefore, the flare sources in a cloud do indeed reduce the signal-to-noise transmittance.

6.   VARIATION OF FLARE PARAMETERS

In this section we examine the variation in the parameters that are used in the complete description of the model. It is important to look at how the various system parameters vary with each other over an extended range in magnitude. To accomplish this we make extensive use of the equations in section 2.
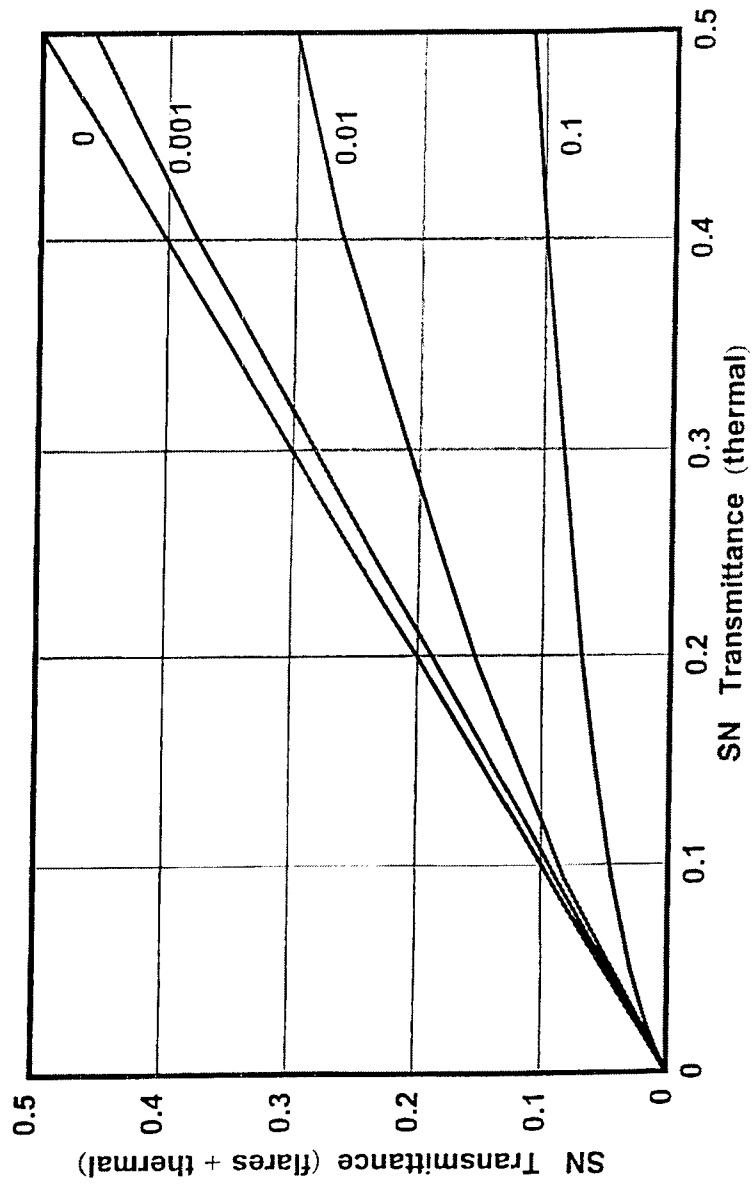
Figure 22. Variation in the Signal-to-Noise Transmittance for a "Flare" Cloud vs. the Signal-to-Noise Transmittance in a "Thermal" Cloud. Target Temperature = 100°F, Background Temperature = 90°F.

6.1   Flare Radius.

Figure 23 depicts the variation of the radius of a flare as a function of the total number of flares in the medium for three flare concentrations. One should note that the total number of flares varies from only 1000 to 1 million. The corresponding change in the flare radius is a factor of 10. Likewise, we can look at the variation in the flare radius as a function of the flare concentration for several numbers of flares in the medium as illustrated in figure 24. One can see that the flare radius varies in a nonlinear manner as the flare concentration goes from 10^{-9} to 10^{-7}. The greatest variation, however, is for a small number of flares.

6.2   Flare Temperature.

Now we analyze the physics of the flares by looking at the variation in the flare temperature as a function of the number of flares in one dimension for three concentrations. This is indicated in figure 25. One can see that for a fixed concentration the temperature decreases as the number of flares increases. The time for the flare to drop in this case is 10 seconds. Likewise, the flare temperature decreases with an increase in the number of flares for a specific flare heat content. This is depicted in figure 26 for four values of the heat content for concentration of 10^{-8}. Now we can examine the variation in the flare temperature as a function of the number of flares in the medium for several drop times as is indicated in figure 27. It should be noted that for a small drop time of only 1 second there is a more rapid temperature decrease than for the case when the drop time is large. It is of some interest to look at the increase in the flare temperature as a function of the concentration for several values of the total number of flares in the medium. This is illustrated in figure 28. Here the total number varies from 1000 to 1,000,000. The variation in the temperature with the flare heat content can be seen in figure 29 for four values of the total number of flares in the medium. Here it is to be noticed that there is a pronounced increase as the heat content increases. In fact the temperature increases by a factor of about 6 for an increase in the heat content from 10^8 to 10^{11} for 1000 flares. Finally, we can illustrate the decrease in temperature as a function of the flare drop time for several values for the total number of flares. This is clearly shown in figure 30.

6.3   Flare Power.

For our analysis of the physical properties of the flares in a cloud we should examine the variation in the total power output of the flares with respect to the parameters that define the physics of the flare. In figure 31 we depict the variation in the total flare power as a function of the number of flares in one dimension of the cubic medium for three values of the flare concentration. It is important to remember that this corresponds to a change in the total number of flares from 1000 to 1 million! It should be noted that there is very little change in power output of the flares. Likewise, we can see the variation in the power as a function of the number of flares in one dimension for several values of the flare heat content. Again, we note that there is very little change as is indicated in figure 32. A similar effect is seen when we illustrate the variation in the power as a function of the number of flares in one dimension for three flare drop times. In figure 33 we see that there is a very small change. The variation of the power with flare concentration, however, shows a very large change as can be seen in figure 34. Here it is to be noted that the flare power changes by a factor of 100 as the concentration also changes by a
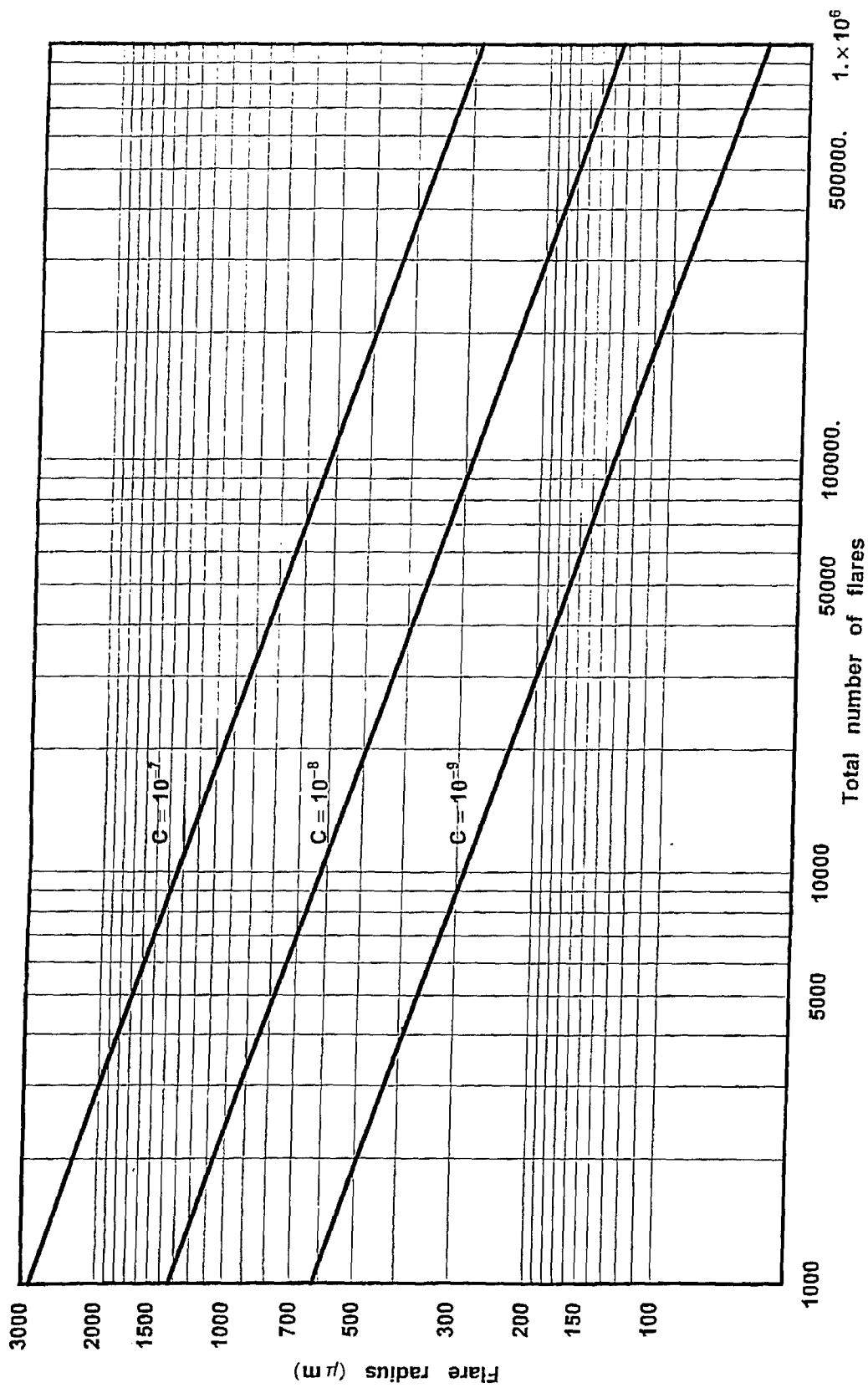
Figure 23. Flare Radius *vs.* the Total Number of Flares for Several Concentrations in a Cube of Length 10 Meters.

50
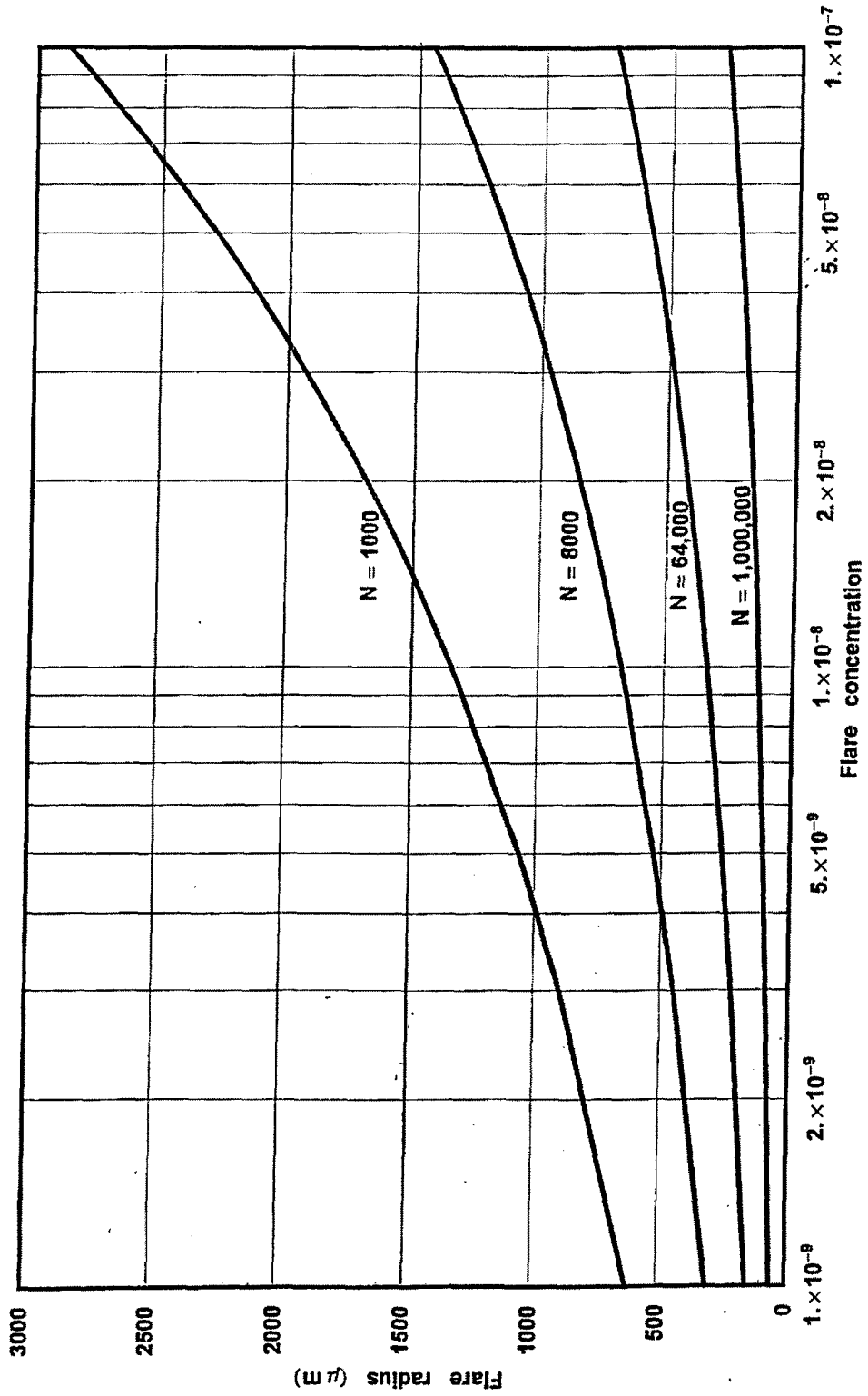
Figure 24. Flare Radius vs. Flare Concentration for N Flares in a Cube of Length 10 Meters.

51
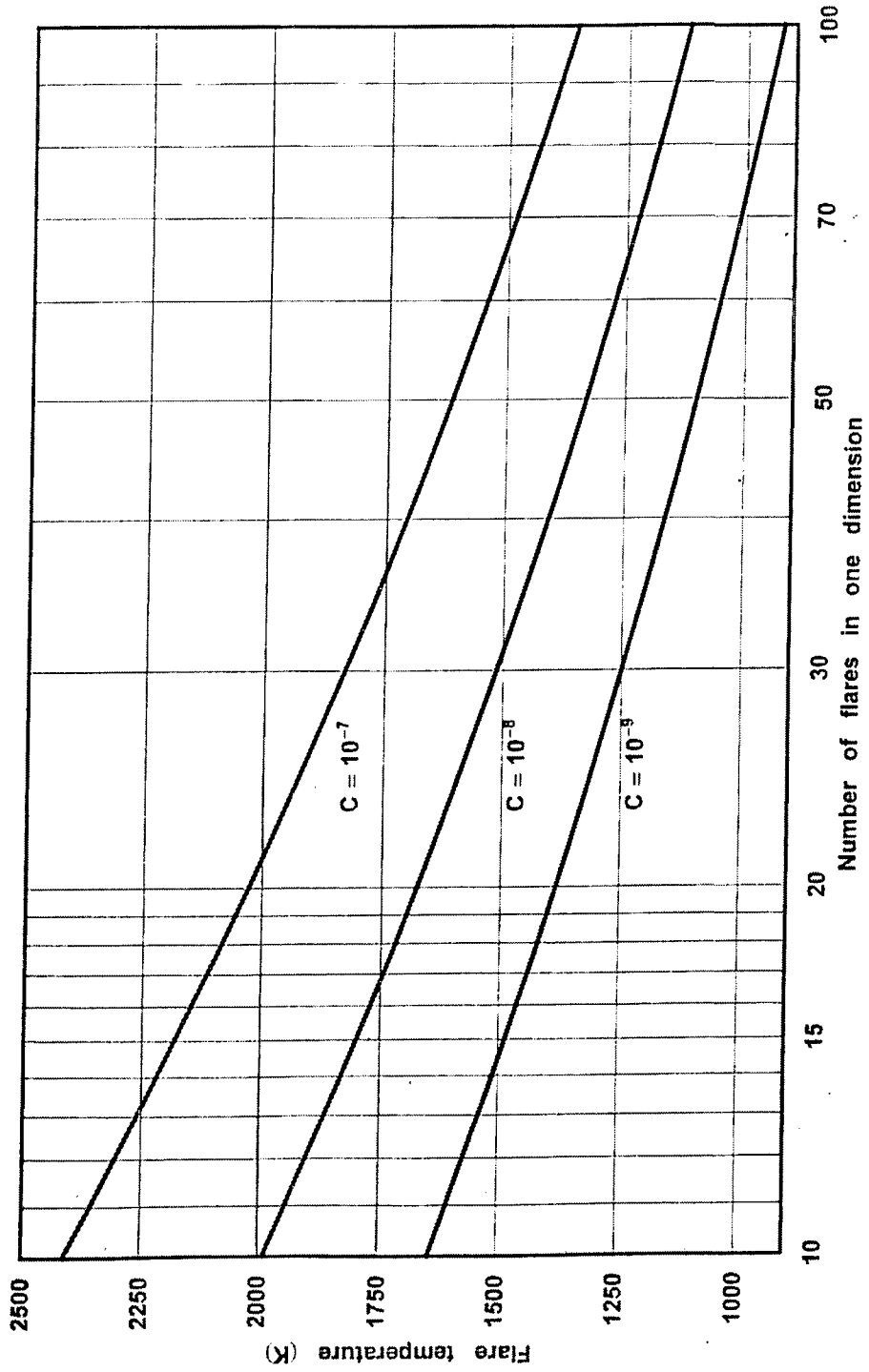
Figure 25. Flare Temperature (K) vs. the Number of Flares in One Dimension for Several Flare Concentrations in a Cube of Length 10 Meters. Ambient Temperature = 300 K, Flare Drop Time = 10 Seconds, Flare Heat Content = 2.0×10^{10} J-m^{-3}.
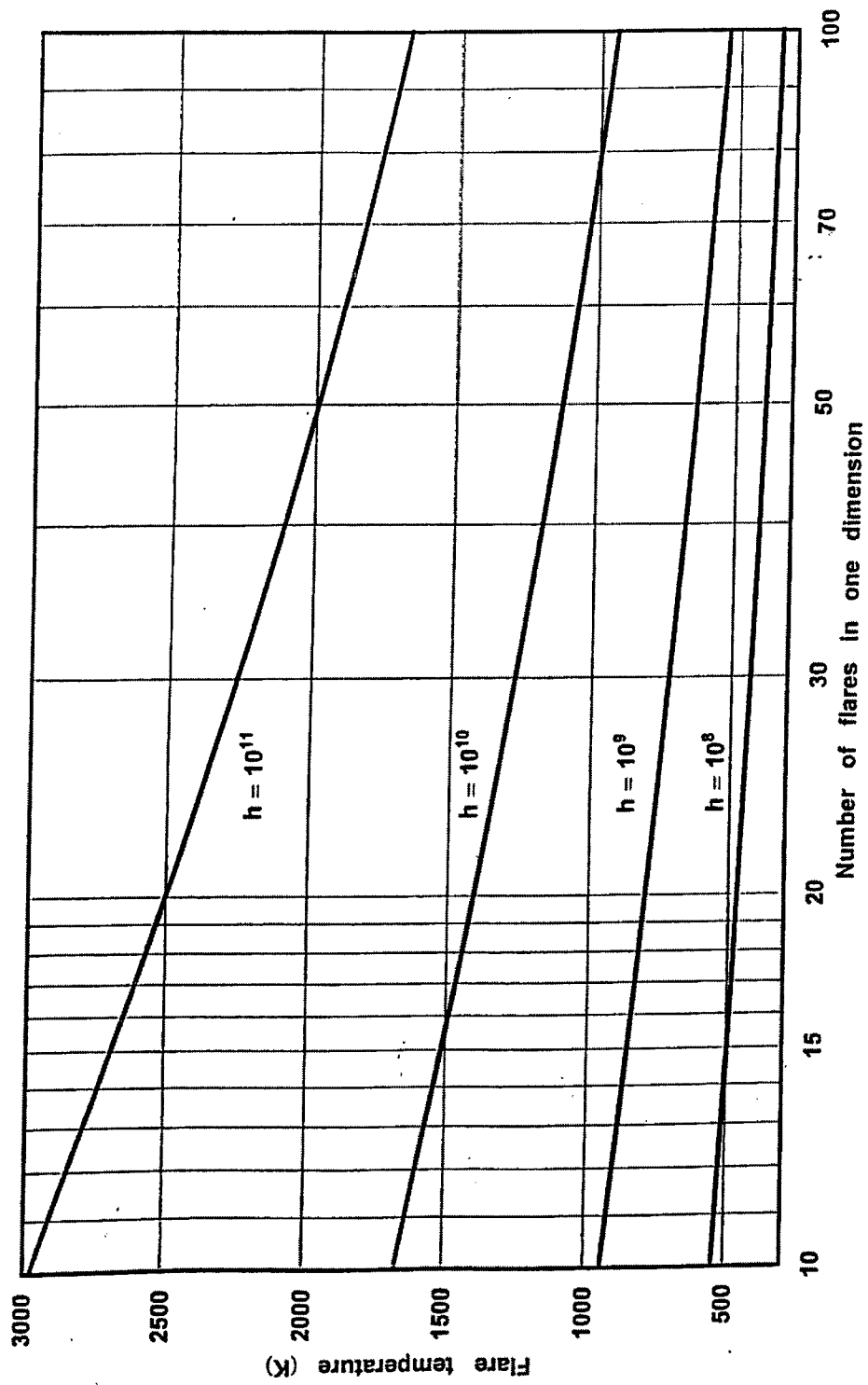
Figure 26. Flare Temperature (K) vs. the Number of Flares in One Dimension for Several Flare Heat Content Values (J-m^{-3}) in a Cube of Length 10 Meters. Ambient Temperature = 300 K, Flare Drop Time = 10 Seconds, Flare Concentration = 10^{-8}.

53
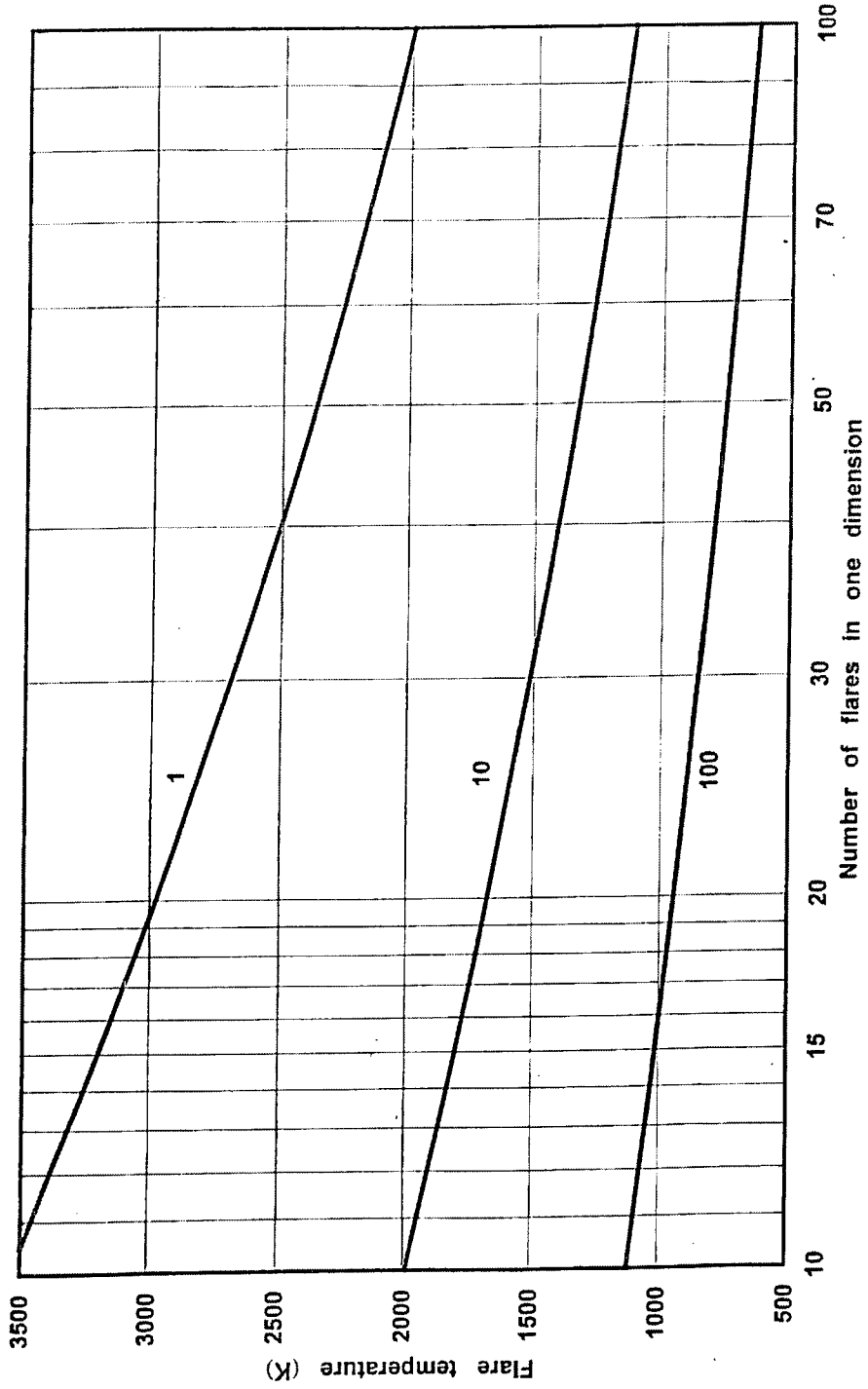
Figure 27. Flare Temperature (K) vs. the Number of Flares in One Dimension for Several Flare Drop Times (Seconds) in a Cube of Length 10 Meters. Ambient Temperature = 300 K, Flare Heat Content = 2.0×10^{11} J-m^{-3}, Flare Concentration = 10^{-8}.
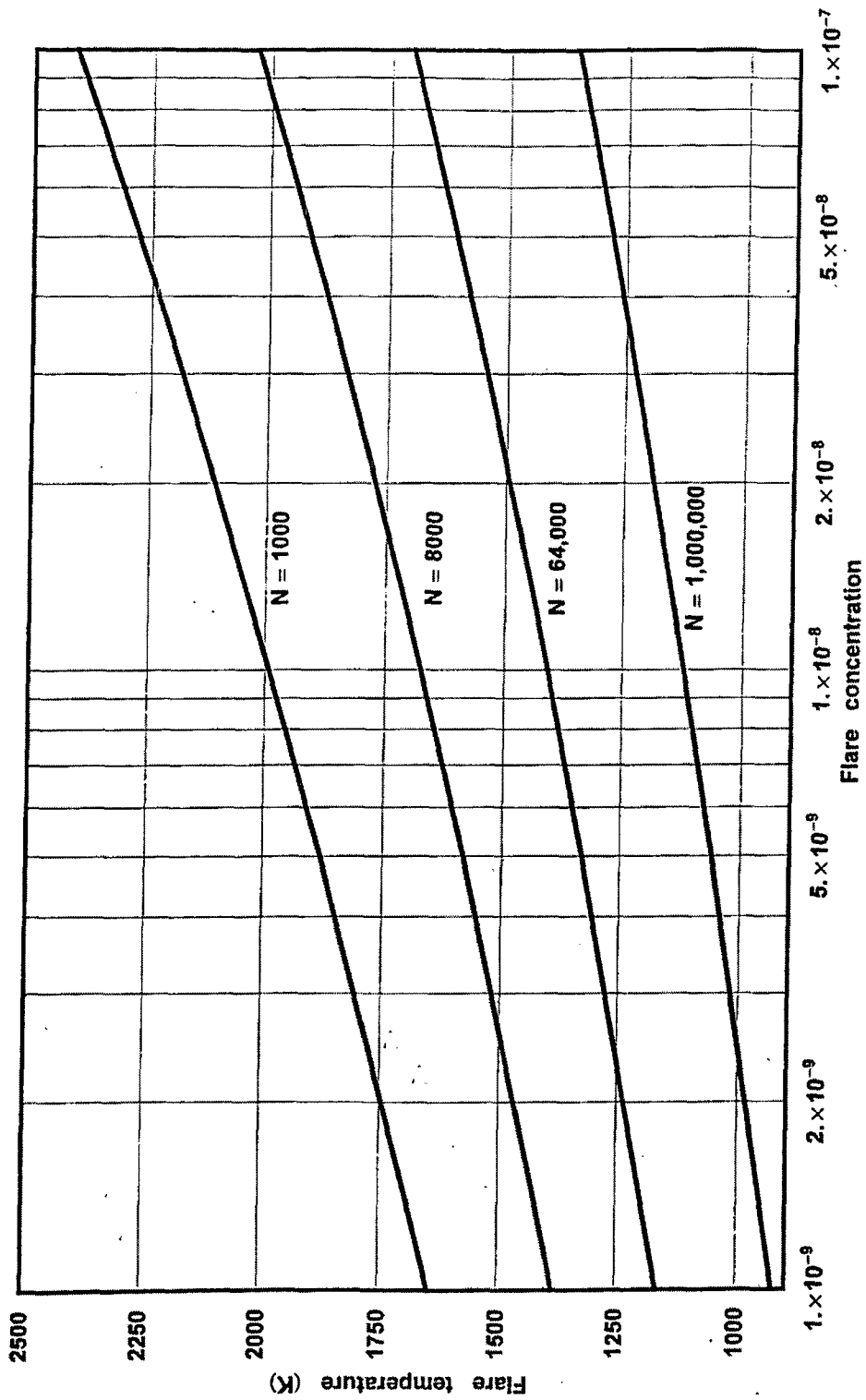
Figure 28. Flare Temperature (K) vs. the Flare Concentration for N Flares in a Cube of Length 10 Meters. Ambient Temperature = 300 K, Flare Drop Time = 10 Seconds, Flare Heat Content = 2.0×10^{11} J-m^{-3}.
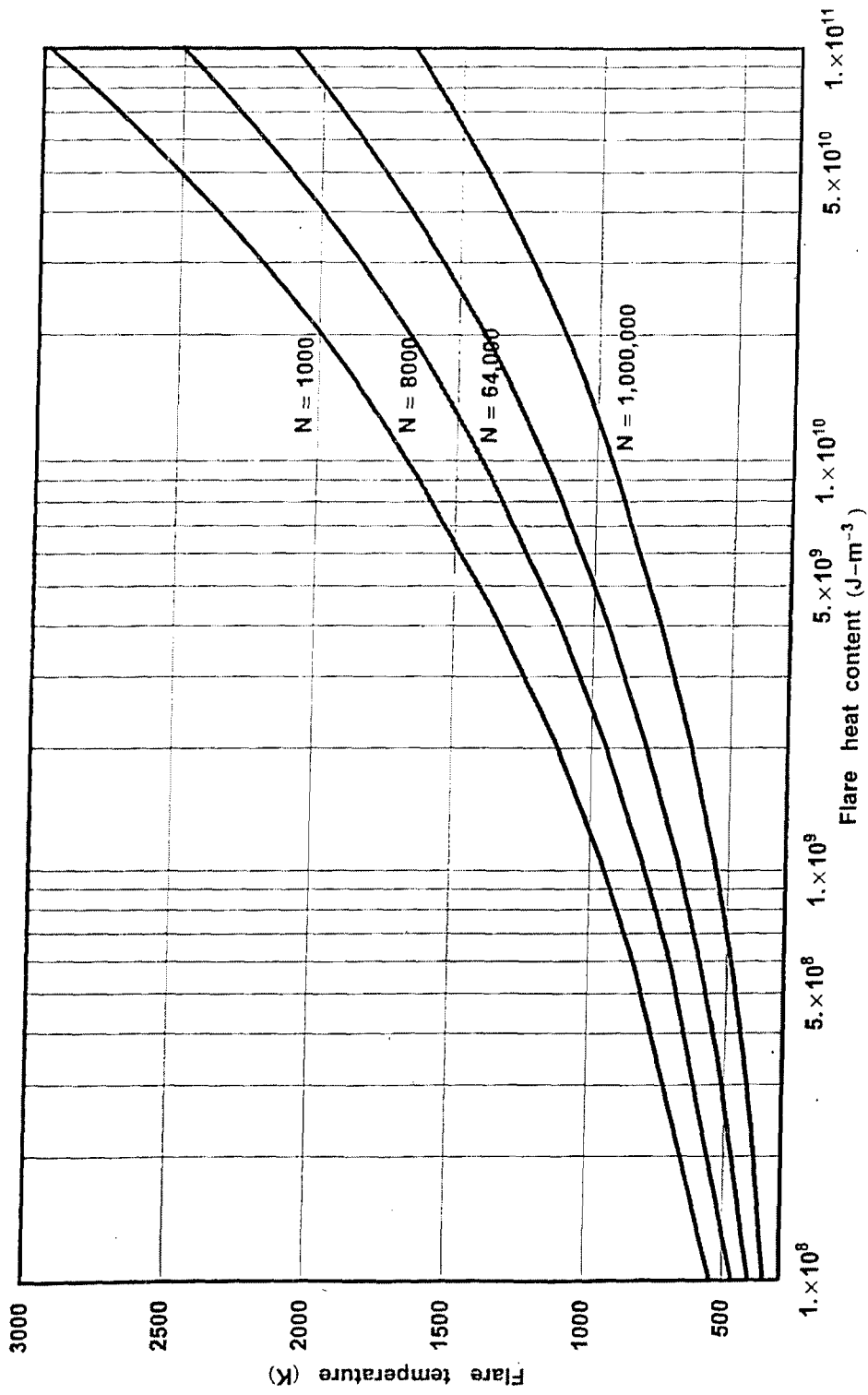
Figure 29. Flare Temperature (K) vs. the Flare Heat Content for N Flares in a Cube of Length 10 Meters. Ambient Temperature = 300 K, Flare Drop Time = 10 Seconds, Flare Concentration = 10^{-8}.
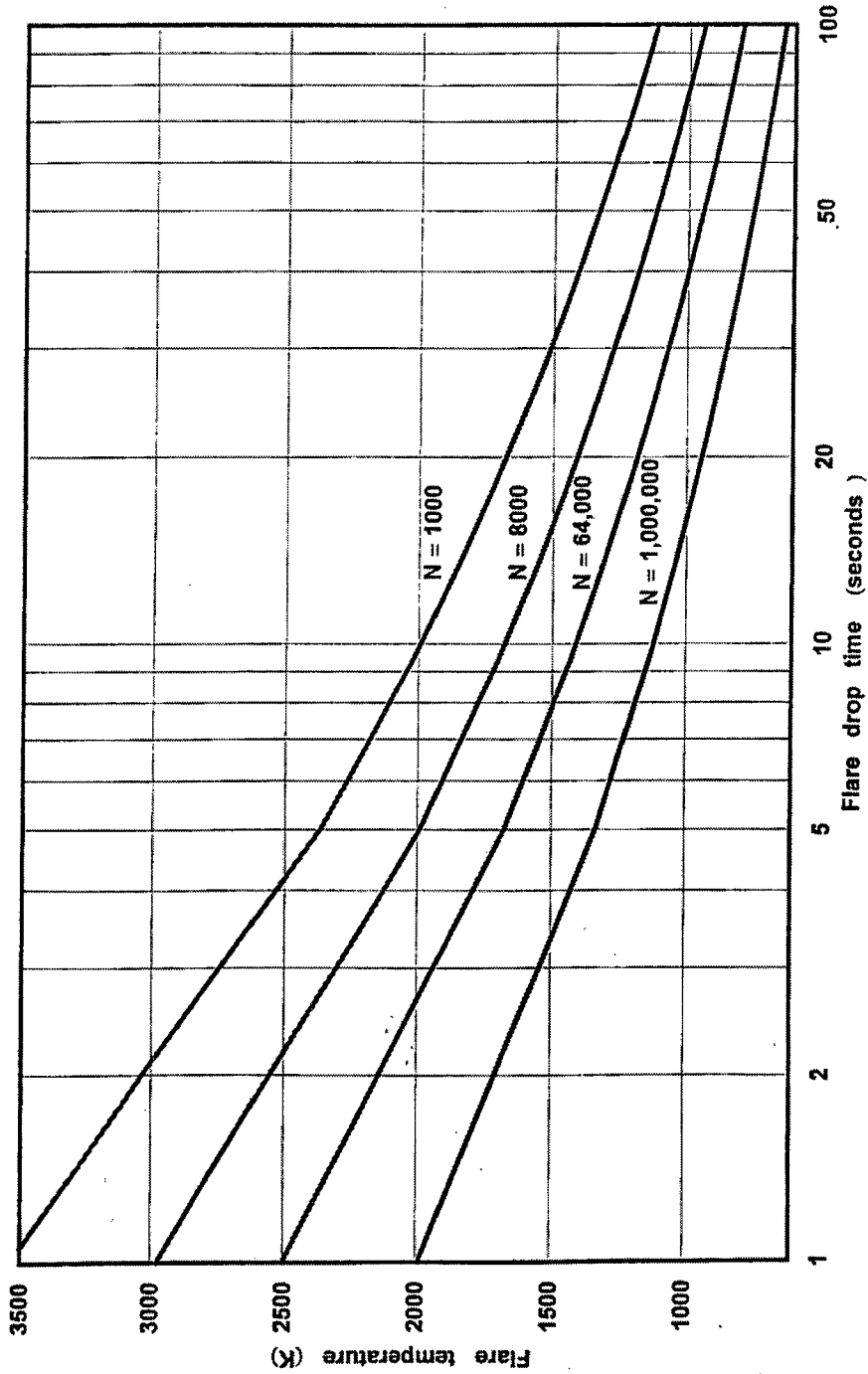
Figure 30. Flare Temperature (K) vs. the Flare Drop Time for N Flares in a Cube of Length 10 Meters. Ambient Temperature = 300 K, Flare Heat Content = 2.0×10^{10} J-m^{-3}, Flare Concentration = 10^{-8}.

e 31. Total Power of All Flares *vs.* the Number of Flares in One Dimension for Several Flare Concentration Values in a
of Length 10 Meters. Ambient Temperature = 300 K, Flare Drop Time = 10 Seconds, Flare Heat Content = 2.0×10^{10} J-m^{-3}.

Best Available Copy

58
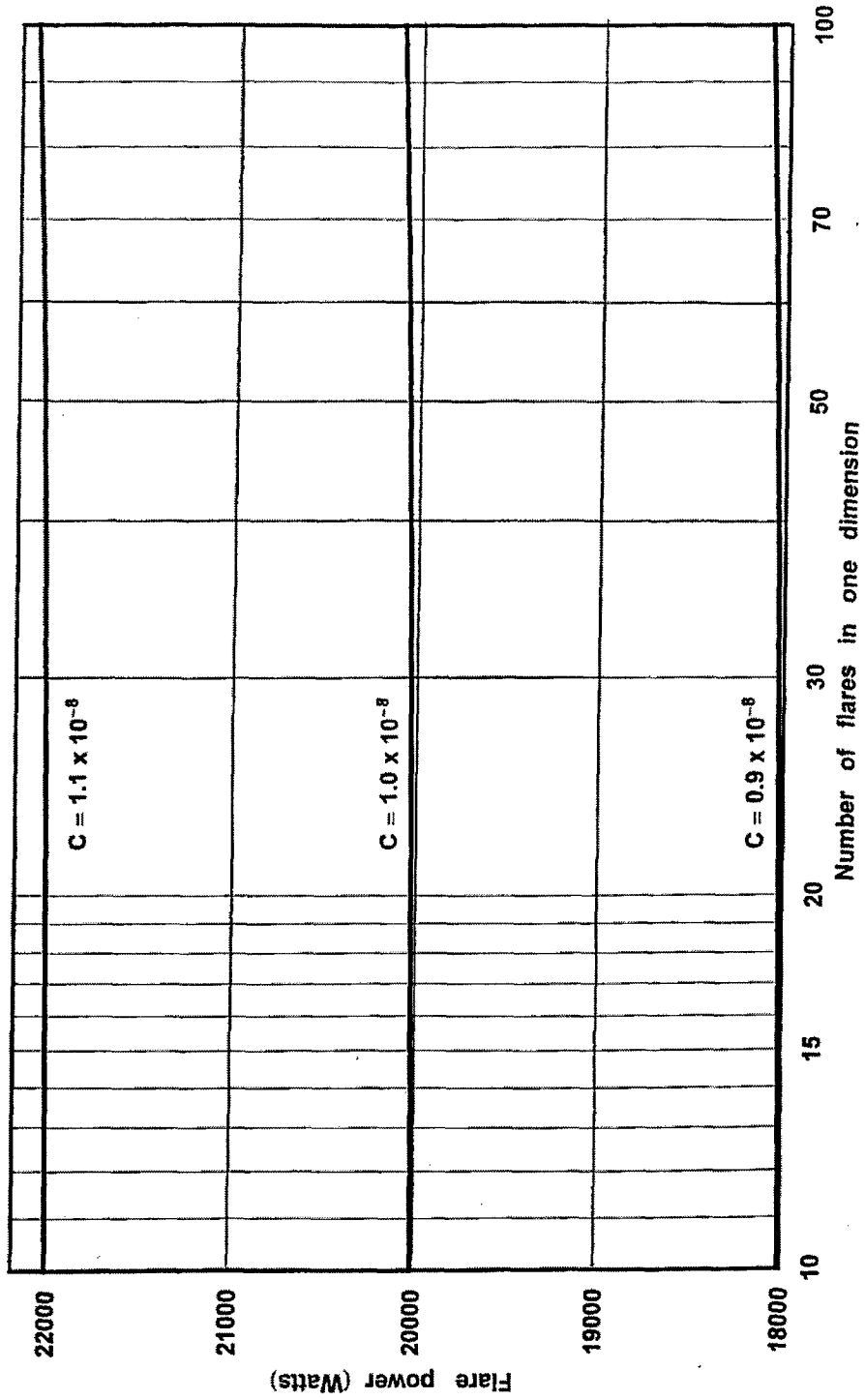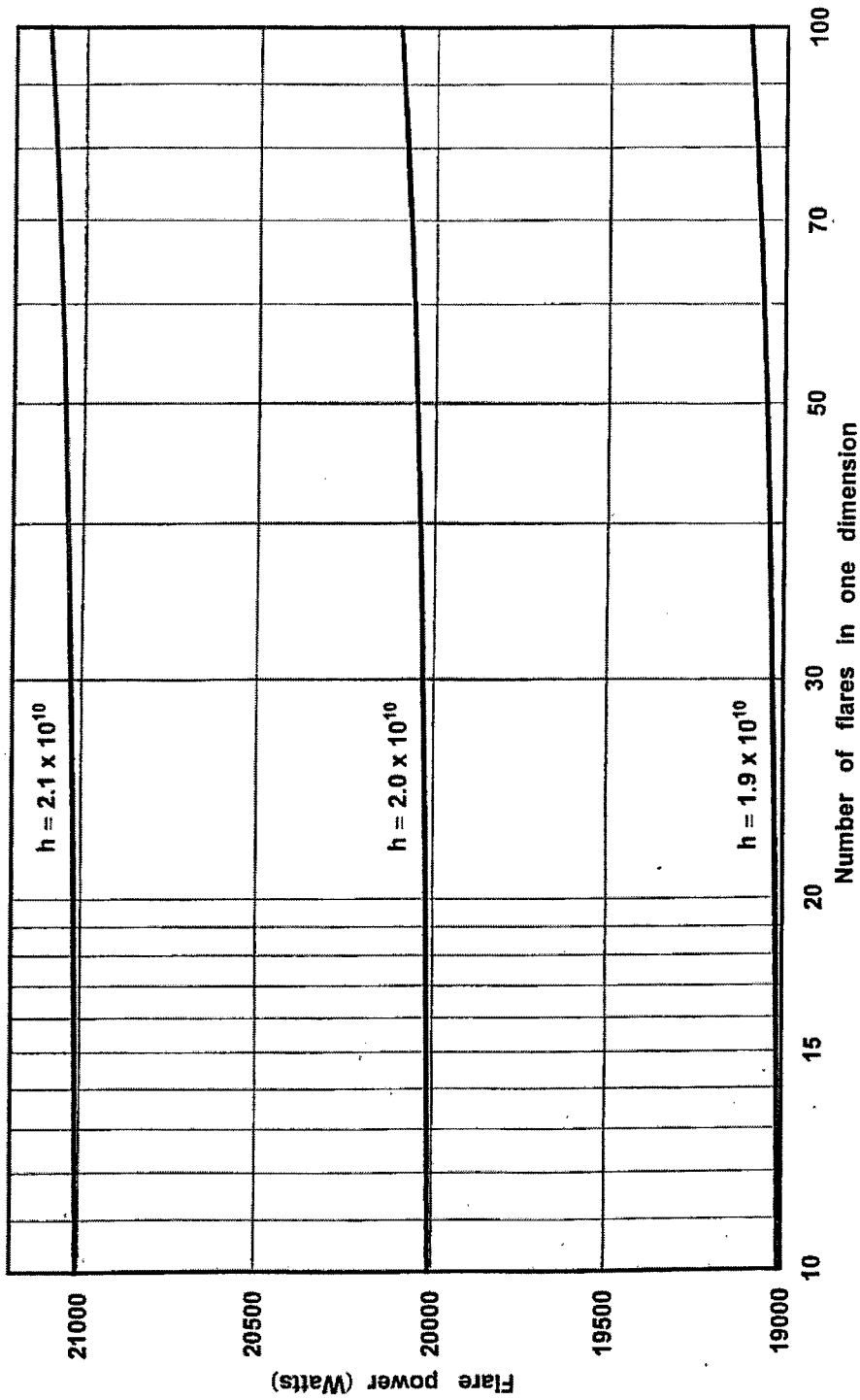
Figure 32. Total Power of All Flares vs. the Number of Flares in One Dimension for Several Flare Heat Content Values $(J\text{-}m^{-3})$ in a Cube of Length 10 Meters. Ambient Temperature = 300 K, Flare Drop Time = 10 Seconds, Flare Concentration = 10^{-8}.
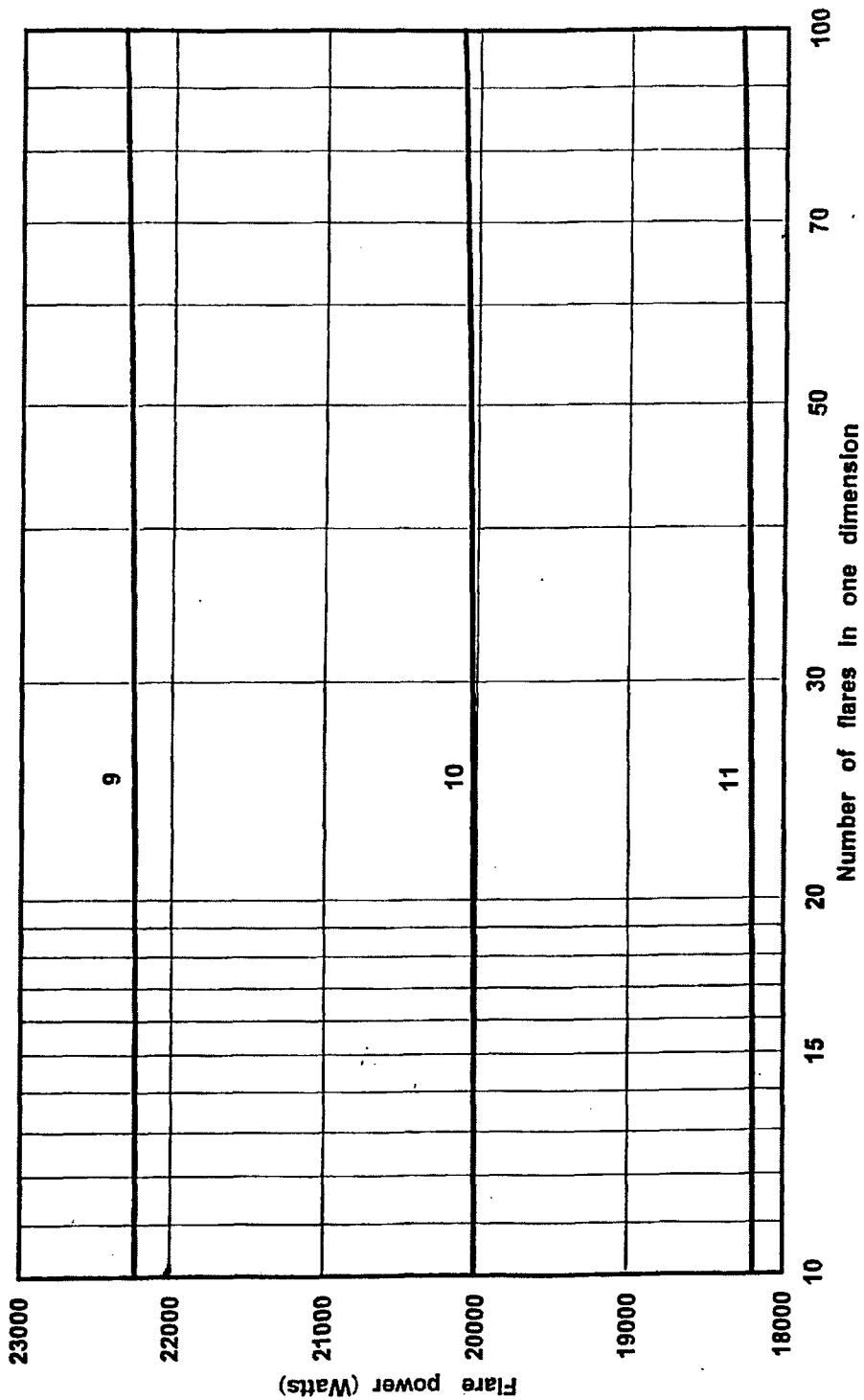
Figure 33. Total Power of All Flares vs. the Number of Flares in One Dimension for Several Flare Drop Time Values (Seconds) in a Cube of Length 10 Meters. Ambient Temperature = 300 K, Flare Heat Content = 2.0×10^{10} J-m^{-3}, Flare Concentration = 10^{-8}.
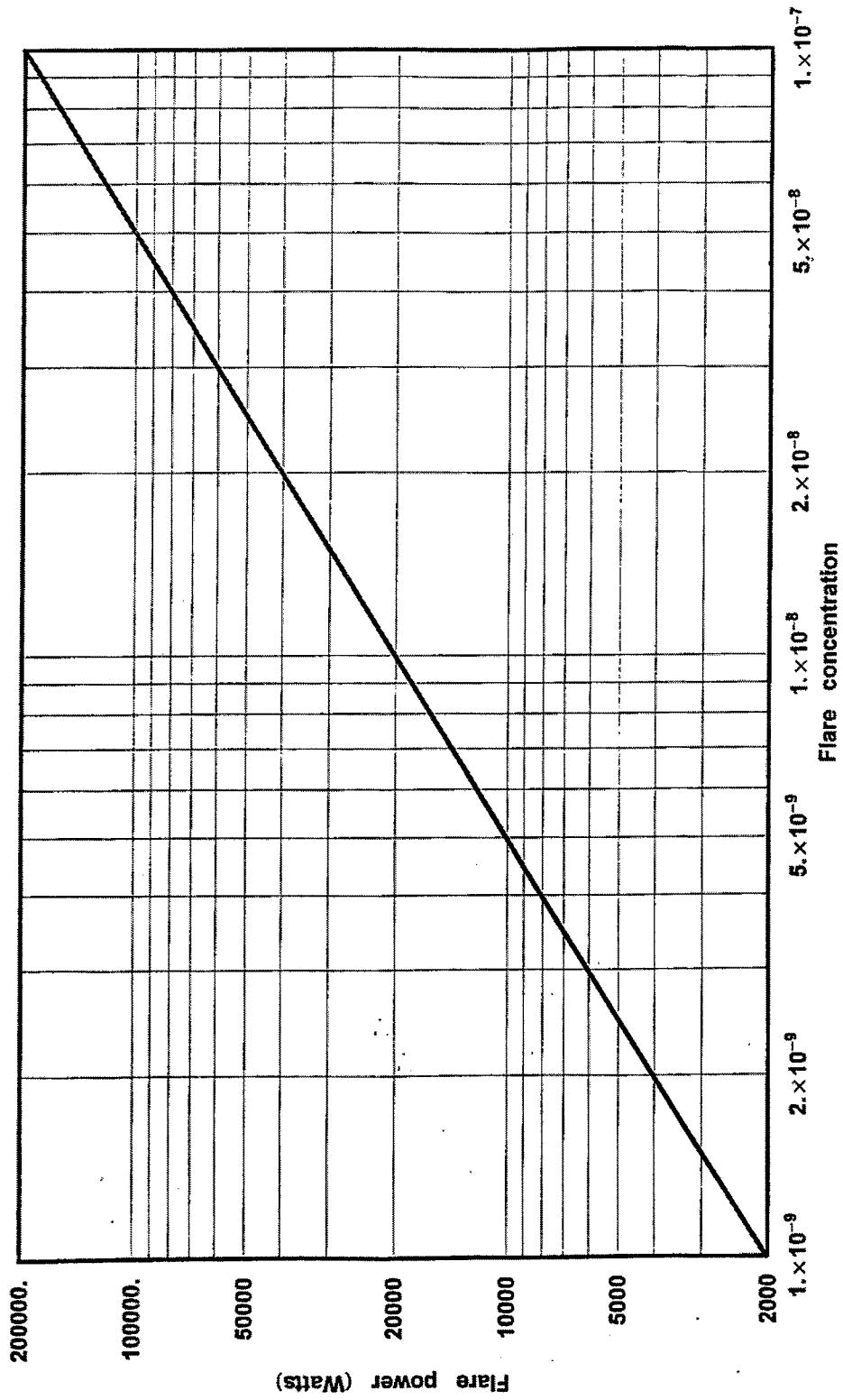
Figure 34. Total Power of All Flares vs. the Flare Concentration for N Flares in a Cube of Length 10 Meters. Ambient Temperature = 300 K, Flare Drop Time = 10 Seconds, Flare Heat Content = 2.0×10^{10} J-m^{-3}.

factor of 100. This is nearly true regardless of the total number of flares in the medium! There is indeed some dependence on the total number of flares, however, as can be seen in figure 35 where we allow a small change in the concentration. There is a very large change in the flare power as a function of the heat content as shown in figure 36 for four values of the total number of flares. It should be noted that for large values of the heat content there is a very small dependence on the total number of flares in the medium. Now we can examine the variation in the power output as a function of the drop time. This is illustrated in figure 37 for a range in the drop time from 1 to 100 seconds. The power decreases by a factor of 100! It is also almost independent of the total number of flares but not quite as can be seen in figure 38 for a more limited range in the flare drop time. Because of the large number of flares that can be used in a cloud it is important to investigate the variation in the flare power density, that is, in the power output per flare. In figure 39 we plot the variation in the power density as a function of the total number of flares in the cloud for three values of the flare heat content. It is to be noted that as the number of flares goes from 1000 to 1 million the flare power density drops by a factor of 1000. A similar decrease in the power density can be seen as a function of the number of flares for three values of the flare concentration as is indicated in figure 40. Finally, we examine the change in the flare power density as a function of the total number of flares for three values of the flare drop time. This is illustrated in figure 41 for drop time from 1 to 100 seconds.

7.   CLOUD RADIATION MODEL

In this section we describe in some detail the geometry and the physics of the cubic radiation model for a smoke cloud.

7.1   Geometry.

For simplicity we chose a geometry for the smoke cloud that is easy to understand and that is also easy to implement in practice. Let the cloud be of cubic shape with a lattice arrangement of the flares inside so that no flare is ever on a side or on an edge of the cloud. The user can select any number of flares in one dimension of the cloud. The lattice arrangement of the flares for one quadrant of the cube is illustrated in figure 4 where L is the length of a side of the cube. The origin of the coordinate system is at 0 and the line of sight (LOS) through the cloud is always along the vertical z axis with the "observer" looking in the positive Z direction. The total number of flares in the cloud is then automatically computed as the cube of the number in one dimension. Thus, if the user enters a number of 1000 for the number of flares in one dimension the total number in the cloud is 1 billion. The scattering of a photon from one of the isotropic flares to the LOS can easily be calculated using equation (30). For higher order scatterings the problem is more complicated. Figure 2 illustrates this for a second order scattering process. The radiation emanating form a flare at point S is attenuated to point P in the cloud. From this point there are many possible interactions with the LOS along the z axis. This process must be accounted for by using some method of tracking the photons and then using the single-scattering integral of equation (30).
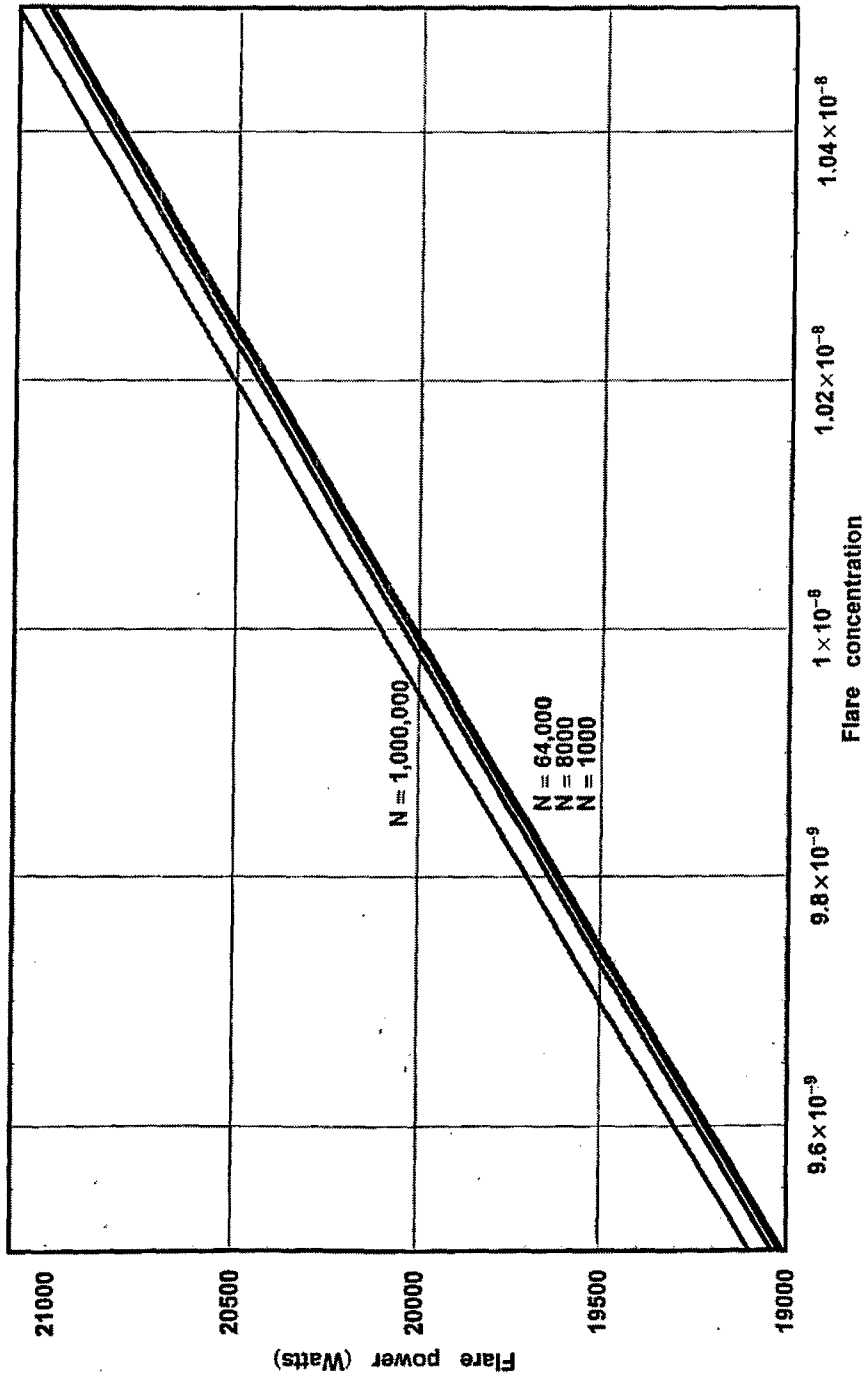
Figure 35. Total Power of All Flares vs. the Flare Concentration in a Cube of Length 10 Meters. Ambient Temperature = 300 K, Flare Drop Time = 10 Seconds, Flare Heat Content = 2.0×10^{10} J-m^{-3}.
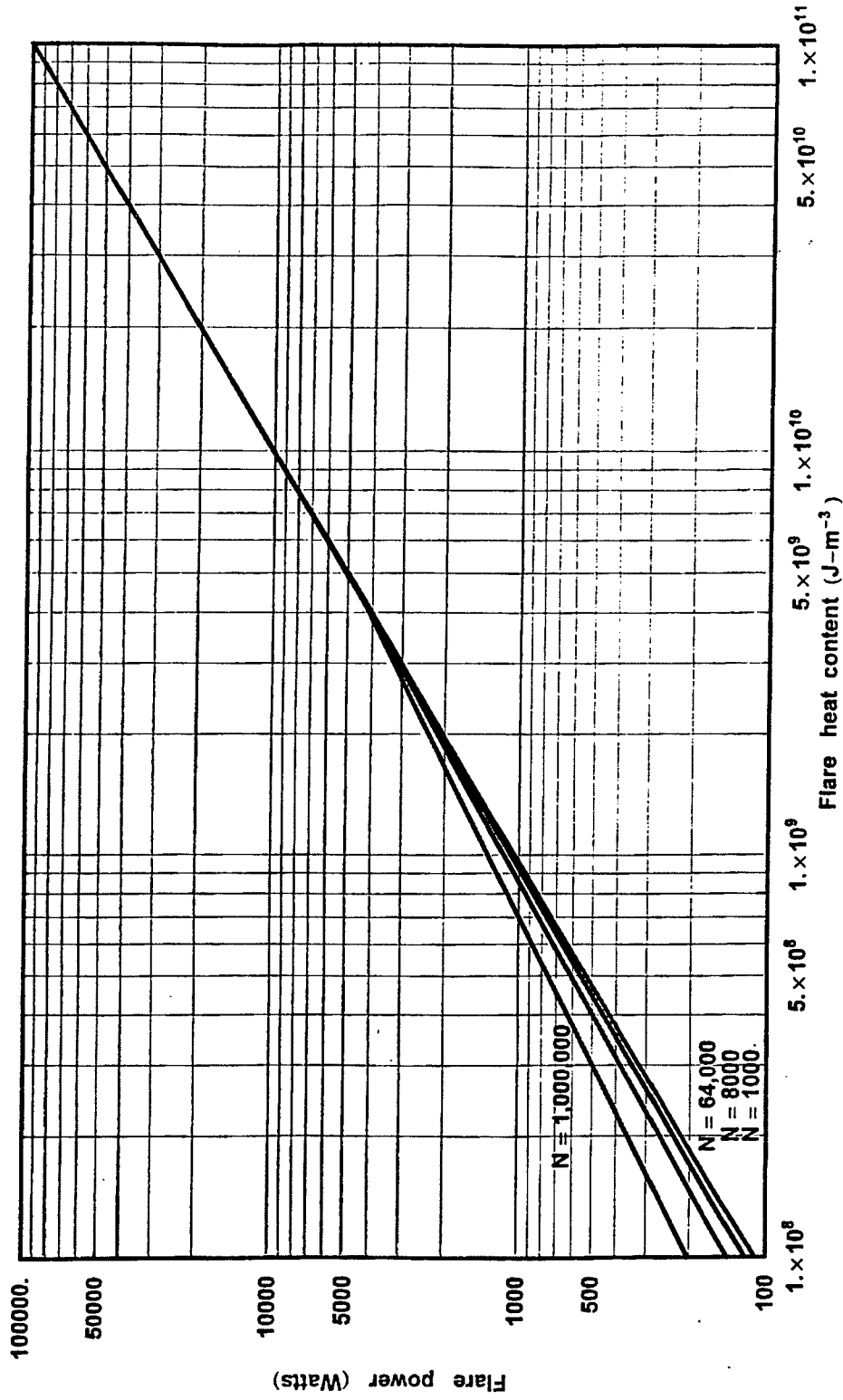
Figure 36. Total Power of All Flares vs. the Flare Heat Content for N Flares in a Cube of Length 10 Meters. Ambient Temperature = 300 K, Flare Drop Time = 10 Seconds, Flare Concentration = 10^{-8}.
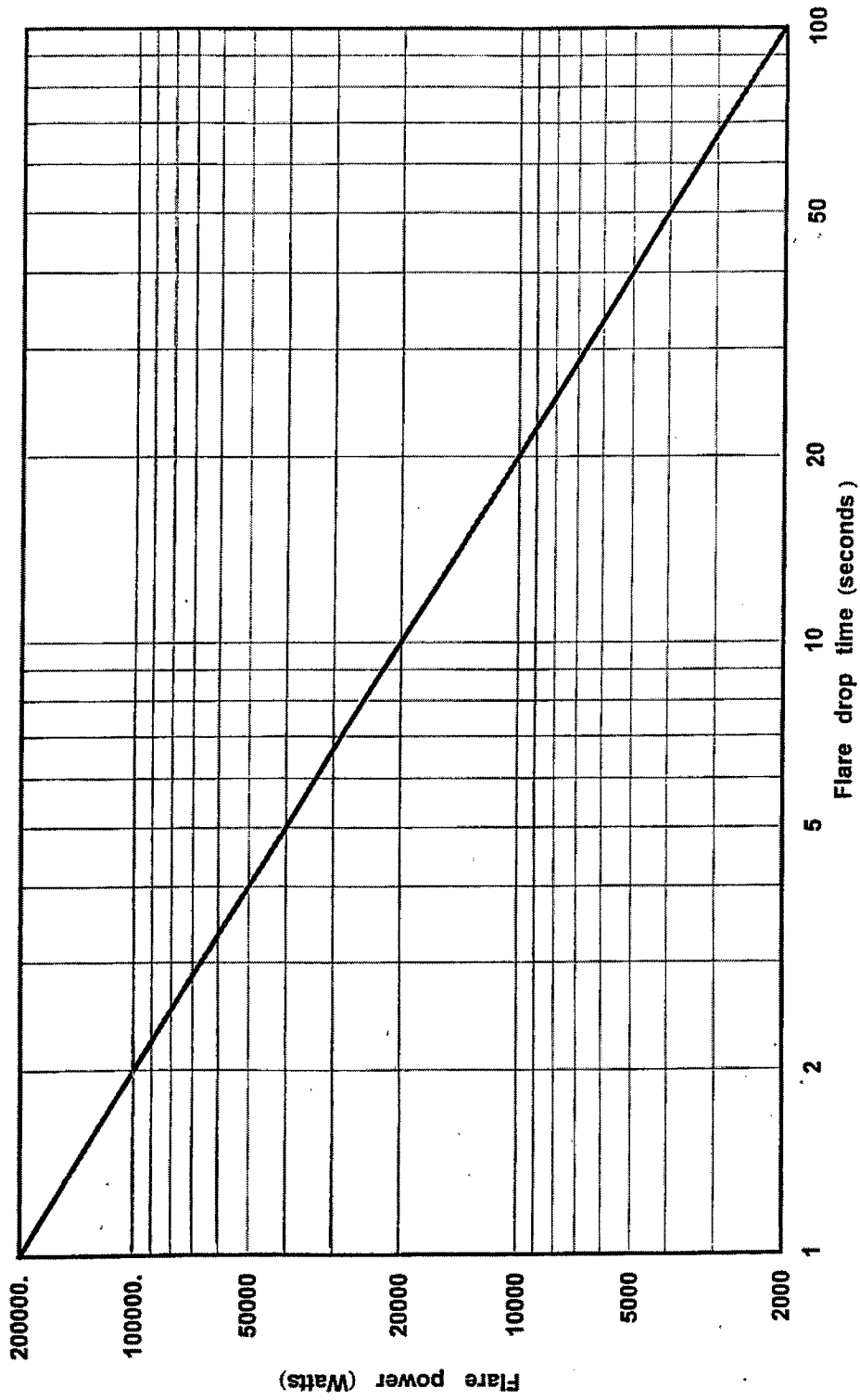
Figure 37. Total Power of All Flares vs. the Flare Drop Time for N Flares in a Cube of Length 10 Meters. Ambient Temperature = 300 K, Flare Concentration = 10^{-8}, Flare Heat Content = 2.0×10^{10} J-m^{-3}.

65
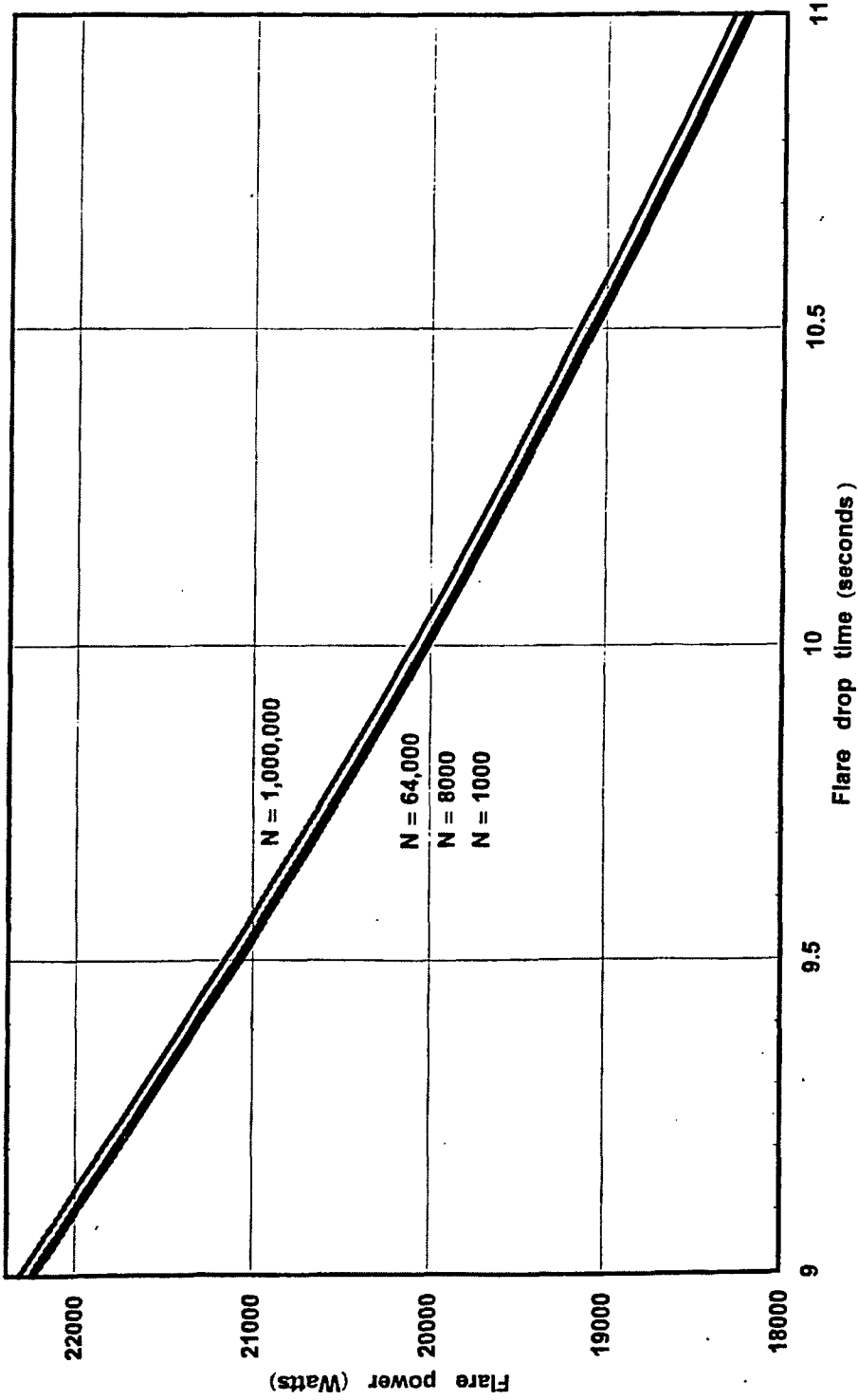
Figure 38. Total Power of All Flares vs. the Flare Drop Time for N Flares in a Cube of Length 10 Meters. Ambient Temperature = 300 K, Flare Concentration = 10^{-8}, Flare Heat Content = 2.0×10^{10} J-m^{-3}.
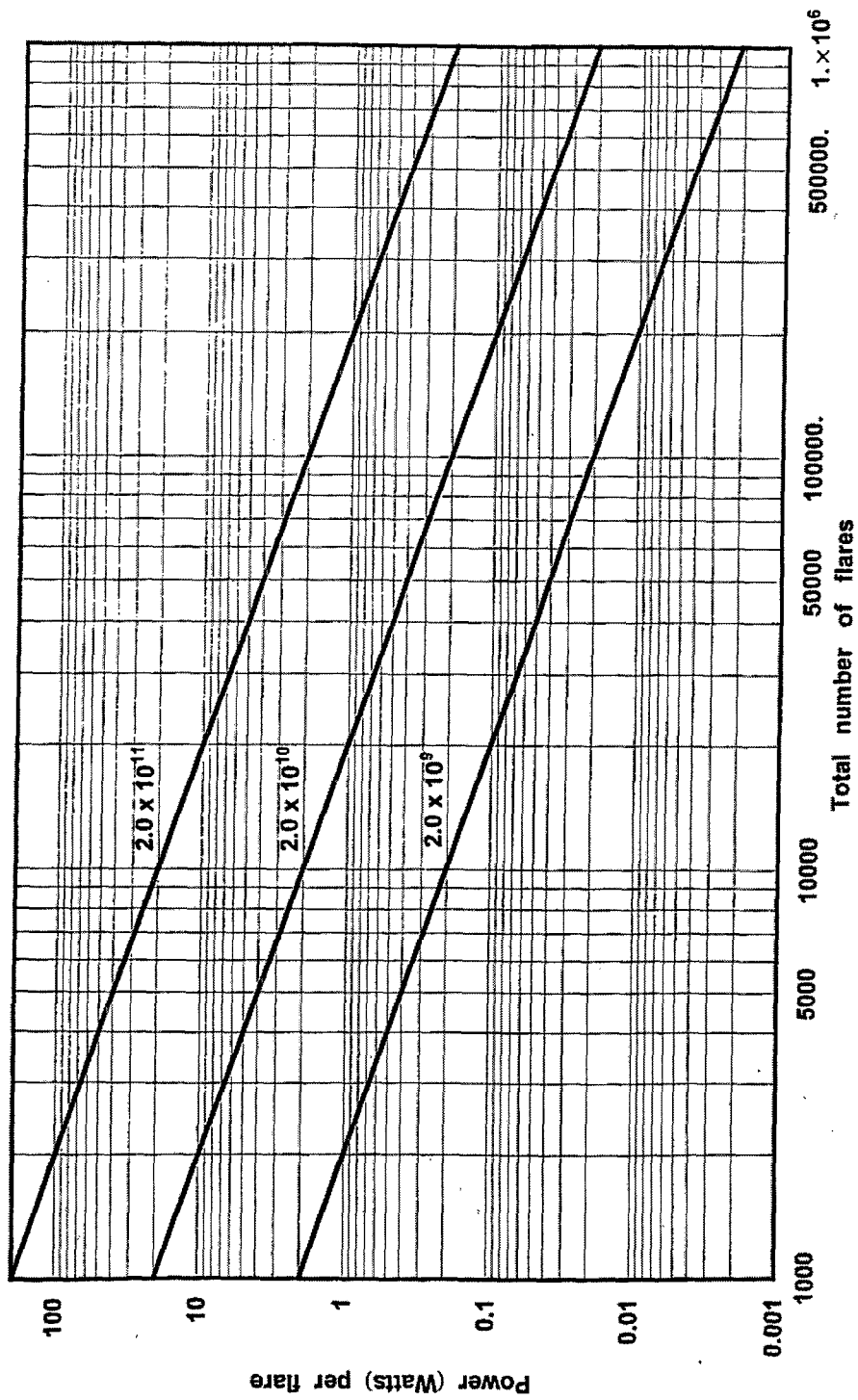
Figure 39. Power Density vs. the Total Number of Flares for Several Flare Heat Content Values ($J \cdot m^{-3}$) in a Cube of Length 10 Meters. Ambient Temperature = 300 K, Flare Drop Time = 10 Seconds, Flare Concentration = 10^{-8}.
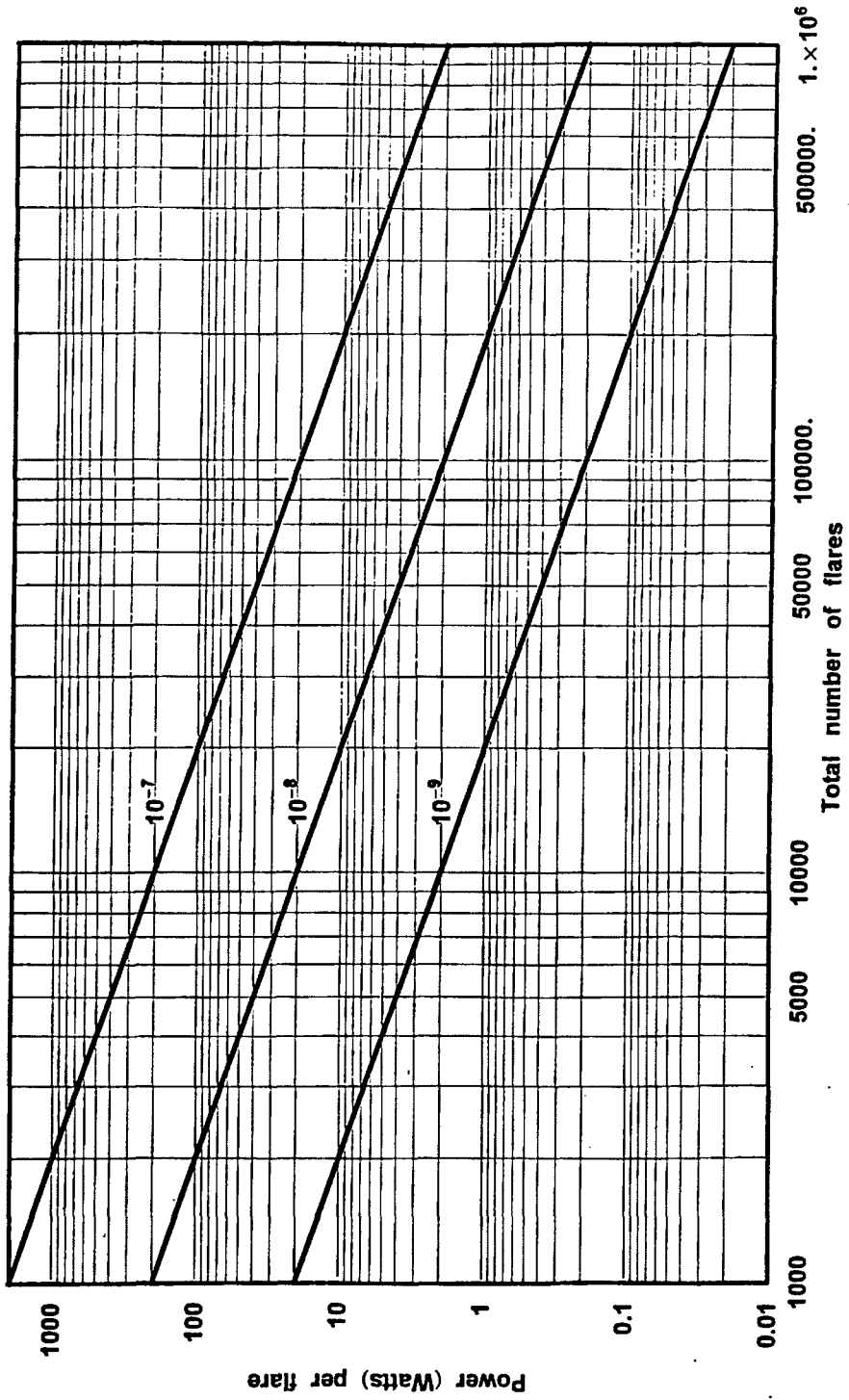
Figure 40. Power Density vs. the Total Number of Flares for Several Flare Concentration Values in a Cube of Length 10 Meters. Ambient Temperature = 300 K, Flare Drop Time = 10 Seconds, Heat Content Value = 2.0×10^{10} J-m^{-3}.
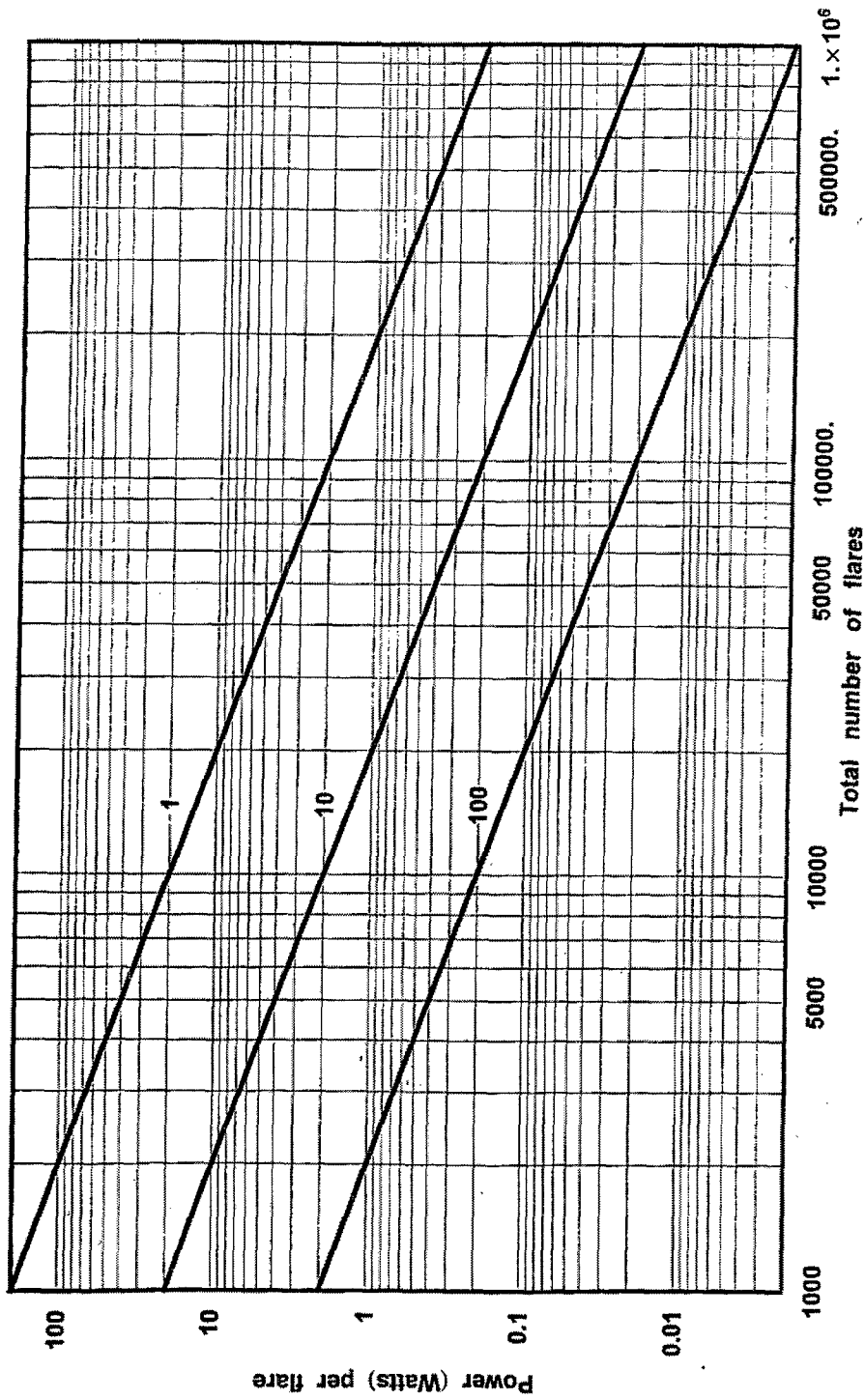
Figure 41. Power Density vs. the Total Number of Flares for Several Flare Drop Times in a Cube of Length 10 Meters. Ambient Temperature = 300 K, Flare Concentration = 2.0×10^{-8}, Flare Heat Content Value = 2.0×10^{10} J-m^{-3}.

7.2   Physics.

A standard method of solving complicated problems involving the multiple scattering of particles in a medium is to use the well-known Monte Carlo technique. A pseudorandom number generator (rng) is used to choose a random number (rnd) from 0 to 1 and this is then mapped into a corresponding number for the physical process that is being analyzed. The physical process for our photon scatterings is described as follows:

1.   Photons are released from an isotropic point source (flare).

2.   The direction cosines of the photons are selected using the rng.

3.   The distance along the path from the source to the boundary of the cloud is determined using the specified coordinates and the rng according to the equation.

4.   The photon weight function is determined as $w = w\,[1-\exp(-\tau_{Max})]$ where τ_{Max} is the maximum optical thickness along the path. This is a Fortran algorithm and not an algebraic equation for the weight factor w.

5.   The optical path is then selected using the rng to select a number rnd as in the following equation:

   Path = -Log(one –rnd(one – exp(-ke dist)))/ke

   Where ke is the volume extinction coefficient of the smoke medium. It should be noted that rnd ranges from zero to one. Thus, as can be seen from the above equation the path ranges from zero to the maximum distance dist.

6.   The maximum and minimum scattering angles are then calculated for the end points along the line of sight.

7.   The scattering integral is evaluated by using Gaussian quadrature.

8.   This entire process is then repeated for a new photon.

The key factor in all of this is the determination of the optical path for the photon. Figure 42 illustrates the variation in the photon's optical path as a function of the random number x where x ranges from 0 to 1.
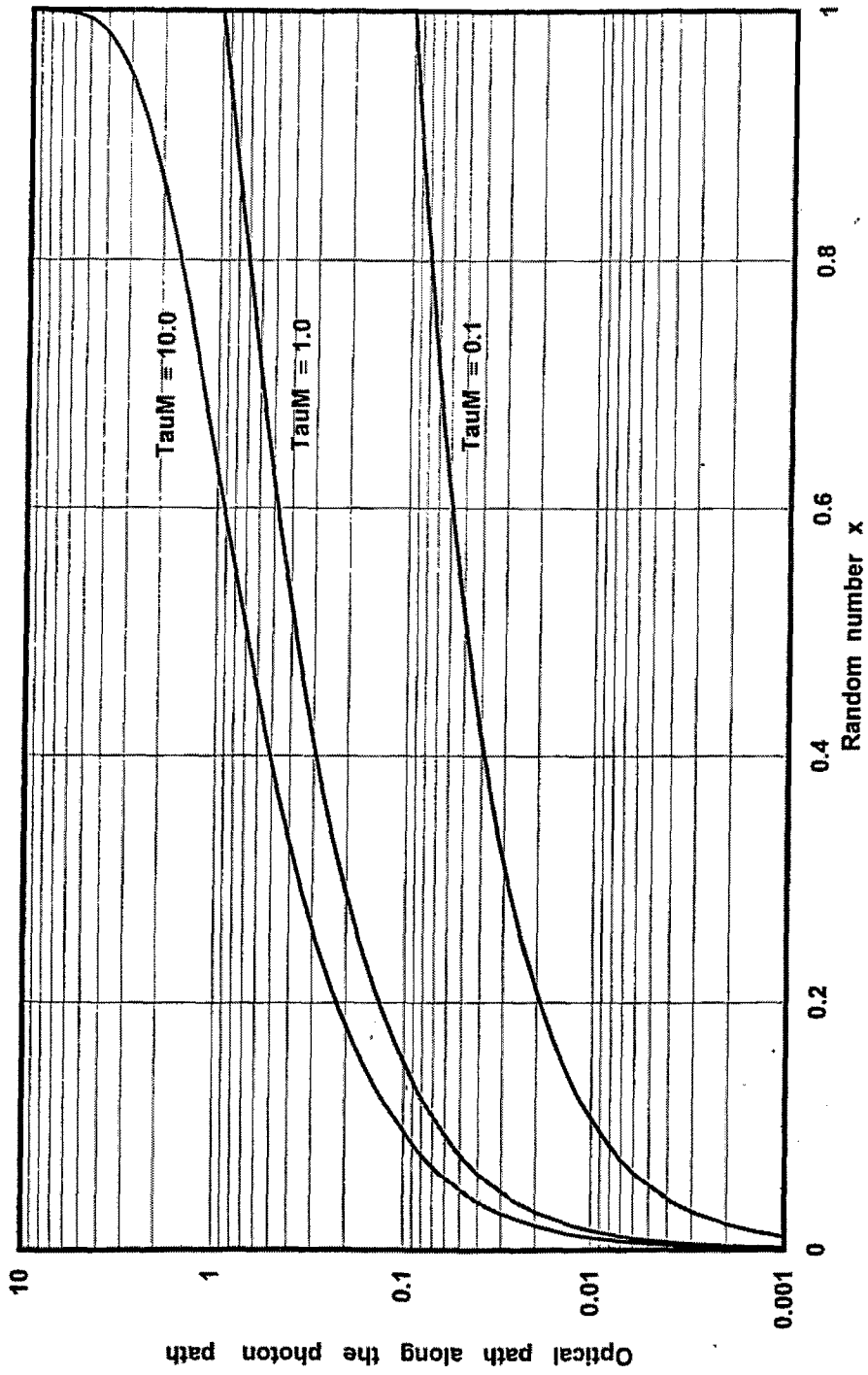
Figure 42. Variation in the Photon Optical Path as a Function of the Random Number x for three Values of the Maximum Optical Thickness.

71

7.3   Basic Algorithm.

The radiation model is a spectral model. The spectral range is from 0.1 μm (ultraviolet) to 1 m (radio wave). It is easy to show that the spectral power output of a flare particle is given by the following:

$$P(\lambda, T) = 15 \left(\frac{hc}{\pi kT} \right)^4 \frac{P(T)}{\lambda^5 [\exp(hc / \lambda kT) - 1]} \qquad (86)$$

where

   h ~ Planck's constant

   k ~ Boltzmann's constant

   c ~ speed of light

   λ ~ wavelength of the radiation

   T ~ absolute temperature of the flare

and P(T) is the total (spectrally integrated) power output of the flare. Thus, knowing the flare temperature from the equations in section 2, the spectral power output of the flare can be calculated from equation (86).

7.4   Comprehensive Model Description.

In the previous sections we described the cloud model as an abstract entity unto itself. For a practical model, however, we consider the cubic cloud in a more realistic setting with radiation sources outside with a target and a background. The targets and background chosen are rather simplistic because the emphasis in this investigation is on the physics of multiple scattering in an emissive smoke cloud rather than on the detailed geometry and physics of targets and backgrounds. In figure 43 we depict a typical scene with the radiation components. All these components are to be used in the computer model. The user enters typical values for the effective temperatures of the thermal radiation that enters the cloud from the near side, that is, from the side of the cloud that is closest to the sensor as well as the temperature of the radiation that enters the cloud from the far side, that is, from the side of the cloud that is farther from the sensor. One must also enter the effective temperatures of the target and the background as well as the temperature of the air inside the cloud. Thus, five temperatures must be entered by the user. The temperature of the flares is, of course, determined by the values of the other flare parameters. The model does contain considerable flexibility in that one can choose radiation components that are different for the near and far sides of the cloud. This may happen for example if the cloud is facing a snow-covered mountain but the back of the cloud is facing a lake. Likewise, one can easily understand that the air temperature in the cloud could be quite different from the temperature of the other external radiation components.
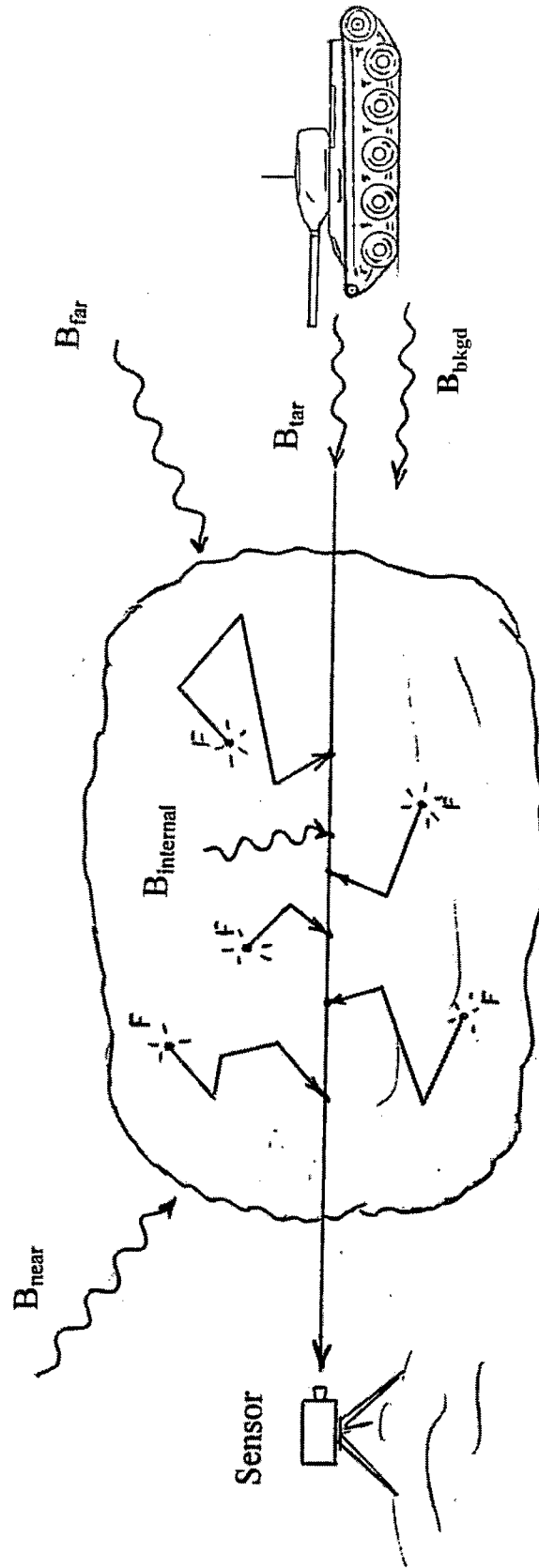
Figure 43. Illustration of the Radiation Components for the Comprehensive Radiation Model for an Emissive Smoke Cloud.

73

8. COMPUTER PROGRAM

In this section we describe the details of the computer model for an emissive smoke cloud.

8.1 System Constraints.

One can specify the variables in the analysis in different ways. We chose the following:

Specify the length L of the side of the smoke cloud, the concentration C_F of the flares, and the total number N_T of flares in the cloud. This then determines the radii of the flares. Thus,

$$r_F \sim r_F (L, C_F, N_T)$$

One can also specify the ambient temperature T_0 of the cloud, the flare heat content h_F, the flare radius r_F, and the flare drop time t. These quantities then determine the final temperature of the flares. Thus,

$$T_F \sim T_F (T_0, h_F, r_F, t)$$.

Finally, one can then specify the ambient temperature of the cloud, the final flare temperature, the total number of flares, the heat content of the flares, and the flare drop time to get the total power output of the flares. Thus,

$$P_F \sim P_F (T_0, T_F, N_{T,} h_F, t)$$

These are the functional relations that are used in the computer model.

An explicit formula for the flare power output is given by the following equation:

$$P_F = 36 N_T \pi \sigma^3 \left(\frac{t}{h_F} \right)^2 T_F^4 (T_F^4 - T_0^4)^2 \qquad (87)$$

8.2 Model Input Quantities.

The computer program called FlareW makes use of an input file called FlareW.in. The quantities that are to be entered into this file by the user are given below with the limits on the ranges clearly specified. Nominal values for the parameters are given in the brackets.

L ~ length of the side of the cubic smoke cloud (m) [nominal value = 10]
 0.1 < L < 1000
κ_e ~ volume extinction coefficient of the medium (m^{-1}) [nominal value = 0.1]
 0.00001 < κ_e < 1000.0
C_F ~ concentration (volume of the flare particles/volume of the medium)
 (dimensionless)[nominal value = 10^{-8}]
 0 < C_F < 1

$\varpi_0 \sim$ single-scattering albedo of cloud medium (dimensionless)[nominal value = 0.9999]
$0 < \varpi_0 < 1$

$g \sim$ asymmetry parameter (dimensionless) [nominal value = 0.0]
$-1 < g < 1$

$\lambda \sim$ initial wavelength of the radiation (μm) [nominal value = 3.0]
$0.1 < \lambda < 1,000,000$

DELW $\sim$ wavelength increment (μm) [nominal value = 0.5]

NW $\sim$ number of wavelengths [nominal value = 50]

$N_F \sim$ number of flares along one dimension of cloud (even integer) [nominal value = 10]
$2 < N_F < 1000$

Nhist $\sim$ number of photon histories [nominal value = 50]
$1 < Nhist < 100,000$

Tair $\sim$ ambient (air) temperature of the smoke cloud (K) [nominal value = 300]
$200 < Tair < 400$

Tfar $\sim$ effective temperature of incident radiation on the far side of smoke cloud (K)
[nominal value = 110]
$200 < Tfar < 400$.

Tnear $\sim$ effective temperature of incident radiation on the near side of smoke cloud (K)
[nominal value = 120]
$200 < Tnear < 400$

Ttar $\sim$ effective target temperature of incident radiation on the far side of smoke cloud
(K) [nominal value = 400]
$200 < Ttar < 6000$

Tbkgd $\sim$ effective background temperature of incident radiation on the far side of smoke
cloud (K) [nominal value = 350]
$200 < Tbkgd < 6000$

$f_h \sim$ Flare heat content factor (dimensionless) [nominal value = 1.0]
$0.005 < f_h < 5$, where $h = h_0 f_h$ and $h_0 = 2.0 \times 10^{10}$ J-m^{-3}

$f_t \sim$ Flare drop time factor (dimensionless) [nominal value = 1.0]
$0.1 < f_t < 10.0$, where $t = t_0 f_t$ and $t_0 = 10.0$ seconds

ISEED $\sim$ seed value for the pseudorandom number generator [nominal value = 305]
ISEED = any positive integer

Note that there are two separate temperatures for the effective temperatures of the radiation that are input on either side of the smoke cloud. This is because it is possible to have different radiation fields outside the cloud that arise from sources in different spatial regions. The following quantities are stored in the program:

$h_0 \sim$ heat content of a flare (J-m^{-3}) [default value = 2×10^{10}]

$t_0 \sim$ Flare particle "drop" time (s) [default value = 10]

$\sigma \sim$ Stefan-Boltzmann constant (W-m^{-2}-K^{-4}) [value = 5.670400×10^{-8}]

A typical example of the model input to the computer program is given below.

Side of cubic cloud L(meters)[F7.2]:10.0
Volume extinction coeff. ke(m-1)[F10.5]:0.5
Flare concentration CF[E12.5]:0.10000E-07

Single-scattering albedo w0[F9.6]:1.00000
Asymmetry parameter g[F9.6]:0.0000000
Initial wavelength WV(micrometers)[F12.4]:3.0000
Wavelength increment DELW (micrometers)
No. of flares in one dimension NF[I4]:10
Number of photon histories Nhist.[I6]:50
Air temp. Tair(kelvins)[F6.2]:300.00
Cloud farside temp. Tfar(kelvins)[F6.2]:305.00
Cloud nearside temp. Tnear(kelvins)[F6.2]:305.00
Effective target temp. Ttar(kelvins)[F7.2]:320.00
Effective backgnd temp. Tbkgd.(kelvins)[F7.2]:290.00
Flare heat factor fh [F8.6]:1.000000
Flare drop time factor ft [F5.2]:1.0
Random number seed (integer > 0)[I7]:305

The user should adhere to the specified format given in the brackets. It is assumed that the user understands the format specification in standard Fortran.

8.3   Model Output Quantities.

The quantities that the computer program calculates are the following:

N_T (= $(N_F)^3$) ~ total number of flares in the cloud
h (= $f_h h_0$) ~ actual heat content of the flares (J-m^{-3}) [default value = 2×10^{10}]
t (= $f_t t_0$) ~ actual flare particle "drop" time (s) [default value = 10]
τ_S (= $\kappa_e L$) ~ optical thickness of the smoke cloud (dimensionless)
DEL ~ Distance between the flares (m)
r_F ~ flare particle radius (μm)
T_F ~ flare particle temperature after heating (K)
Total integrated source power (Watts)
Total spectral source power (Watts-μm^{-1})
Single-source integrated power (Watts)
Single-source spectral power (Watts-μm^{-1})
Single-source integrated radiance (Watts-m^{-2}-sr^{-1})
Single-source spectral radiance (Watts-m^{-2}-sr^{-1}-μm^{-1})
Flare path spectral radiance (single scattering) (Watts-m^{-2}-sr^{-1}-μm^{-1})
Flare path spectral radiance (double scattering) (Watts-m^{-2}-sr^{-1}-μm^{-1})
Flare path spectral radiance (triple scattering) (Watts-m^{-2}-sr^{-1}-μm^{-1})
Flare path spectral radiance (total scattering) (Watts-m^{-2}-sr^{-1}-μm^{-1})
Cloud albedo
Cloud diffuse transmission
Cloud emissivity
Cloud line-of-sight transmittance
Cloud far side incident spectral radiance (Watts-m^{-2}-sr^{-1}-μm^{-1})
Cloud near side incident spectral radiance (Watts-m^{-2}-sr^{-1}-μm^{-1})
Cloud internal thermal spectral radiance (Watts-m^{-2}-sr^{-1}-μm^{-1})
Cloud thermal path spectral radiance (Watts-m^{-2}-sr^{-1}-μm^{-1})
Total (flare + thermal) spectral path radiance (Watts-m^{-2}-sr^{-1}-μm^{-1})

Target spectral radiance (at the target) (Watts-m^{-2}-sr^{-1}-μm^{-1})
Background spectral radiance (at the target) (Watts-m^{-2}-sr^{-1}-μm^{-1})
300-degree blackbody spectral radiance (Watts-m^{-2}-sr^{-1}-μm^{-1})
Contrast transmittance (with no flares present)
Contrast transmittance (with flares present)
Signal-to-noise ratio (intrinsic with no cloud present)
Signal-to-noise ratio (with no flares present)
Signal-to-noise ratio (with flares present)
Signal-to-noise ratio transmittance (with no flares present)
Signal-to-noise ratio transmittance (with flares present)
Pseudorandom number seed value
Computer time (minutes and seconds)

A typical example of the model output from the computer program that corresponds to the input file given in section 8.2 is as follows:

Length of side of cubic cloud	=	10.00 meters
Volume extinction coefficient	=	0.50000 per meter
Cloud optical thickness	=	5.000000
Concentration of flares	=	1.00000E-08
Distance between flares	=	9.09091E-01 meters
Radius of the flares	=	1.33650E+03 micrometers
Single-scattering albedo	=	1.000000
Asymmetry parameter	=	0.000000
Wavelength of radiation	=	3.0000 micrometers
Wavelength increment	=	0.05 micrometers
No. of wavelengths	=	5
Number of flares in one dimension	=	10
Total no. of flares in the cloud	=	1000
Ambient air temperature in cloud	=	300.00 K = 80.33 F
Temperature at far side of cloud	=	305.00 K = 89.33 F
Temperature at near side of cloud	=	305.00 K = 89.33 F
Effective target temperature	=	320.00 K = 116.33 F
Effective background temperature	=	290.00 K = 62.33 F
Temperature of the flares	=	1991.23 K = 3124.55 F
Heat content of a flare	=	2.000000E+10 J per m^3
Flare drop time	=	10.00 seconds
Total integrated source power	=	2.001031E+04 Watts
Total spectral source power	=	3.416262E+03 Watts/micrometer
Single source power	=	2.001031E+01 Watts
Single source spectral power	=	3.416262E+00 Watts/micrometer
Single source radiance	=	2.837613E+05 Watts/m^2/sr
Single source spectral radiance	=	4.844517E+04 Watts/m^2/sr/um
Number of photon histories	=	50
Flare path radiance (single scat.)	=	4.118574E-01 Watts/m^2/sr/um
Flare path radiance (double scat.)	=	4.096055E-01 Watts/m^2/sr/um
Flare path radiance (triple scat.)	=	3.626195E-01 Watts/m^2/sr/um
Flare path radiance (total scat.)	=	3.005133E+00 Watts/m^2/sr/um

Cloud albedo = 0.83333333	=	83.333333 %
Cloud transmission = 0.16666667	=	16.666667 %
Cloud emissivity = 0.00000000	=	0.000000 %
LOS transmittance = 0.00673795	=	0.673795 %
Cloud far side radiance	=	7.266681E-02 Watts/m^2/sr/um
Cloud near side radiance	=	7.266681E-02 Watts/m^2/sr/um
Cloud internal thermal radiance	=	5.591389E-02 Watts/m^2/sr/um
Cloud thermal path radiance	=	7.266681E-02 Watts/m^2/sr/um
Total path radiance	=	3.077800E+00 Watts/m^2/sr/um
Target radiance (at target)	=	1.518605E-01 Watts/m^2/sr/um
Background radiance (at target)	=	3.221905E-02 Watts/m^2/sr/um
300 degree blackbody radiance	=	5.591389E-02 Watts/m^2/sr/um
Contrast transmittance (no flares)	=	0.0103023
Contrast transmittance (with flares)	=	0.0002457
SNR (intrinsic, no cloud)	=	0.7706835
SNR (cloud without flares)	=	0.0077779
SNR (cloud with flares)	=	0.0001852
SNR transmittance (cloud without flares)	=	0.0100922
SNR transmittance (cloud with flares)	=	0.0002403
Random number seed value	=	305
Computer time = 6.34375 seconds	=	0.10573 minutes

It should be noted that in addition to the computed output the program also prints out the input quantities. Thus, the user has a complete record of all the model parameters in one file called FlareW.out each time the program is run.

8.4   Operation of the Computer Program.

All one needs to run the computer program FlareW is the program itself and the input file called FlareW.in. Upon operation, the output file called FlareW.out is automatically generated. It is assumed that the user has some background in computers and a basic knowledge of radiometry and thermal physics in order to understand the input required and the output quantities. It is suggested that the user begin in a conservative manner, that is, try a small number of flares, say about 10, and a small number of photon histories, say about 50 in order to gain some experience. The computer time is strongly dependent on the values of these quantities as the user will understand after making a few runs. If a large number of flares and a large number of photon histories are input to the program it can take a very long time to run. This author has let the program run on a standard PC for up to 16 hours! One will find, however, that this level of accuracy is rarely necessary. One can get reasonably good results in a few minutes of computer time. It is easy to make successive runs with the program. Each time the program is run the user can either print out the output file FlareW.out or rename the file each time for inventory.

9.   FINAL RESULTS

In this section we show the results of many computer runs for the metrics that were described in section 5. More explicitly, we illustrate the results for the path radiance, the contrast transmittance, the signal-to-noise ratio, and the signal-to-noise ratio transmittance for various values of the parameters in the model.

9.1   Variation with the Single-Scattering Albedo.

The single-scattering albedo is a measure of the relative amount of scattering versus absorption in a medium. Therefore, it can be an important factor in the analysis of the metrics. In figure 44 we illustrate the dependence of the path radiance on the single-scattering albedo with and without flares in the cloud. One can see that the path radiance increases as the single-scattering albedo approaches 1, indicating pure scattering. The difference, however, between the cloud with and without flares appears to be rather small. It is important to note that the cloud optical thickness in this case is 5, a rather significant amount that can cause considerable scattering. In figure 45 we show the corresponding variation in the contrast transmittance. Here we see a dramatic difference between the case of a cloud with and without flares. It clearly illustrates the effect of the presence of flares. The flares do indeed produce enough radiance to act as a blocking factor of the input radiation from a target or a background. It also indicates that the optimum single-scattering albedo is not necessarily the one in which the single-scattering albedo is 1. In figures 46 and 47 we illustrate the same effect for the variation in the signal-to-noise ratio and the signal-to-noise ratio transmittance with single-scattering albedo. The pattern is very similar to that for the contrast transmittance. These graphs suggest that it may be possible to design smoke particles to maximize the difference between the metrics with and without flares.

9.2   Variation with the Flare Heat Content.

The heat content of the flares is a driving factor in the flare-produced radiance. In figure 48 we illustrate the variation in the path radiance in a smoke cloud as a function of the flare heat content for three values of the volume extinction coefficient. Since the cloud length is 10 meters the smoke optical thickness is just equal to 10 times the volume extinction coefficient. Thus, the figure is for cases for optical thickness values from 1 to 5. As expected the path radiance increases with an increase in the heat content as well as for an increase in the optical thickness. It should be noted that this case probably represents the optimum or near optimum in that the single-scattering albedo is 1,that is pure scattering. The variation in the contrast transmittance as a function of the flare heat content can be seen in figure 49. As one might expect, the contrast transmittance decreases with increasing flare heat content and with increasing optical thickness. Figures 50 and 51 illustrate a similar variation for the signal-to-noise ratio and the signal-to-noise ratio transmittance.

9.3   Variation with the Volume Extinction Coefficient.

Volume extinction coefficient or equivalently, the optical thickness of the smoke medium is obviously an important factor in the evaluation of the metrics. In figure 52 we depict the variation in the path radiance as a function of the volume extinction coefficient for a single-scattering albedo = 1.0 for the case when there are flares in the cloud and for the case when there are flares plus the thermal component in the cloud. This graph is for a wavelength of 5.0 μm. One might wonder why there is a non-zero value for the case when there are flares and the thermal radiation. This means that the flares contribute nothing for a volume extinction coefficient of 0 since there is no scattering by a medium but there is a thermal component because the atmosphere (where a cloud should be) is radiating as a simple blackbody. In figure 53 we illustrate the variation in the contrast transmittance as a function of the volume extinction coefficient for a similar case. It is interesting to notice that the contrast transmittance hardly changes for the case when there are no flares to the case when flares are present. The
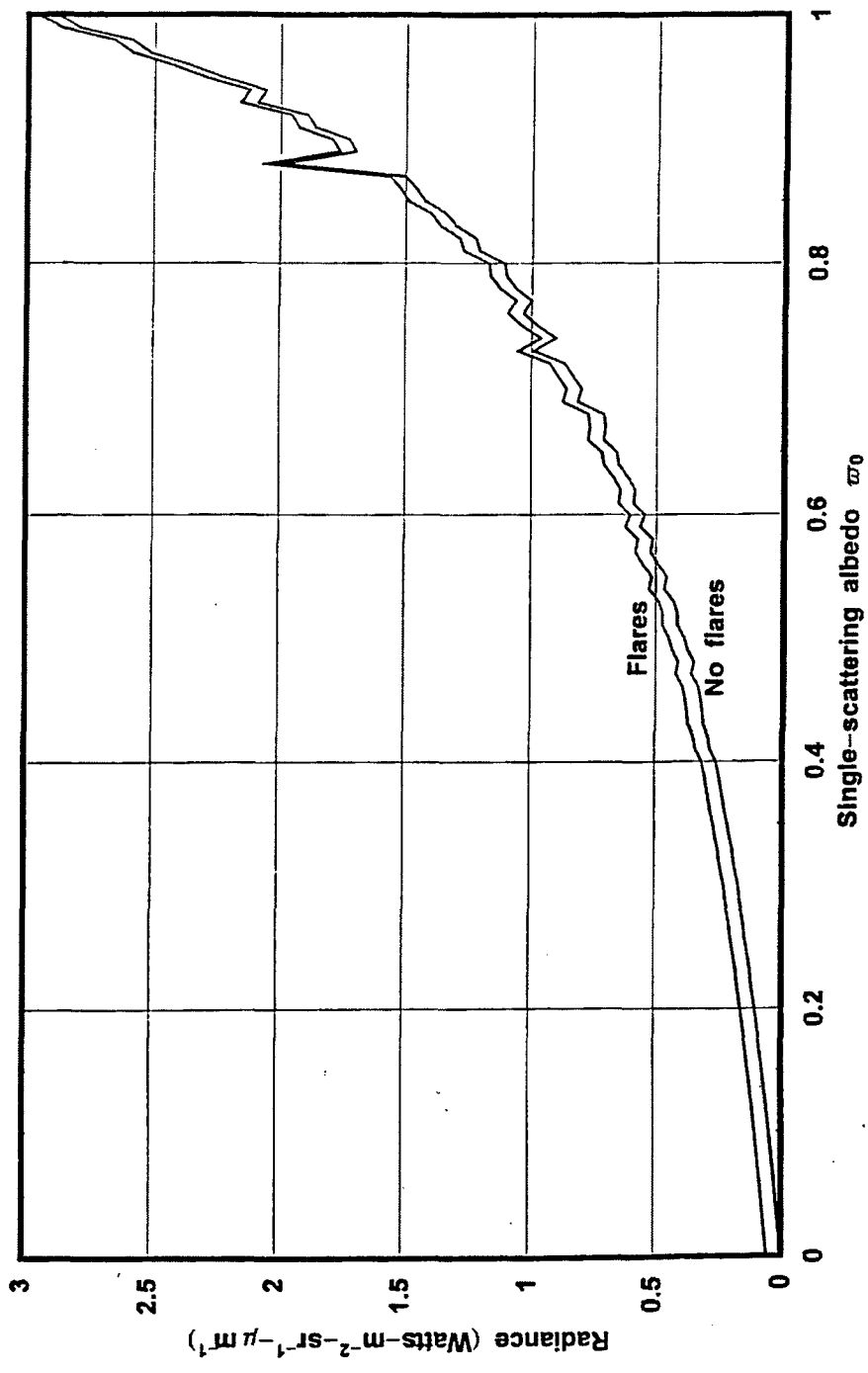
Figure 44. Variation in the Path Radiance as a Function of the Single-Scattering Albedo for a Volume Extinction Coefficient of 0.5 m^{-1} for a Wavelength = 3.0 μm for 50 Photon Histories for 1000 Source Points in a Cube of Length 10 Meters with and without Flares. Total Source Power = 20,000 Watts, Asymmetry Parameter = 0.0, Flare Concentration = 1.0×10^{-8}.

80
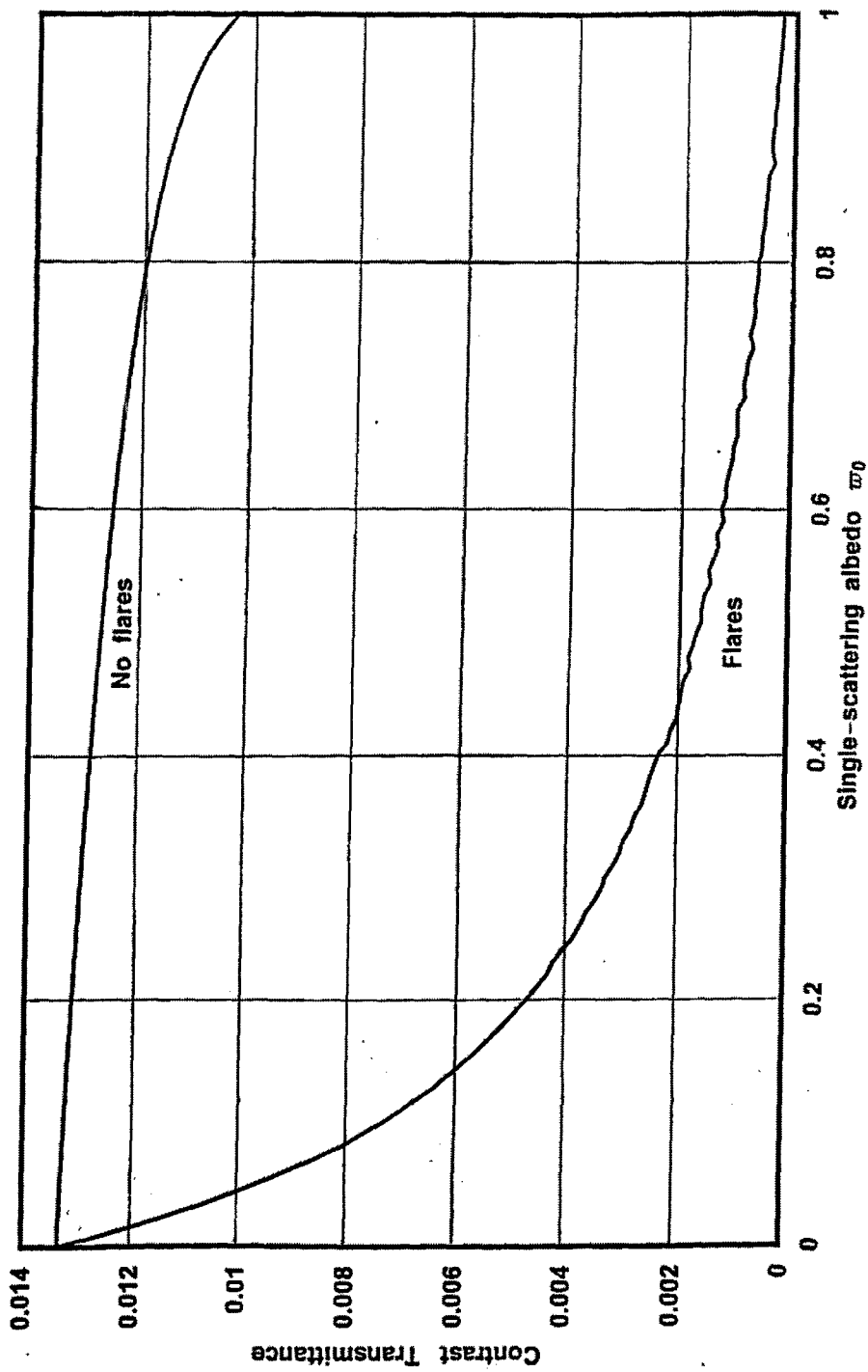
Figure 45. Variation in the Contrast Transmittance as a Function of the Single-Scattering Albedo for a Volume Extinction Coefficient of 0.5 m^{-1} for a Wavelength = 3.0 μm for 50 Photon Histories for 1000 Source Points in a Cube of Length 10 Meters with and without Flares. Total Source Power = 20,000 Watts, Asymmetry Parameter = 0.0, Flare Concentration = 1.0 × 10^{-8}.
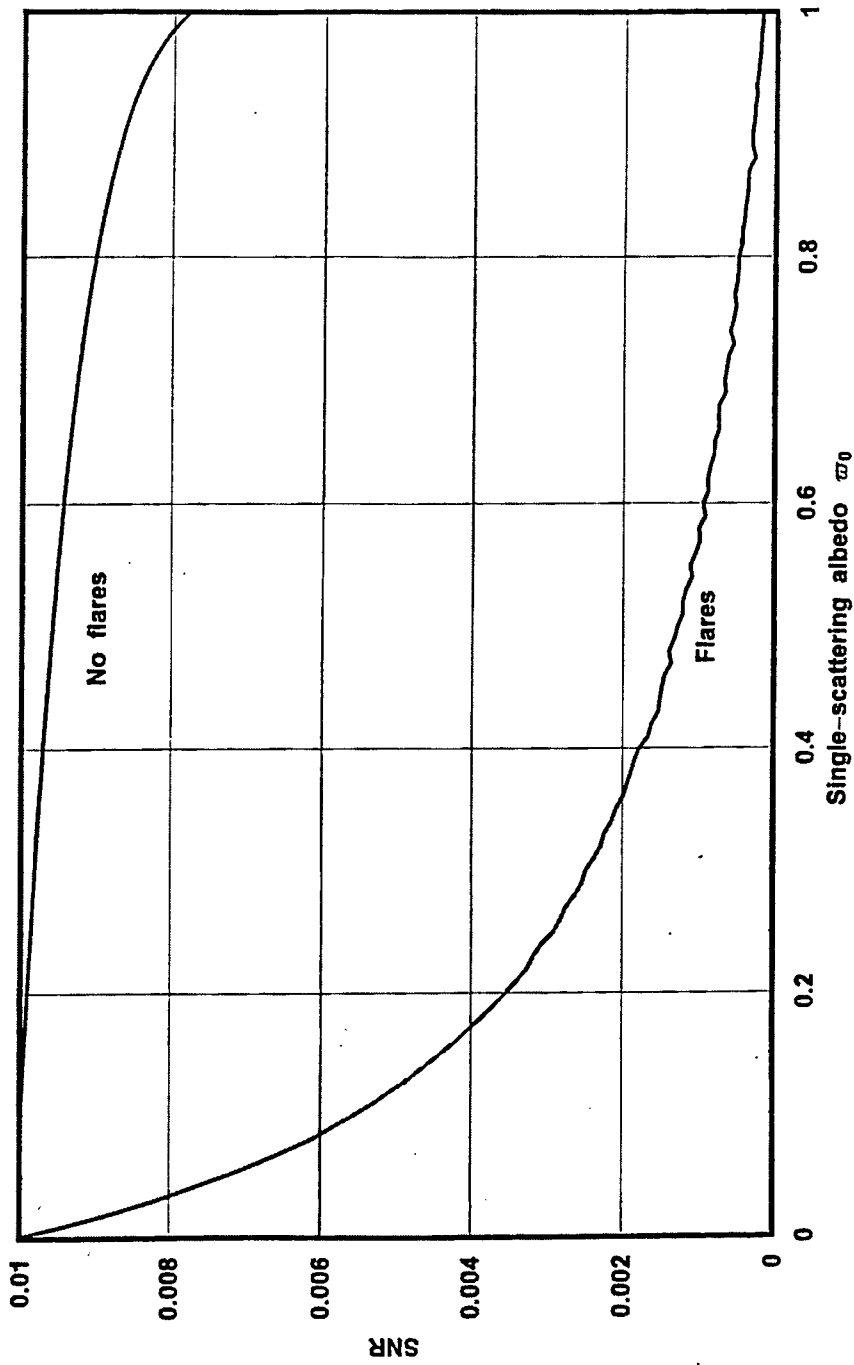
Figure 46. Variation in the Signal-to-Noise Ratio as a Function of the Single-Scattering Albedo for a Volume Extinction Coefficient of 0.5 m^{-1} for a Wavelength = 3.0 μm for 50 Photon Histories for 1000 Source Points in a Cube of Length 10 Meters with and without Flares. Total Source Power = 20,000 Watts, Asymmetry Parameter = 0.0, Flare Concentration = 1.0×10^{-8}.
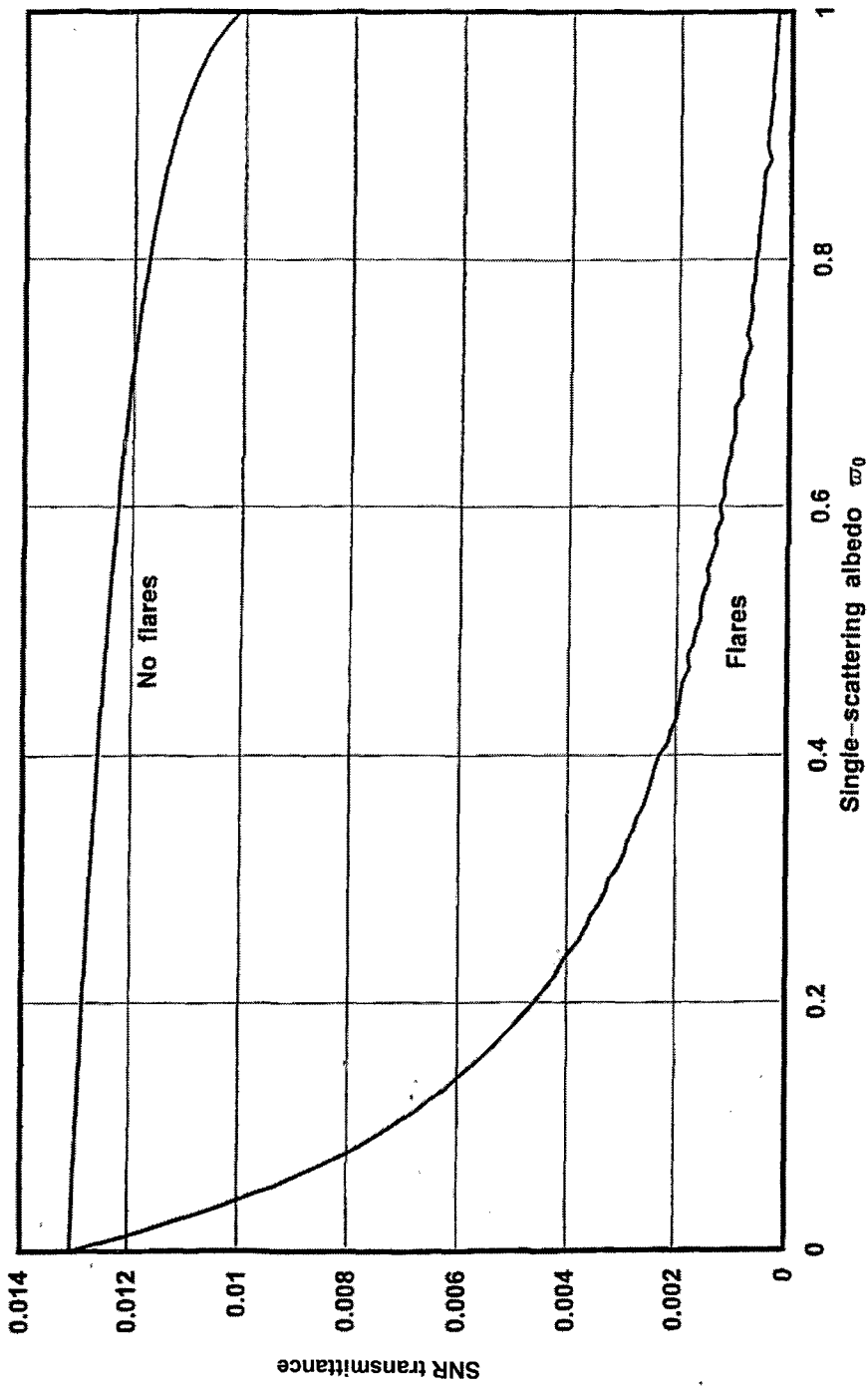
Figure 47. Variation in the Signal-to-Noise Ratio Transmittance as a Function of the Single-Scattering Albedo for a Volume Extinction Coefficient of 0.5 m^{-1} for a Wavelength = 3.0 μm for 50 Photon Histories for 1000 Source Points in a Cube of Length 10 Meters with and without Flares. Total Source Power = 20,000 Watts, Asymmetry Parameter = 0.0, Flare Concentration = 1.0×10^{-8}.
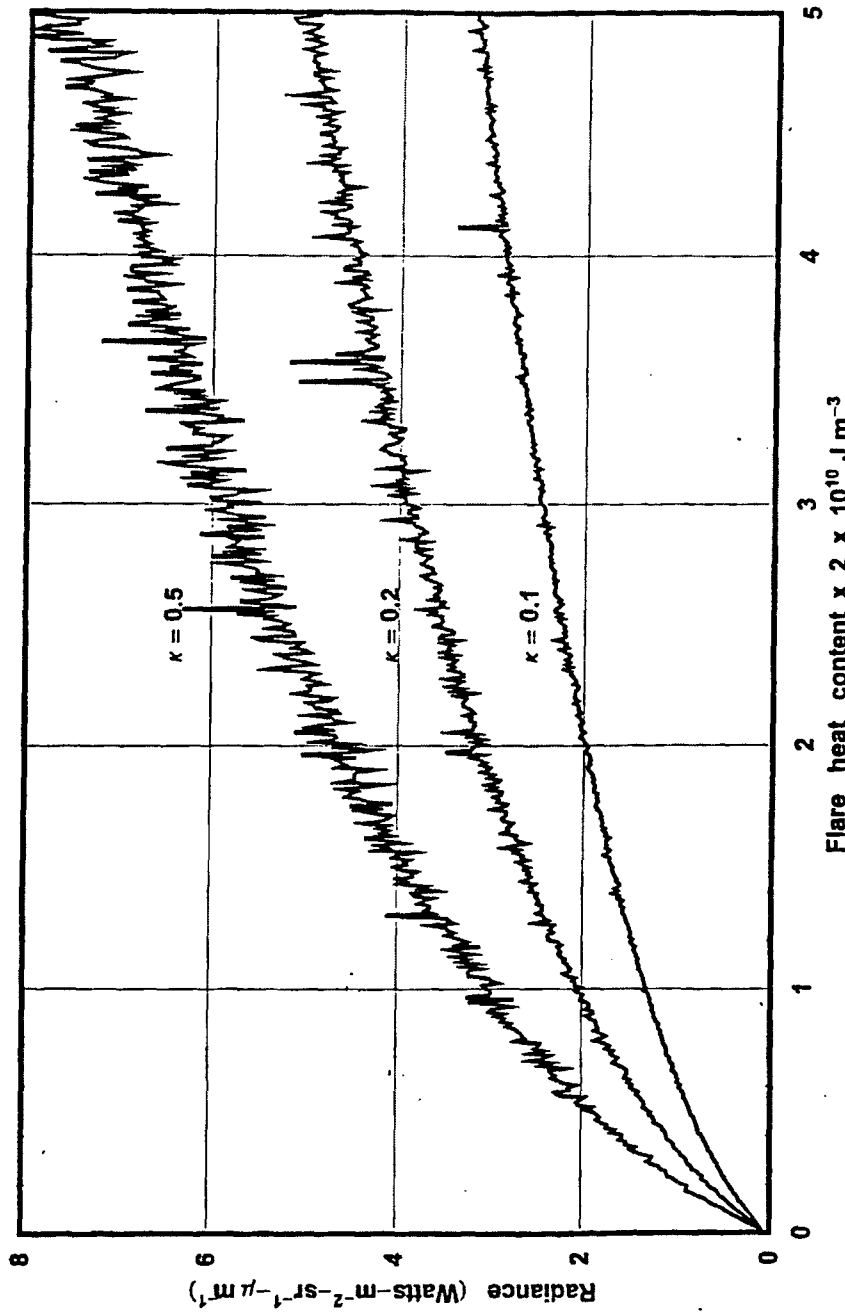
Figure 48. Variation in the Path Radiance as a Function of the Flare Heat Content for a Single-Scattering Albedo = 1.0 and for Three Volume Extinction Coefficients for a Wavelength = 3.0 μm for 50 Photon Histories for 1000 Source Points in a Cube of Length 10 Meters. Total Source Power = Variable, Asymmetry Parameter = 0.0, Flare Concentration = 1.0×10^{-8}.
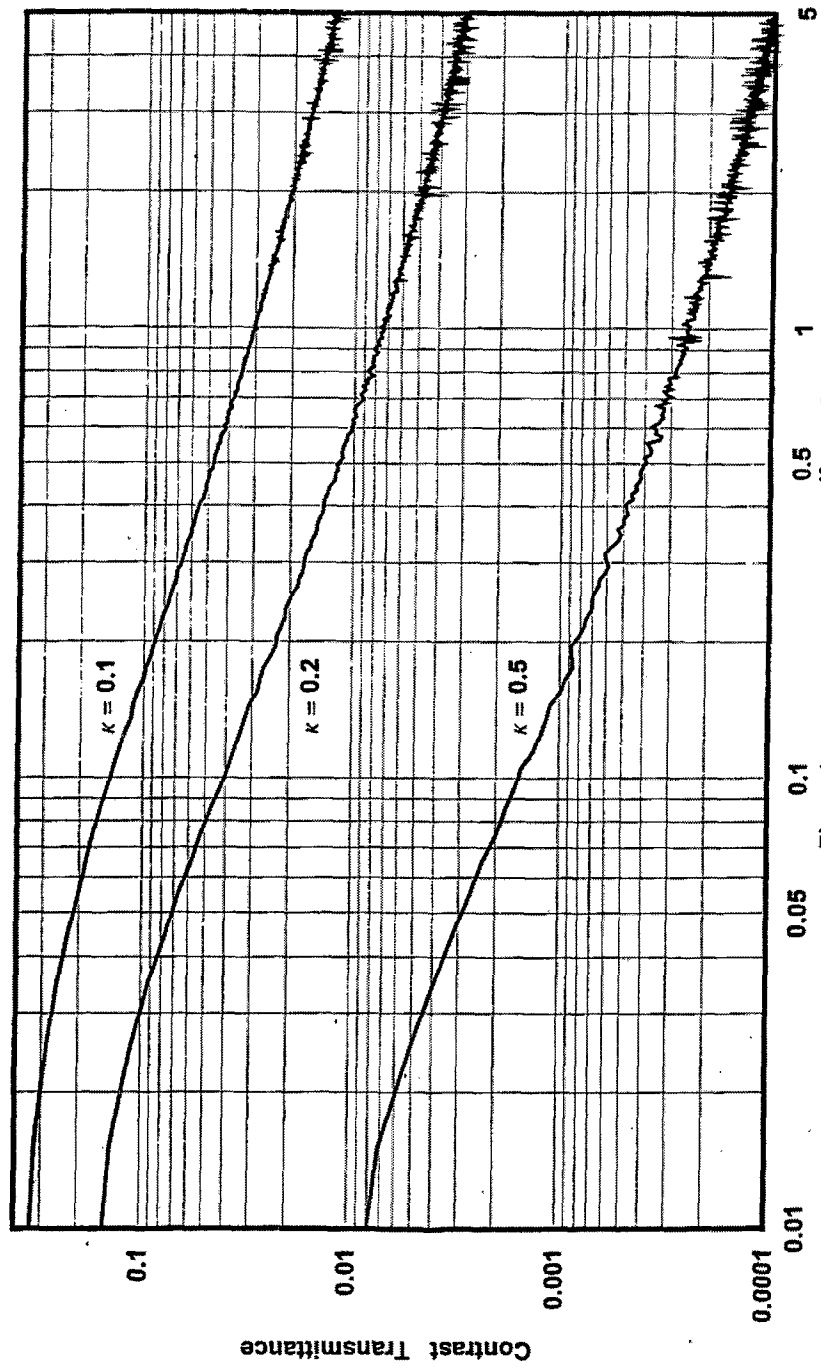
Figure 49. Variation in the Contrast Transmittance as a Function of the Flare Heat Content for a Single-Scattering Albedo = 1.0 and for Three Volume Extinction Coefficients for a Wavelength = 3.0 μm for 50 Photon Histories for 1000 Source Points in a Cube of Length 10 Meters. Total Source Power = Variable, Asymmetry Parameter = 0.0, Flare Concentration = 1.0×10^{-8}.
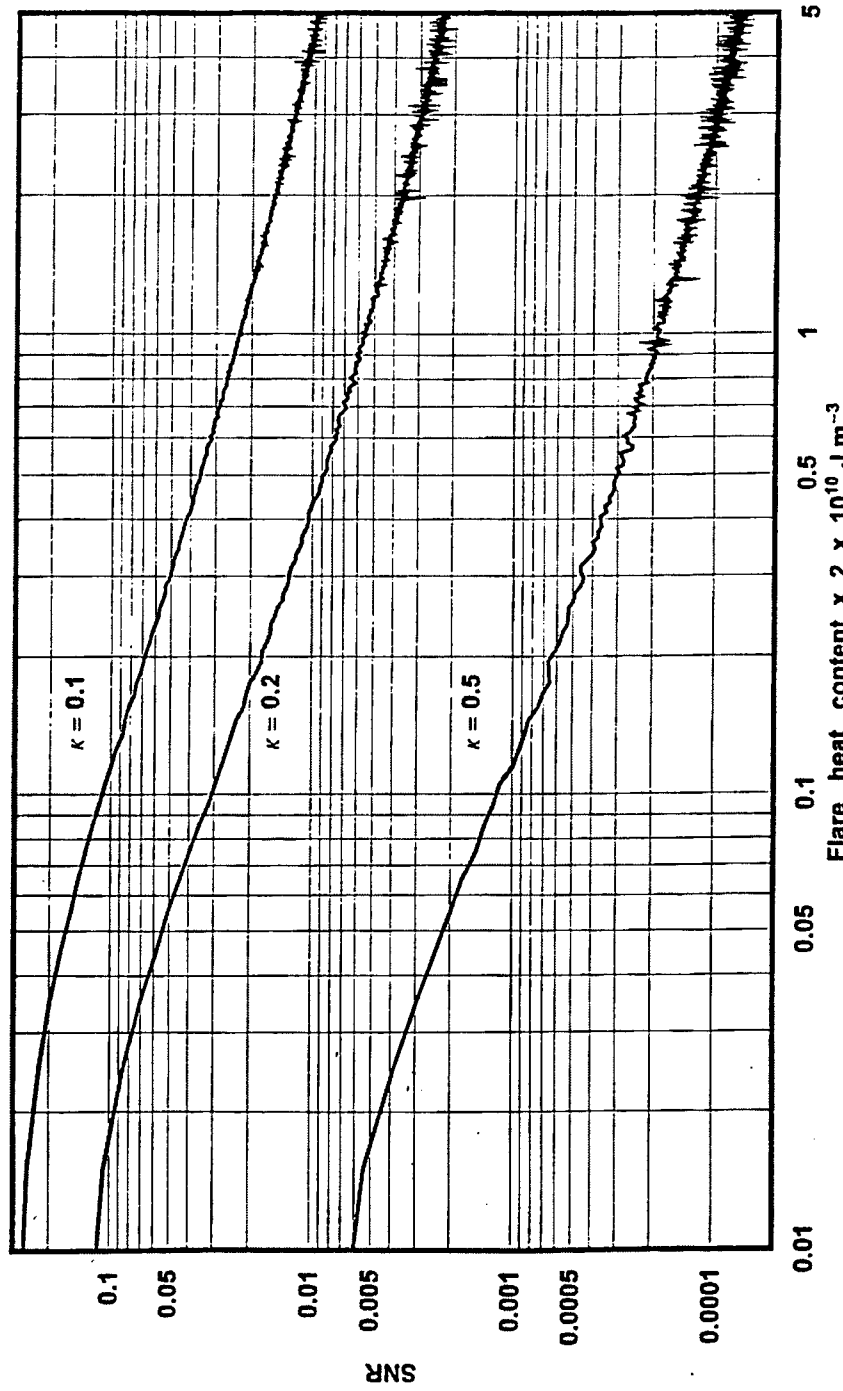
Figure 50. Variation in the Signal-to-Noise Ratio as a Function of the Flare Heat Content for a Single-Scattering Albedo = 1.0 and for Three Volume Extinction Coefficients for a Wavelength = 3.0 μm for 50 Photon Histories for 1000 Source Points in a Cube of Length 10 Meters. Total Source Power = Variable, Asymmetry Parameter = 0.0, Flare Concentration = 1.0×10^{-8}.
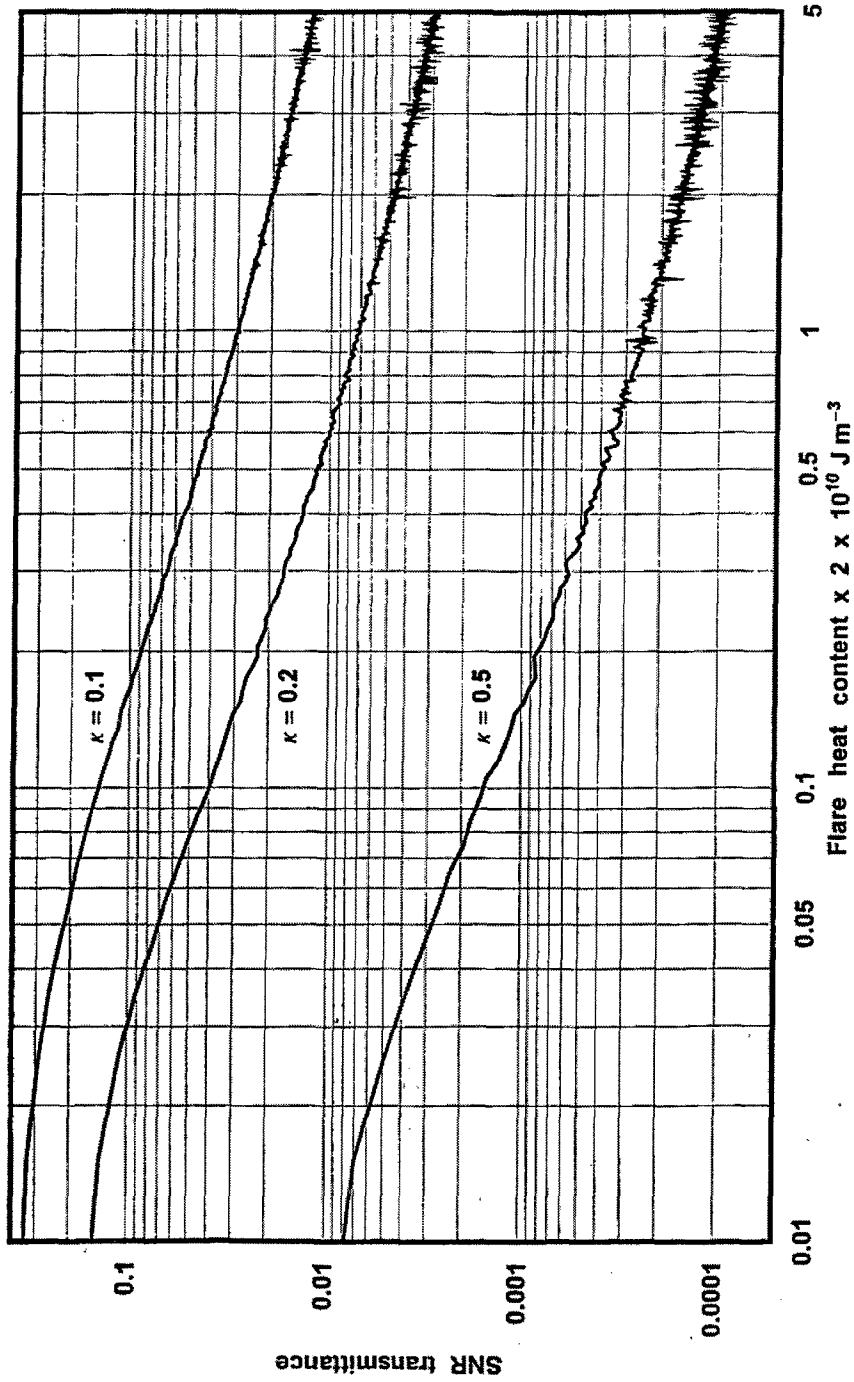
Figure 51. Variation in the Signal-to-Noise Ratio Transmittance as a Function of the Flare Heat Content for a Single-Scattering Albedo = 1.0 and for Three Volume Extinction Coefficients for a Wavelength = 3.0 μm for 50 Photon Histories for 1000 Source Points in a Cube of Length 10 Meters. Total Source Power = Variable, Asymmetry Parameter = 0.0, Flare Concentration = 1.0 × 10^{-8}.
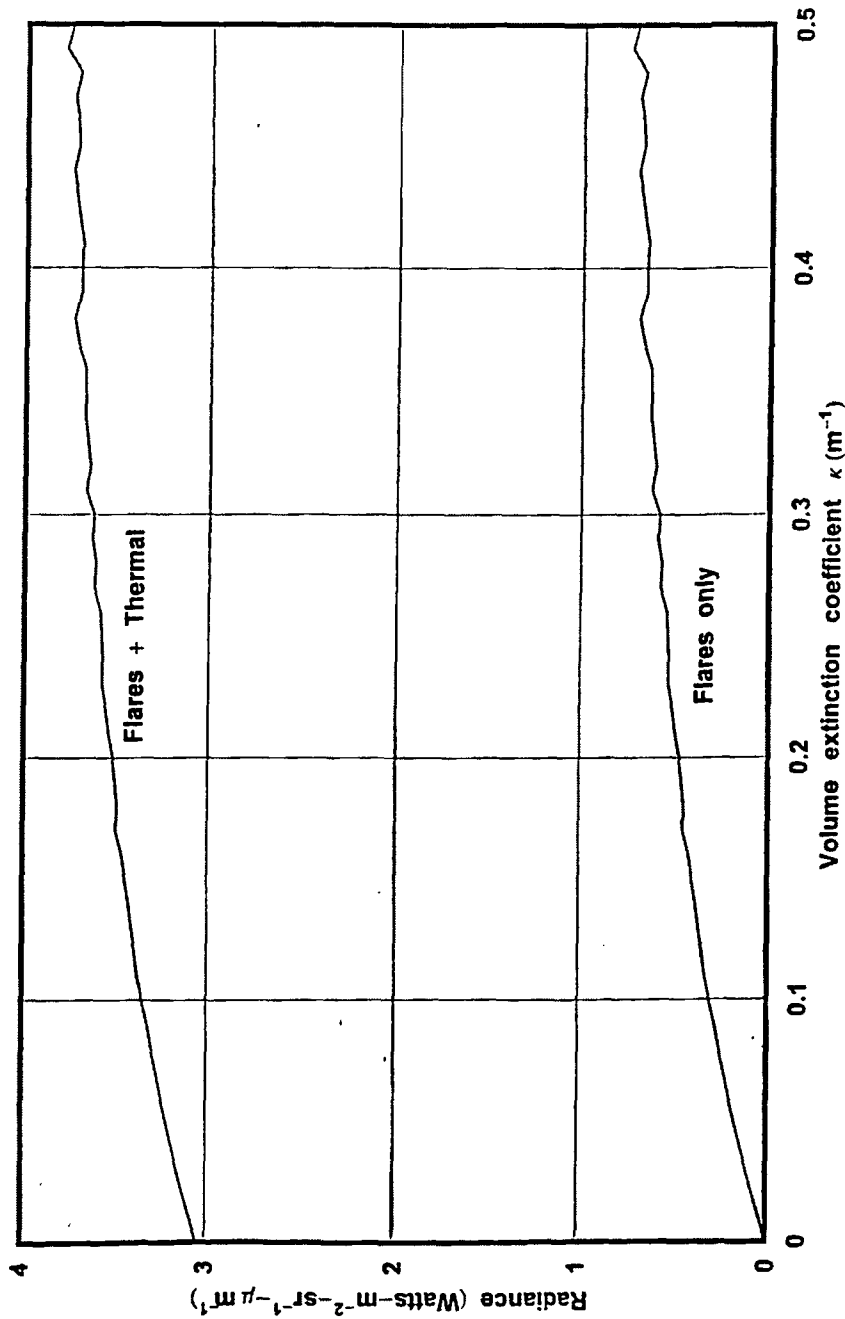
Figure 52. Variation in the Path Radiance as a Function of the Volume Extinction Coefficient for a Single-Scattering Albedo = 1.0 and for a Wavelength = 5.0 μm for 50 Photon Histories for 1000 Source Points in a Cube of Length 10 Meters with Flares Alone and Flares with the Thermal Component. Total Source Power = 20,000 Watts, Asymmetry Parameter = 0.0, Flare Concentration = 1.0×10^{-8}.
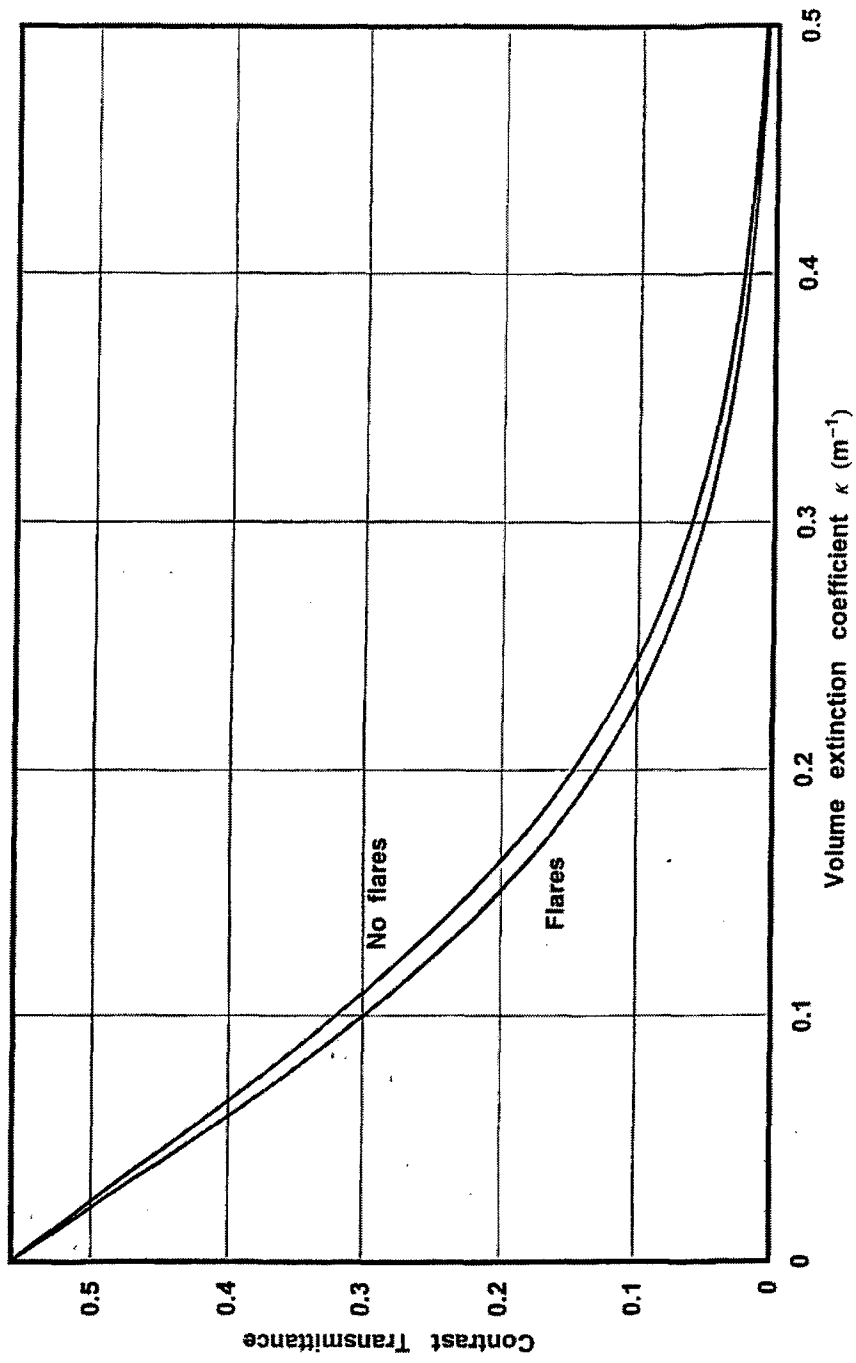
Figure 53. Variation in the Contrast Transmittance as a Function of the Volume Extinction Coefficient for a Single-Scattering Albedo = 1.0 and for a Wavelength = 5.0 μm for 50 Photon Histories for 1000 Source Points in a Cube of Length 10 Meters with and without Flares. Total Source Power = 20,000 Watts, Asymmetry Parameter = 0.0, Flare Concentration = 1.0×10^{-8}.

reason is that for this wavelength the thermal component dominates over the flare component. It is the flare-produced radiance that is most important. We will dispense with the corresponding signal-to-noise ratio and the signal-to-noise ratio transmittance graphs because they are essentially the same as for the contrast transmittance.

Now we illustrate the same graphs as above except for a wavelength of 3.0 μm instead of 5.0 μm. In figure 54 we depict the variation in the path radiance as a function of the volume extinction coefficient for a single-scattering albedo = 1.0 for the case when there are flares in the cloud and for the case when there are flares and the thermal component in the cloud. This graph is for a wavelength of 3.0 μm. In this case we notice that the thermal contribution is much smaller than for the case when the wavelength is 5.0 μm. This arises because the cloud temperature is 300 K and therefore the peak of the blackbody spectrum occurs at a wavelength of 9.66 μm. We are now much farther from the peak value and therefore the thermal component is less. As a result of this fact we would then expect the contribution from the flare radiance to be greater and therefore the contrast transmittance to be less. This is indeed what happens as one can see in figure 55 where we illustrate the variation in the contrast transmittance as a function of the volume extinction coefficient. Here we see a large change in the cases when there are flares and without flares. Finally, we consider the case for a wavelength of 2.5 μm. Here we are much farther from the peak of the blackbody spectrum for 300 K. Indeed, from figure 56 we see that there is essentially no difference in the path radiance. The path radiance for this wavelength for flares dominates over the path radiance without flares. We then expect that the contrast transmittance with flares present to be much smaller than the contrast transmittance for the other wavelengths. This is indeed the case as one can see from figure 57. The effect of wavelength can be more easily seen in figure 58 where we show the variation in the contrast transmittance as a function of the volume extinction coefficient for all three wavelengths with flares. It clearly illustrates the significance of wavelength on the blocking effect of the flares. It should be pointed out that if the cloud had a quite different temperature then the curves would vary somewhat. What is being observed here is the competition between the thermal energy in the cloud and the thermal energy in the flares. They peak at different wavelengths because of the large difference in their respective temperatures.

9.4   Variation with Wavelength.

Since there is a strong effect of the wavelength on the metrics we now take a detailed look at the explicit dependence on wavelength. Figure 59 illustrates the variation in the path radiance as a function of wavelength for a volume extinction coefficient of 0.02 m^{-1} or for an optical thickness of 0.2. This represents a relatively thin cloud and therefore there is not much scattering. As a result the flare path radiance is small. The peak in the flare spectrum occurs at a wavelength of 1.456 μm since the flares have a temperature of 1991.23 K. Likewise, the peak in the cloud thermal spectrum occurs at a wavelength of 9.66 μm since the cloud has a temperature of 300 K. We can also show the same function for a more abbreviated scale as in figure 60. One can see that the thermal component begins to compete with the flare component near a wavelength of about 3.0 μm. In figure 61 we illustrate the corresponding variation in the contrast transmittance with wavelength. Here we see the very strong effect of the wavelength. The contrast transmittance is essentially zero for wavelengths up to about 2.0 μm but it is near its maximum near a wavelength of 4.0 μm. Thus, at least for this thin cloud, flares play an important role for the shorter wavelengths. In figure 62 we see a similar set of curves as in figure 60 except for a volume extinction coefficient of 0.1m^{-1}. Here the optical thickness of the cloud is five times
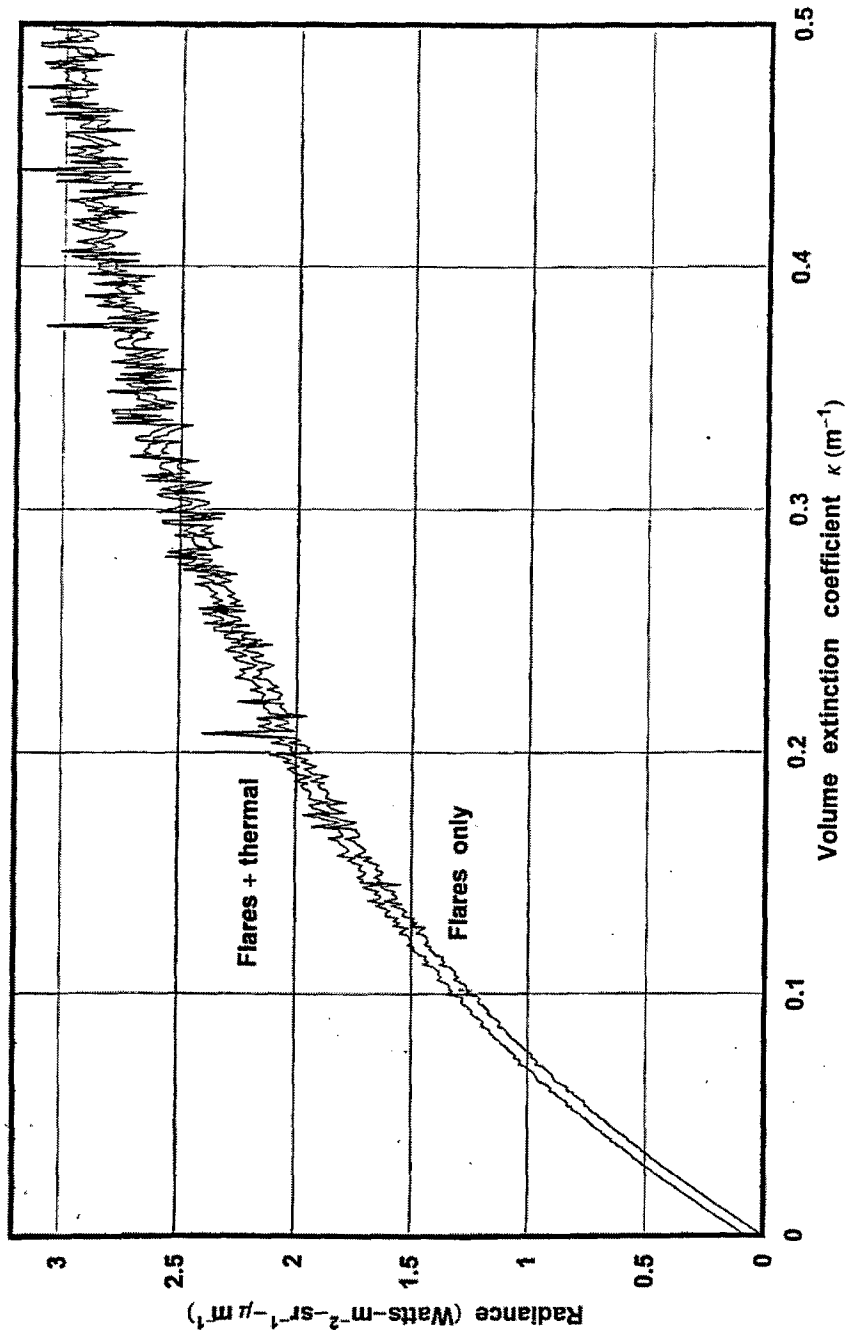
Figure 54. Variation in the Path Radiance as a Function of the Volume Extinction Coefficient for a Single-Scattering Albedo = 1.0 and for a Wavelength = 3.0 μm for 1000 Source Points in a Cube of Length 10 Meters with Flares Alone and Flares with the Thermal Component. Total Source Power = 20,000 Watts, Asymmetry Parameter = 0.0, Flare Concentration = 1.0×10^{-8}.

91
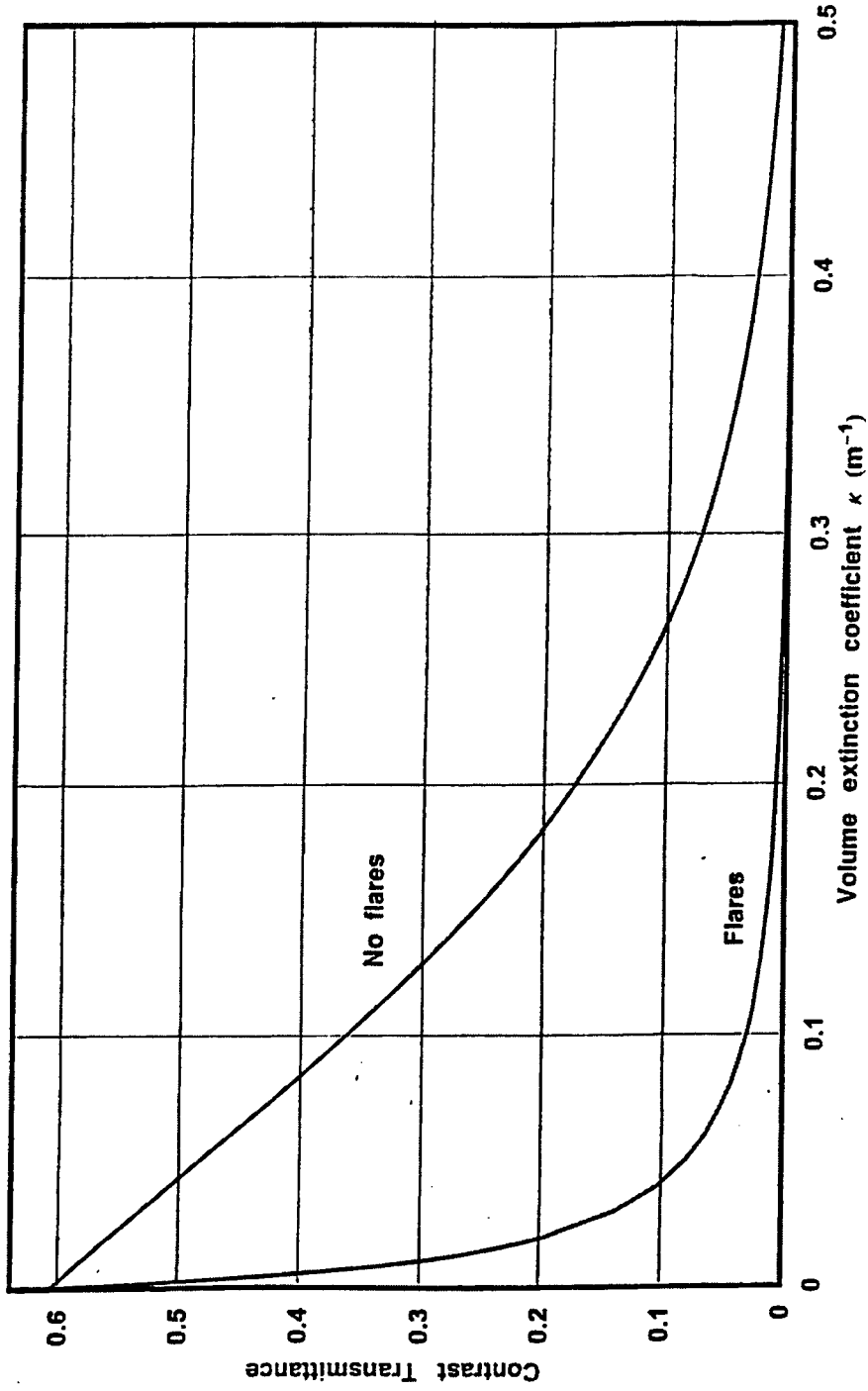
Figure 55. Variation in the Contrast Transmittance as a Function of the Volume Extinction Coefficient for a Single-Scattering Albedo = 1.0 and for a Wavelength = 3.0 μm for 50 Photon Histories for 1000 Source Points in a Cube of Length 10 Meters with and without Flares. Total Source Power = 20,000 Watts, Asymmetry Parameter = 0.0, Flare Concentration = 1.0×10^{-8}.
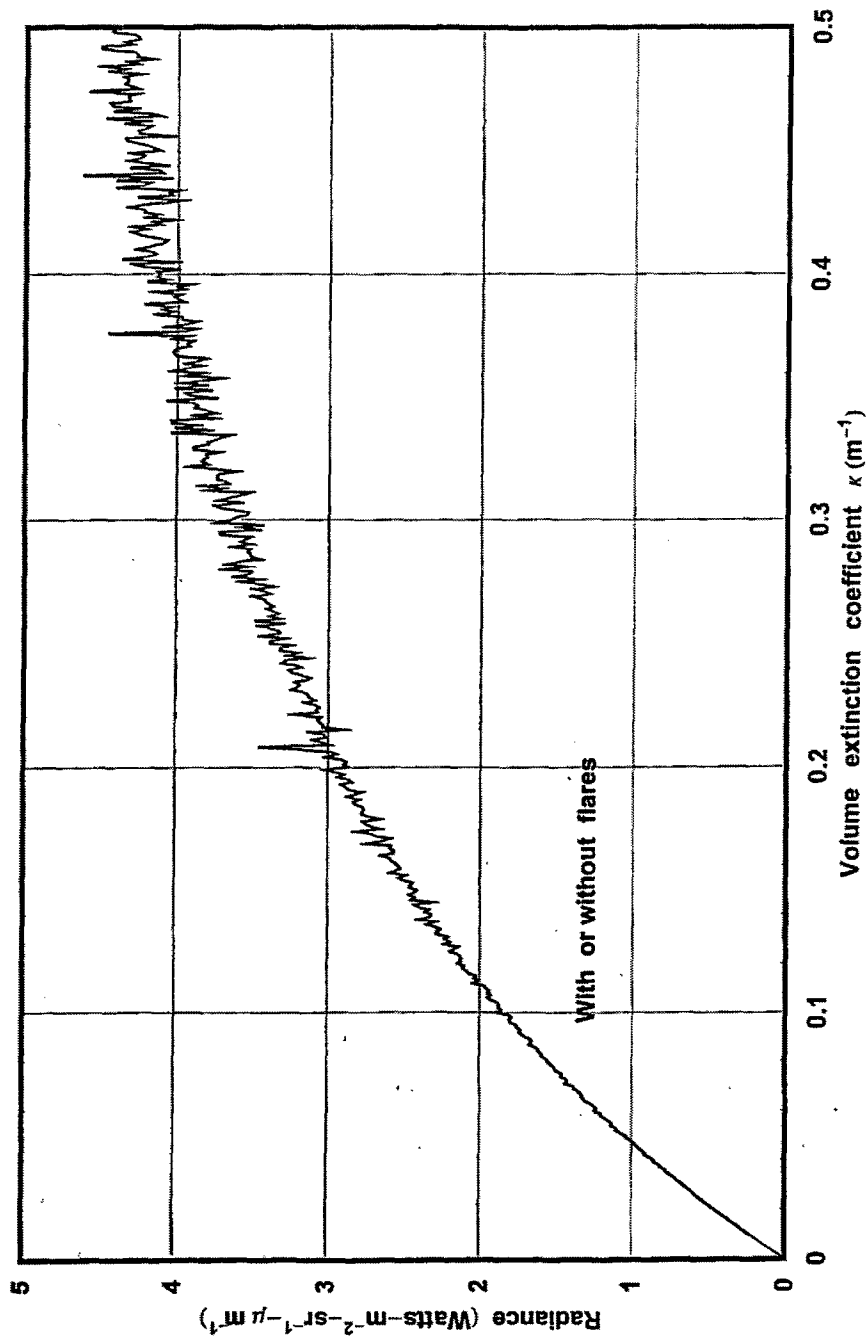
Figure 56. Variation in the Path Radiance as a Function of the Volume Extinction Coefficient for a Single-Scattering Albedo = 1.0 and for a Wavelength = 2.5 μm for 50 Photon Histories for 1000 Source Points in a Cube of Length 10 Meters with and without Flares. Total Source Power = 20,000 Watts, Asymmetry Parameter = 0.0, Flare Concentration = 1.0×10^{-8}.
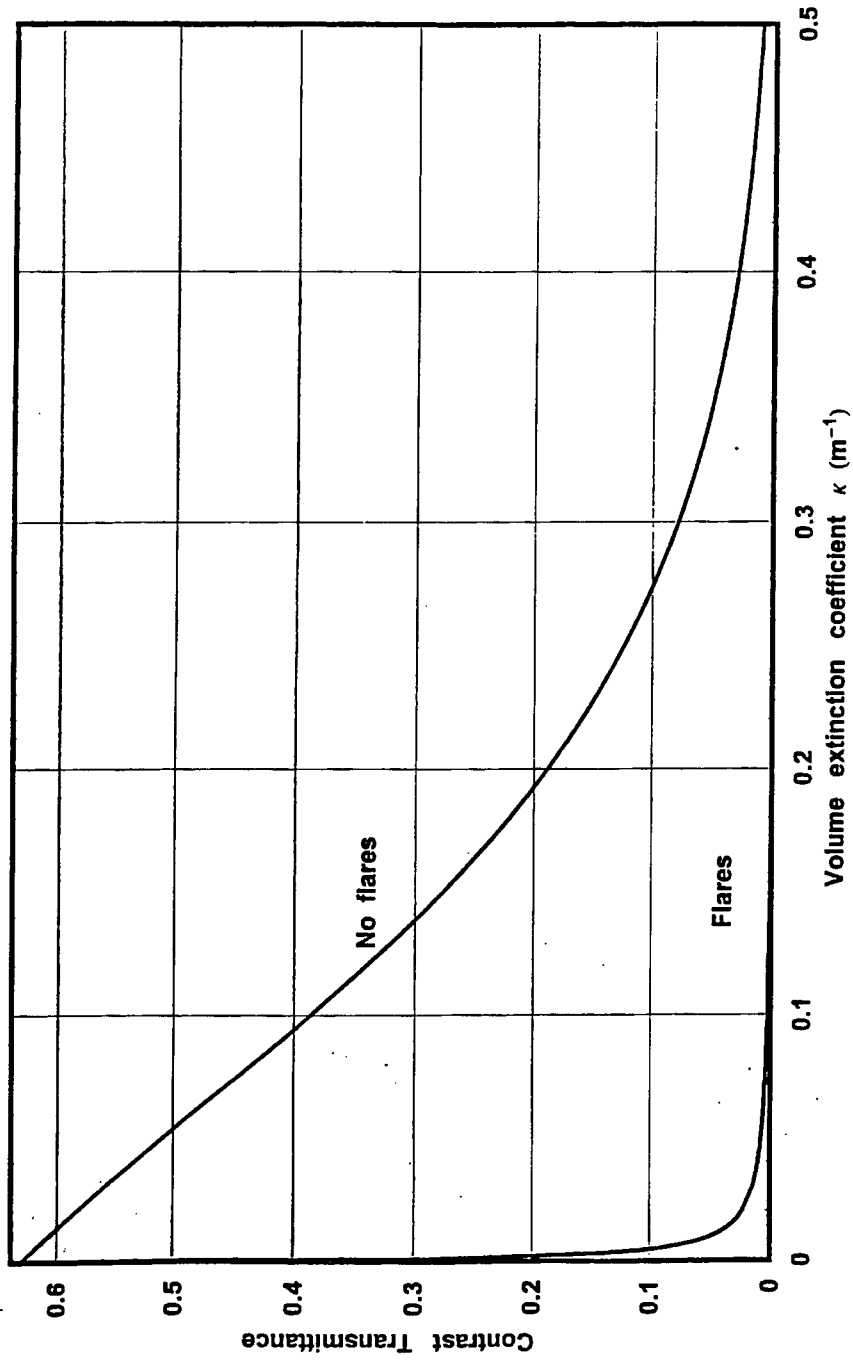
Figure 57. Variation in the Contrast Transmittance as a Function of the Volume Extinction Coefficient for a Single-Scattering Albedo = 1.0 and for a Wavelength = 2.5 μm for 50 Photon Histories for 1000 Source Points in a Cube of Length 10 Meters with and without Flares. Total Source Power = 20,000 Watts, Asymmetry Parameter = 0.0, Flare Concentration = 1.0×10^{-8}.
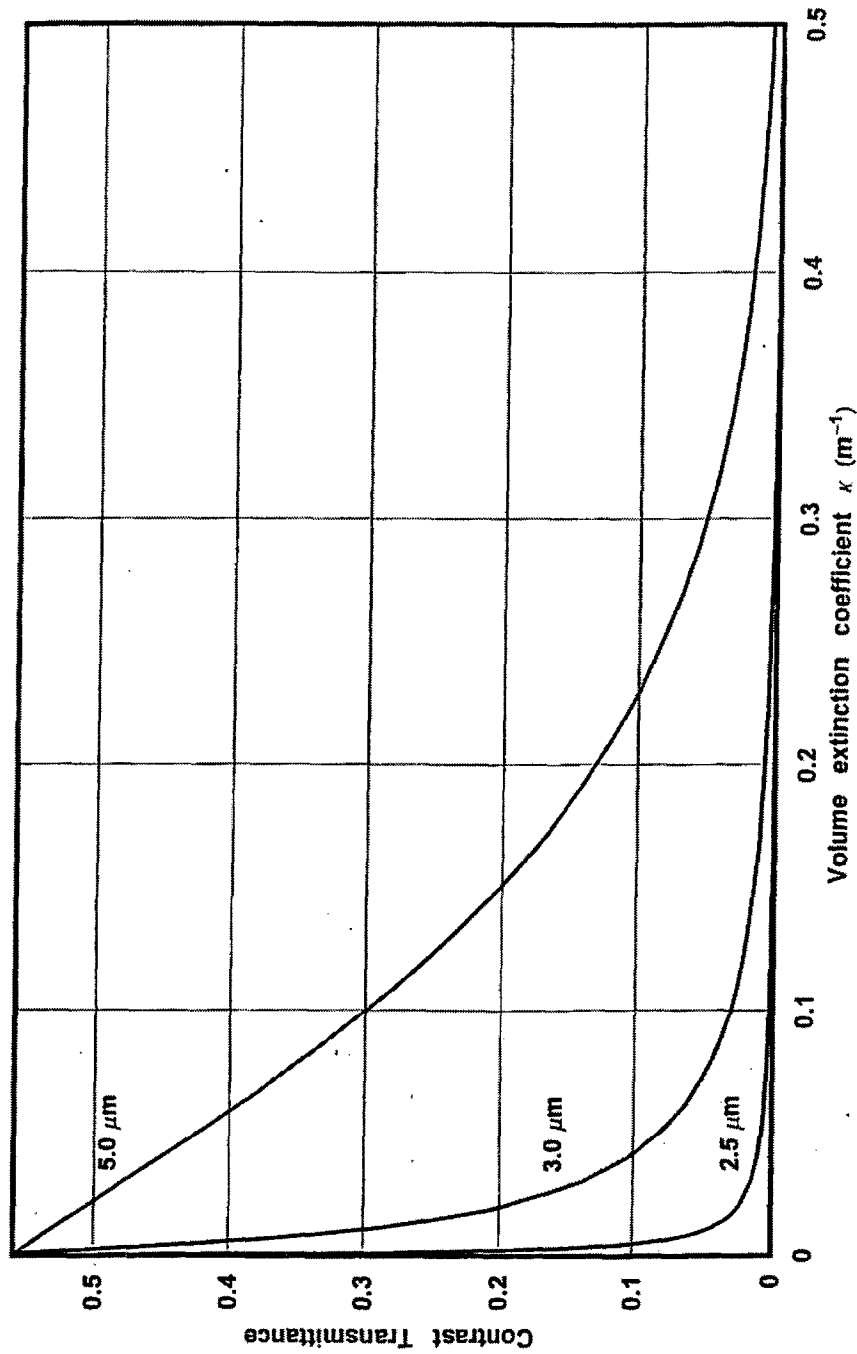
Figure 58. Variation in the Contrast Transmittance as a Function of the Volume Extinction Coefficient for a Single-Scattering Albedo = 1.0 for Three Wavelengths for 50 Photon Histories for 1000 Source Points in a Cube of Length 10 Meters with Flares. Total Source Power = 20,000 Watts, Asymmetry Parameter = 0.0, Flare Concentration = 1.0×10^{-8}.
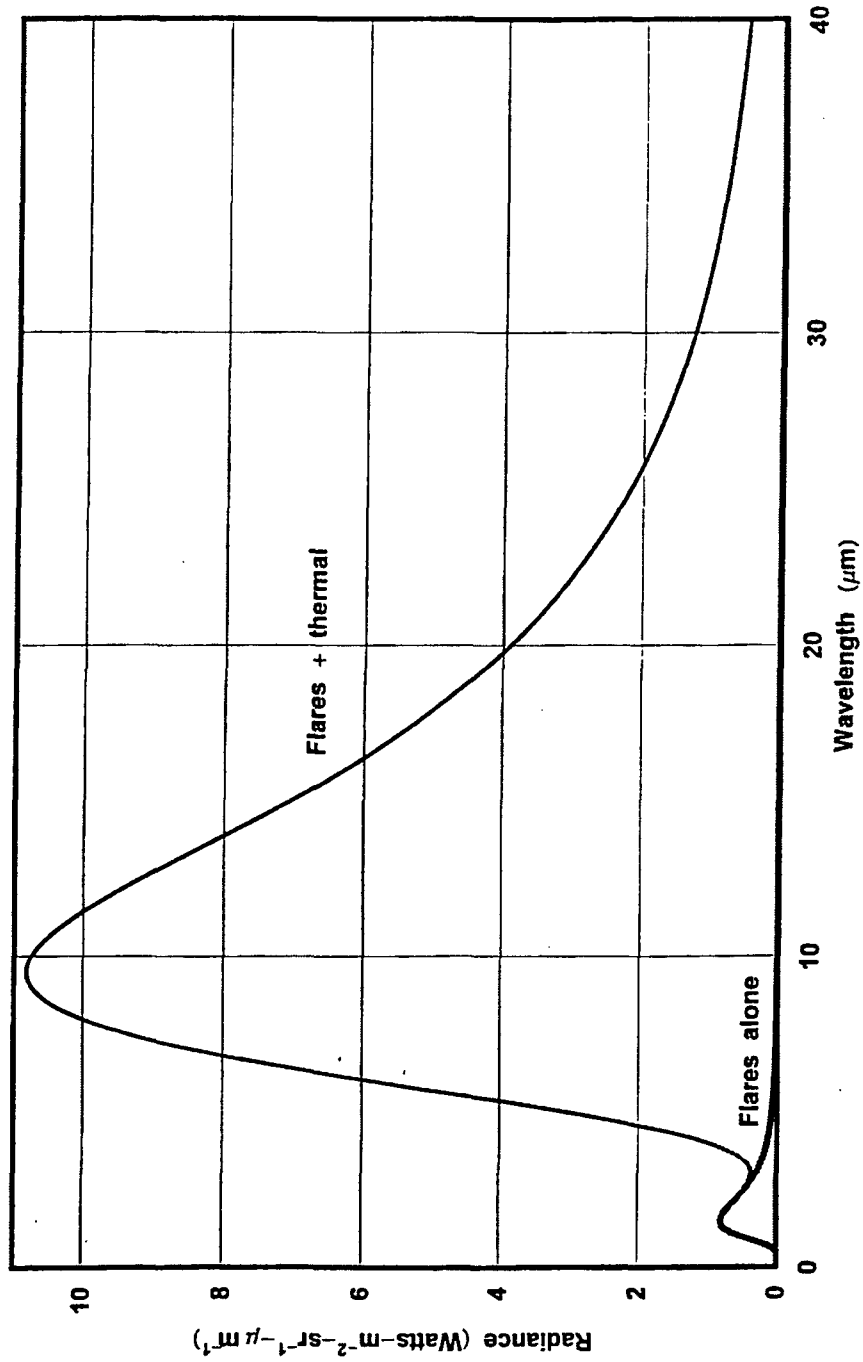
Figure 59. Variation in the Path Radiance as a Function of the Wavelength for a Single-Scattering Albedo = 1.0 for a Volume Extinction Coefficient or 0.02 m^{-1} for 50 Photon Histories for 1000 Source Points in a Cube of Length 10 Meters. Total Source Power = 20,000 Watts, Asymmetry Parameter = 0.0, Flare Concentration = 1.0×10^{-8}.

96
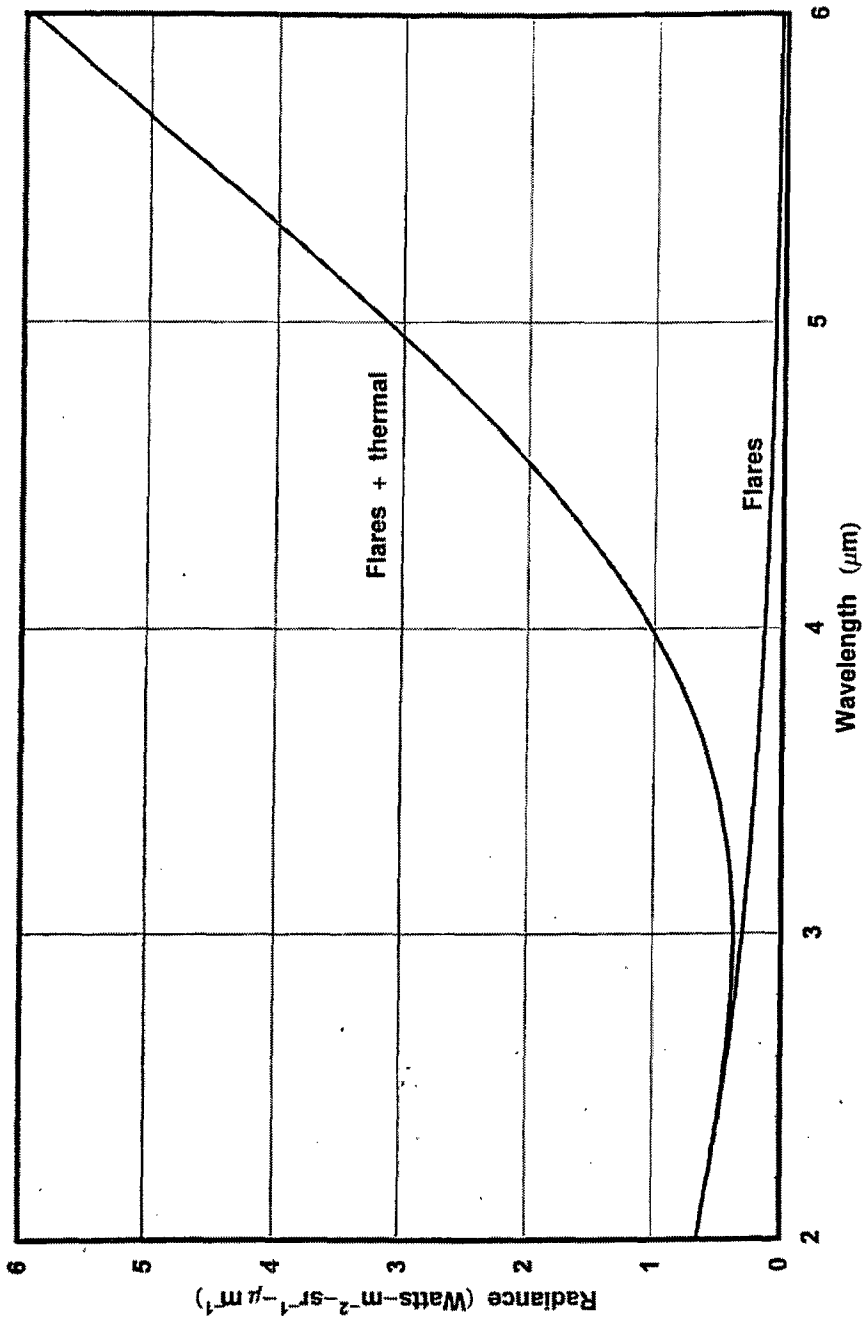
Figure 60. Variation in the Path Radiance as a Function of the Wavelength for a Single-Scattering Albedo = 1.0 for a Volume Extinction Coefficient or 0.02 m^{-1} for 50 Photon Histories for 1000 Source Points in a Cube of Length 10 Meters. Total Source Power = 20,000 Watts, Asymmetry Parameter = 0.0, Flare Concentration = 1.0 × 10^{-8}.
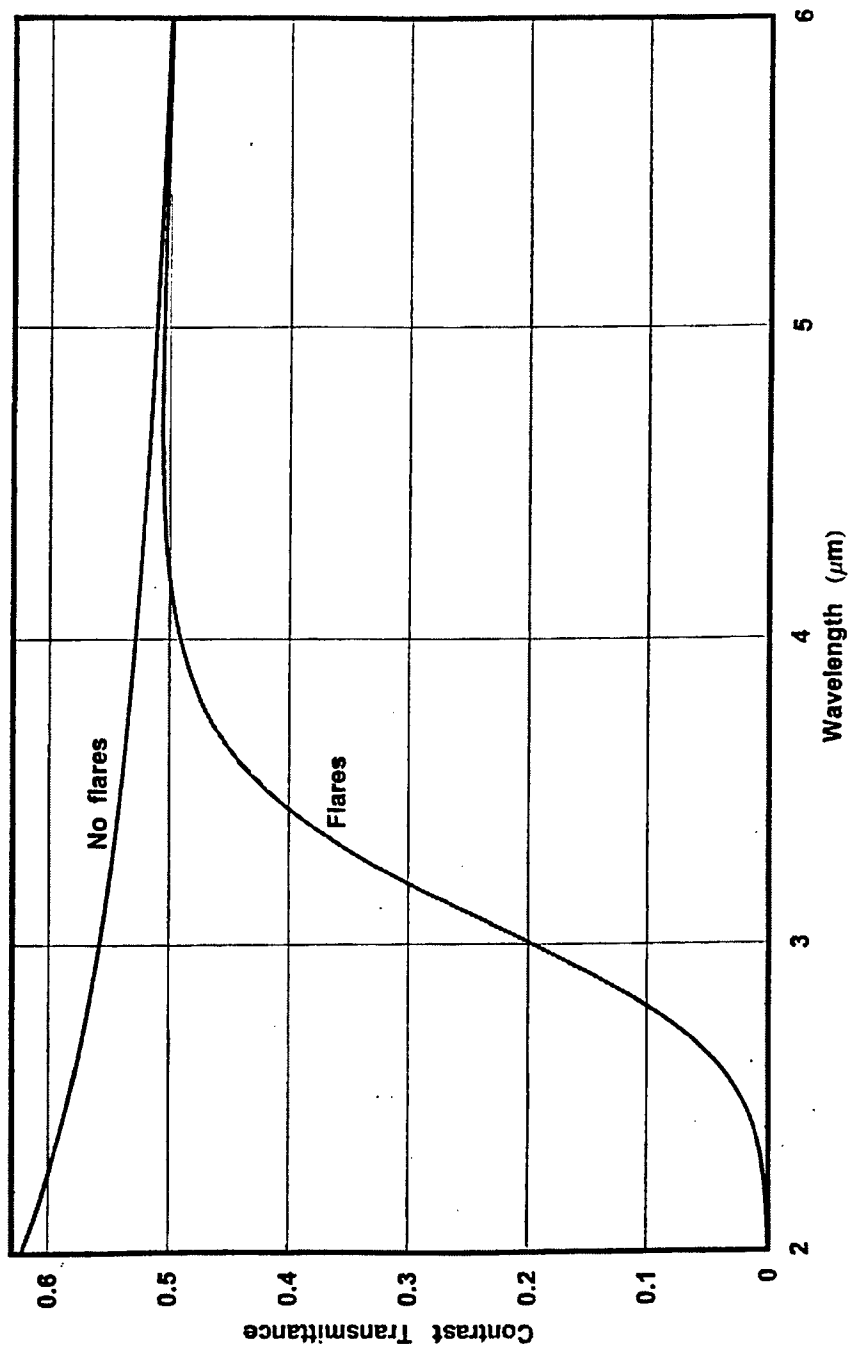
Figure 61. Variation in the Contrast Transmittance as a Function of the Wavelength for a Single-Scattering Albedo = 1.0 for a Volume Extinction Coefficient or 0.02 m^{-1} for 50 Photon Histories for 1000 Source Points in a Cube of Length 10 Meters. Total Source Power = 20,000 Watts, Asymmetry Parameter = 0.0, Flare Concentration = 1.0×10^{-8}.
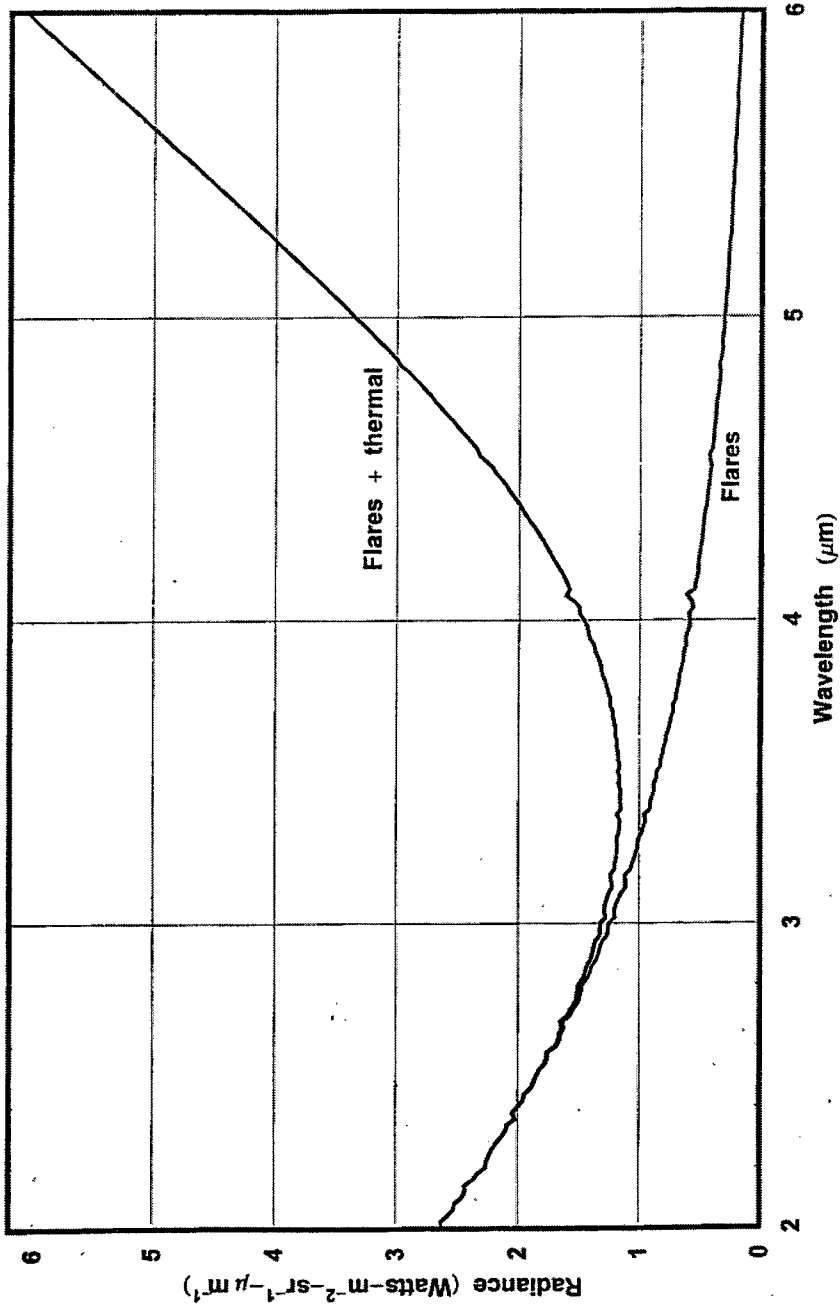
Figure 62. Variation in the Path Radiance as a Function of the Wavelength for a Single-Scattering Albedo = 1.0 for a Volume Extinction Coefficient or 0.1 m^{-1} for 50 Photon Histories for 1000 Source Points in a Cube of Length 10 Meters. Total Source Power = 20,000 Watts, Asymmetry Parameter = 0.0, Flare Concentration = 1.0 × 10^{-8}.

99

larger than in the previous case and the path radiance is larger as a result. The contrast transmittance as illustrated in figure 63 is similar to that in the thin cloud case although it peaks near a wavelength of about 5.0 um. It should be noted, however, that the "asymptotic" value of the contrast transmittance is somewhat lower than for the previous case. In figure 64 we depict the variation in the path radiance as a function of wavelength for a somewhat thicker cloud with a volume extinction coefficient of 0.2 m^{-1}. Once again, the flare path radiance is large because more scattering takes place in the cloud. In this case, however, the contrast transmittance in figure 65 seems to reach a peak near a wavelength of about 6.0 μm. Finally, we consider the case of an optically thick cloud with a volume extinction coefficient of 0.5 m^{-1} or for an optical thickness of 5.0 in figure 66. As before the path radiance is large because of the large optical thickness of the medium. In this case the contrast transmittance depicted in figure 67 has a similar appearance as in the case of a smaller optical thickness but the asymptotic value is considerably less. At a wavelength of 6.0 μm it is now about 0.008 instead of 0.14.

We can now illustrate the variation in the path radiance as a function of wavelength for all four values of the volume extinction coefficient. This is seen in figure 68. Since the total path length is 10 meters the optical thickness varies from 0.2 to 5.0. One can clearly see the strong dependence of the path radiance on wavelength and on optical thickness. Because of the difference in the temperatures between the flares and the cloud the spectral "cross-over" point is somewhere between 3.0 μm and 4.0 μm. In figure 69 we show the corresponding values for the contrast transmittance. Here we see the strong "blocking" capability of the emissive smoke cloud wavelengths less than about 4.0 μm. For completeness we also depict in figure 70 the corresponding values for the signal-to-noise ratio for the four clouds. It is interesting to see that there seems to be an optimum wavelength for which the signal-to-noise ratio reaches a maximum. The signal-to-noise ratio transmittance is very similar to the contrast transmittance as one can see in figure 71.

10.   CONCLUSIONS

During this project we have examined several methods for the calculation of the radiance from a finite cloud medium of moderate optical thickness. The primary computational method to be chosen depends on a least two factors, the optical thickness of the multiple-scattering medium, and the single-scattering albedo. For media of large optical thickness, say about 30, and little absorption there is a very large number of scatterings and one can make use of what is called the diffusion method. On the other hand, if the optical thickness is very small, say about 0.1 then one can probably use a simple-single-scattering approximation. However, for media with intermediate optical thickness values one must use more advanced mathematical techniques to find a solution. The problem we were faced with in this project makes use of the intermediate situation. It was resolved by using the Gaussian quadrature method to evaluate the single-scattering integral and then by using a photon-counting method (Monte Carlo) to evaluate the higher orders of scattering.

Also, not only does multiply-scattered radiation originate from the flares but also it originates from the thermal heating of the smoke as a result of the ambient temperature. The smoke cloud model we have created deals with thermal radiation from these two internal sources. The first is the isotropic thermal radiation emitted by the isolated flares that are situated in a three-dimensional lattice within the cloud. The second source is the thermal radiation that is

100
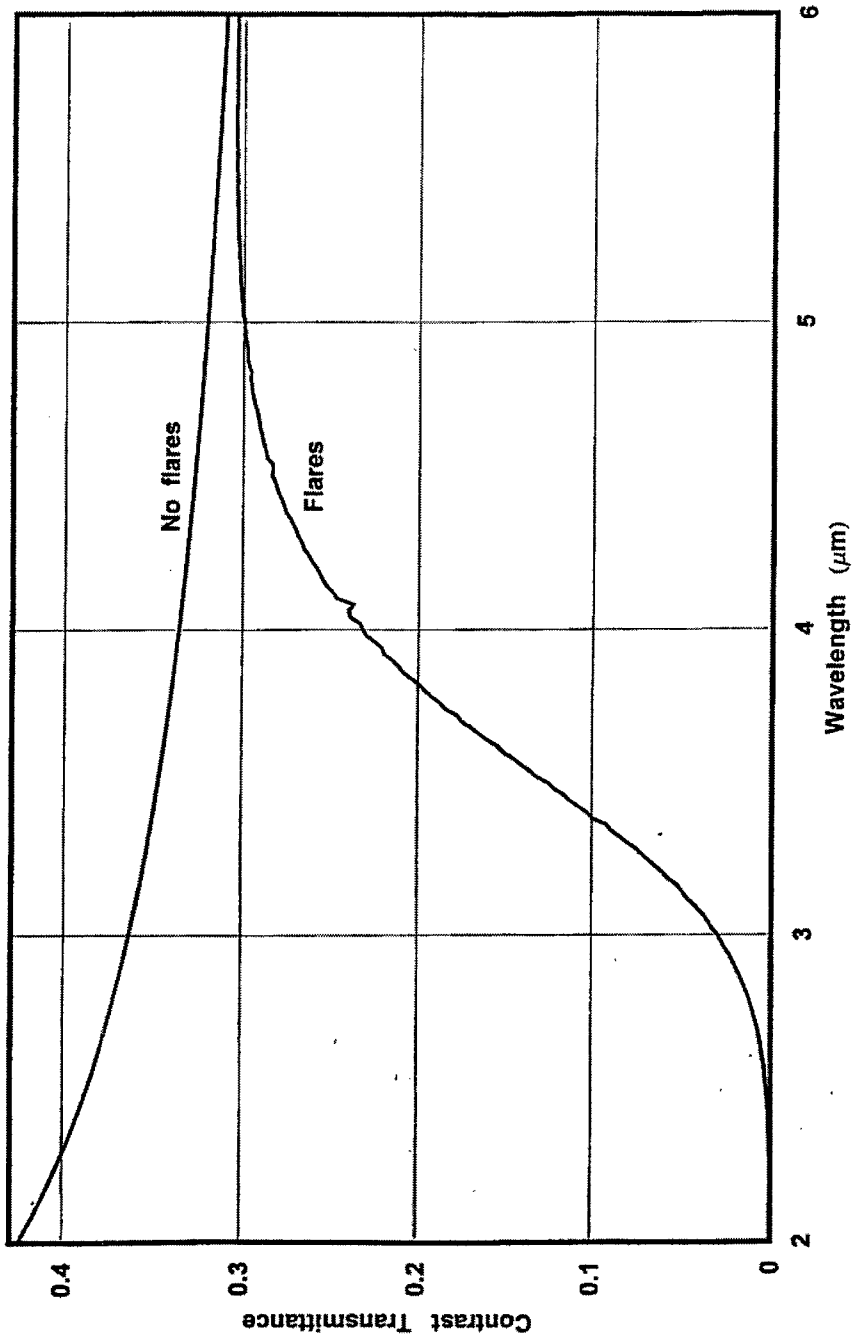
Figure 63. Variation in the Contrast Transmittance as a Function of the Wavelength for a Single-Scattering Albedo = 1.0 for a Volume Extinction Coefficient or 0.1 m^{-1} for 50 Photon Histories for 1000 Source Points in a Cube of Length 10 Meters. Total Source Power = 20,000 Watts, Asymmetry Parameter = 0.0, Flare Concentration = 1.0×10^{-8} .
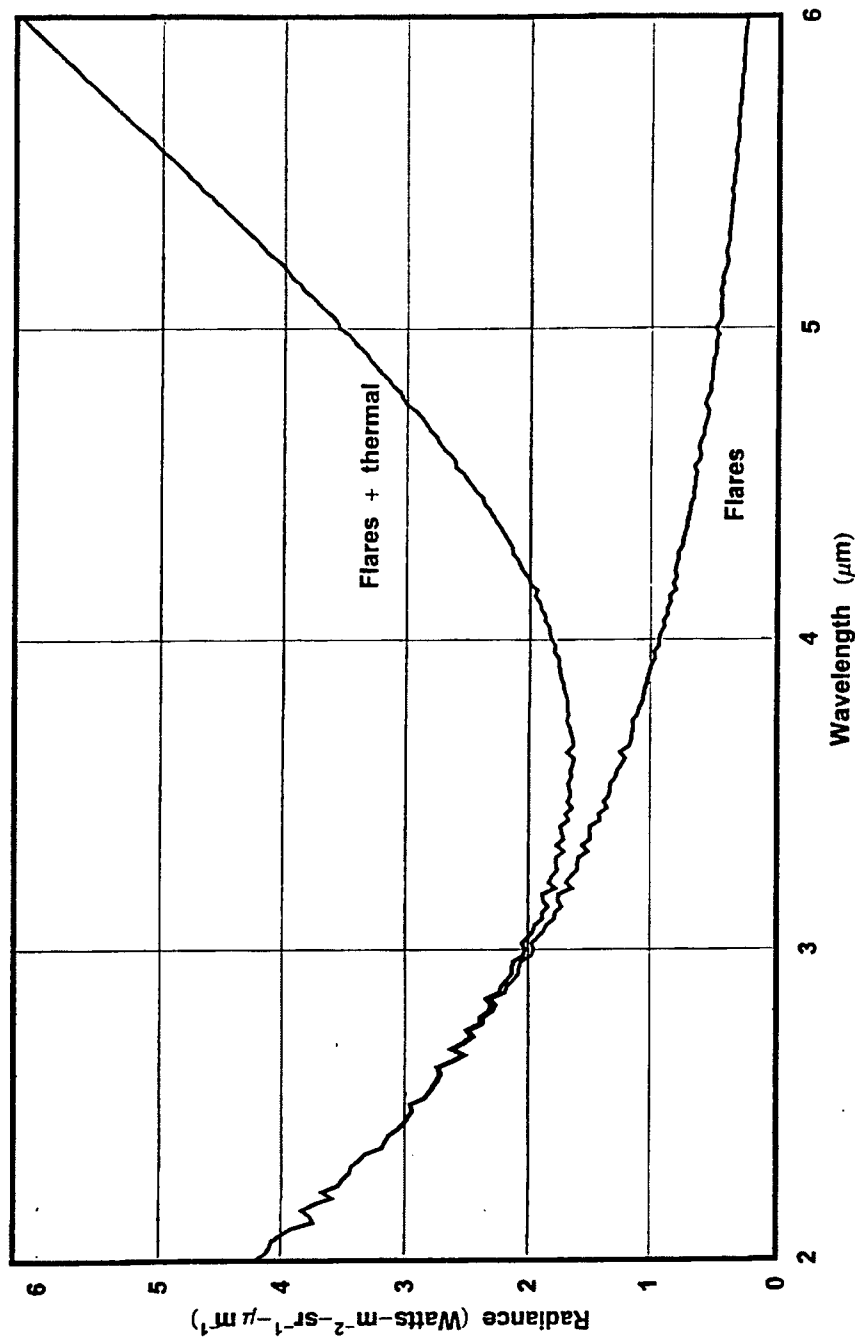
Figure 64. Variation in the Path Radiance as a Function of the Wavelength for a Single-Scattering Albedo = 1.0 for a Volume Extinction Coefficient or 0.2 m^{-1} for 50 Photon Histories for 1000 Source Points in a Cube of Length 10 Meters. Total Source Power = 20,000 Watts, Asymmetry Parameter = 0.0, Flare Concentration = 1.0 × 10^{-8}.
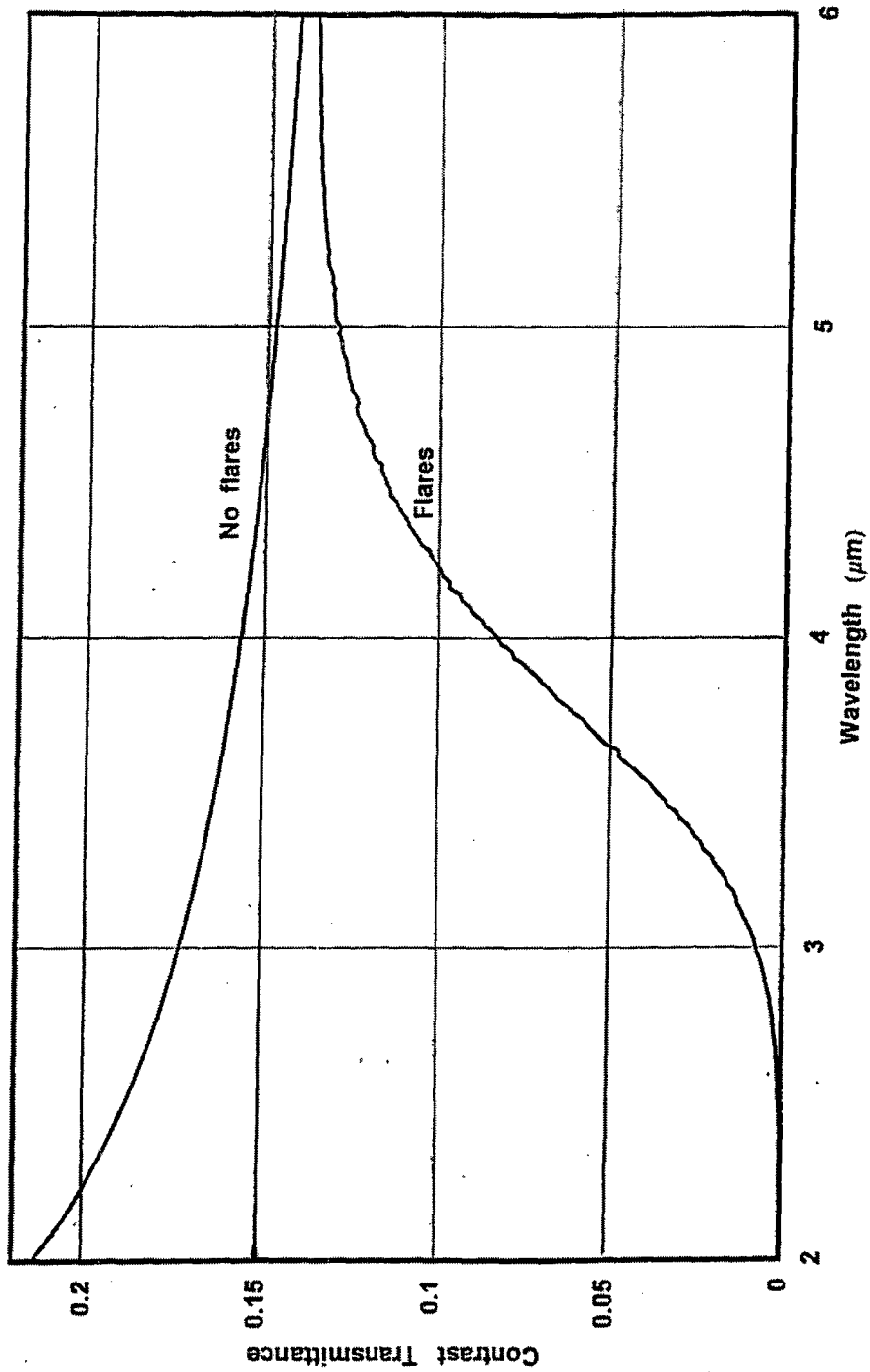
Figure 65. Variation in the Contrast Transmittance as a Function of the Wavelength for a Single-Scattering Albedo = 1.0 for a Volume Extinction Coefficient or 0.2 m^{-1} for 50 Photon Histories for 1000 Source Points in a Cube of Length 10 Meters. Total Source Power = 20,000 Watts, Asymmetry Parameter = 0.0, Flare Concentration = 1.0×10^{-8}.
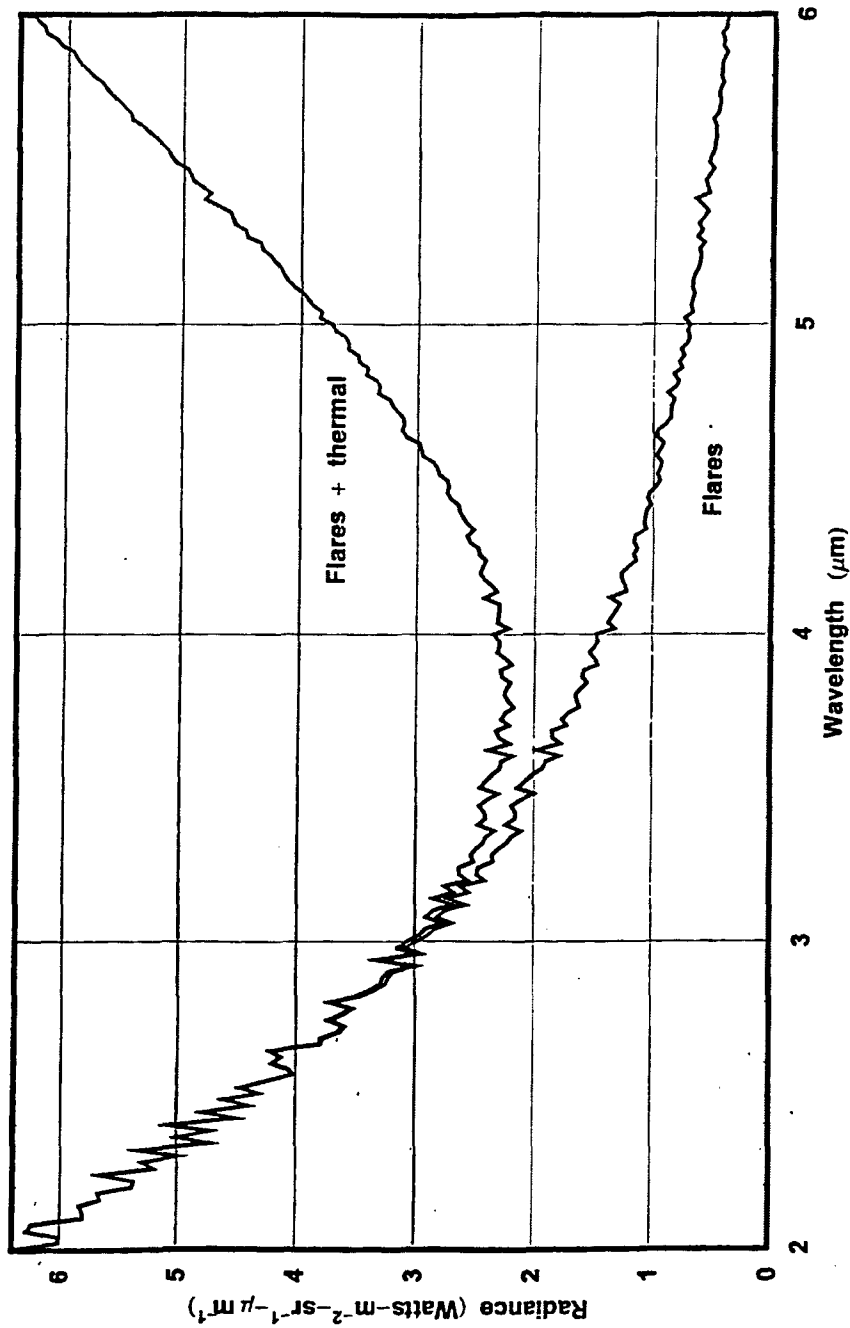
Figure 66. Variation in the Path Radiance as a Function of the Wavelength for a Single-Scattering Albedo = 1.0 for a Volume Extinction Coefficient or 0.5 m^{-1} for 50 Photon Histories for 1000 Source Points in a Cube of Length 10 Meters. Total Source Power = 20,000 Watts, Asymmetry Parameter = 0.0, Flare Concentration = 1.0×10^{-8}.
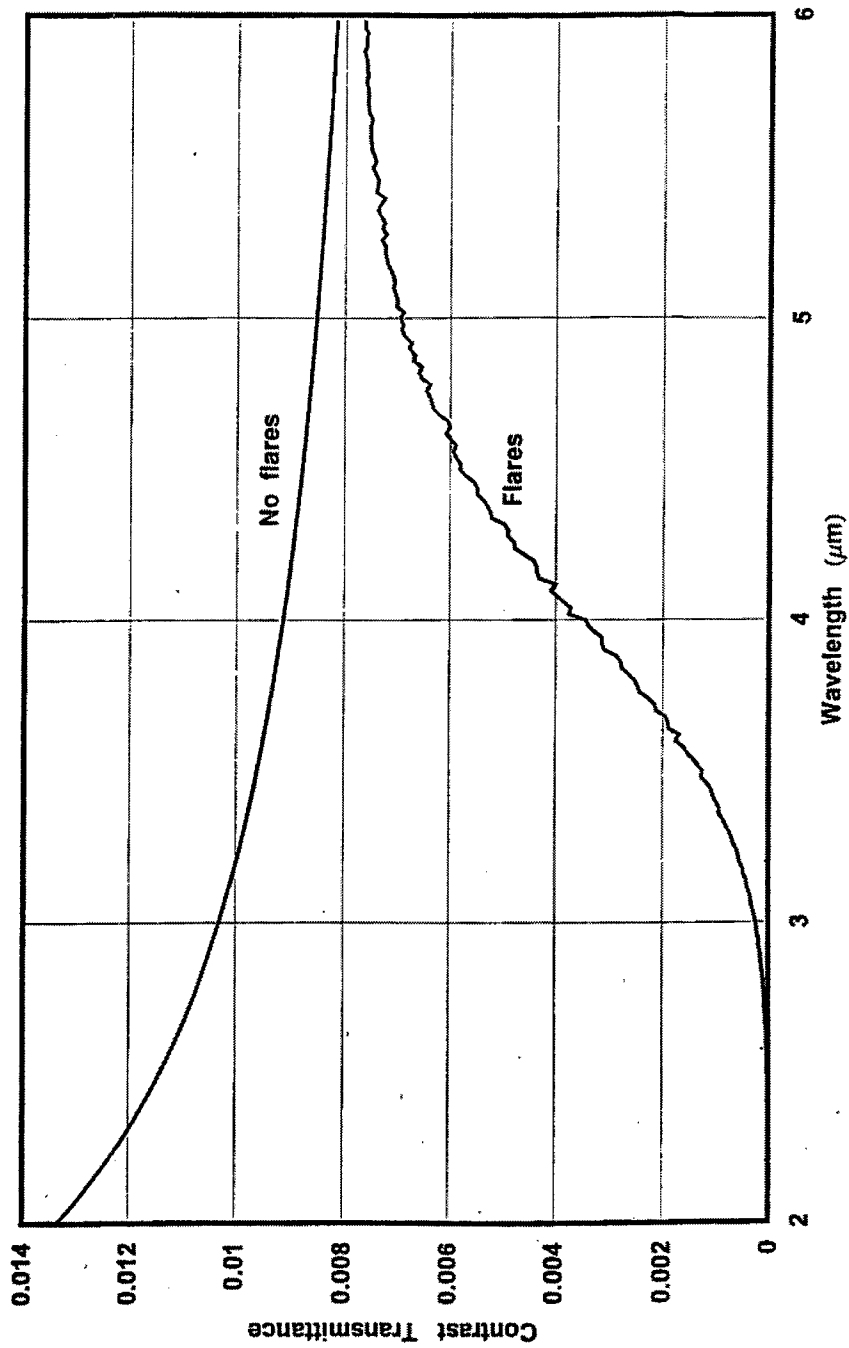
Figure 67. Variation in the Contrast Transmittance as a Function of the Wavelength for a Single-Scattering Albedo = 1.0 for a Volume Extinction Coefficient or 0.5 m^{-1} for 50 Photon Histories for 1000 Source Points in a Cube of Length 10 Meters. Total Source Power = 20,000 Watts, Asymmetry Parameter = 0.0, Flare Concentration = 1.0×10^{-8}.
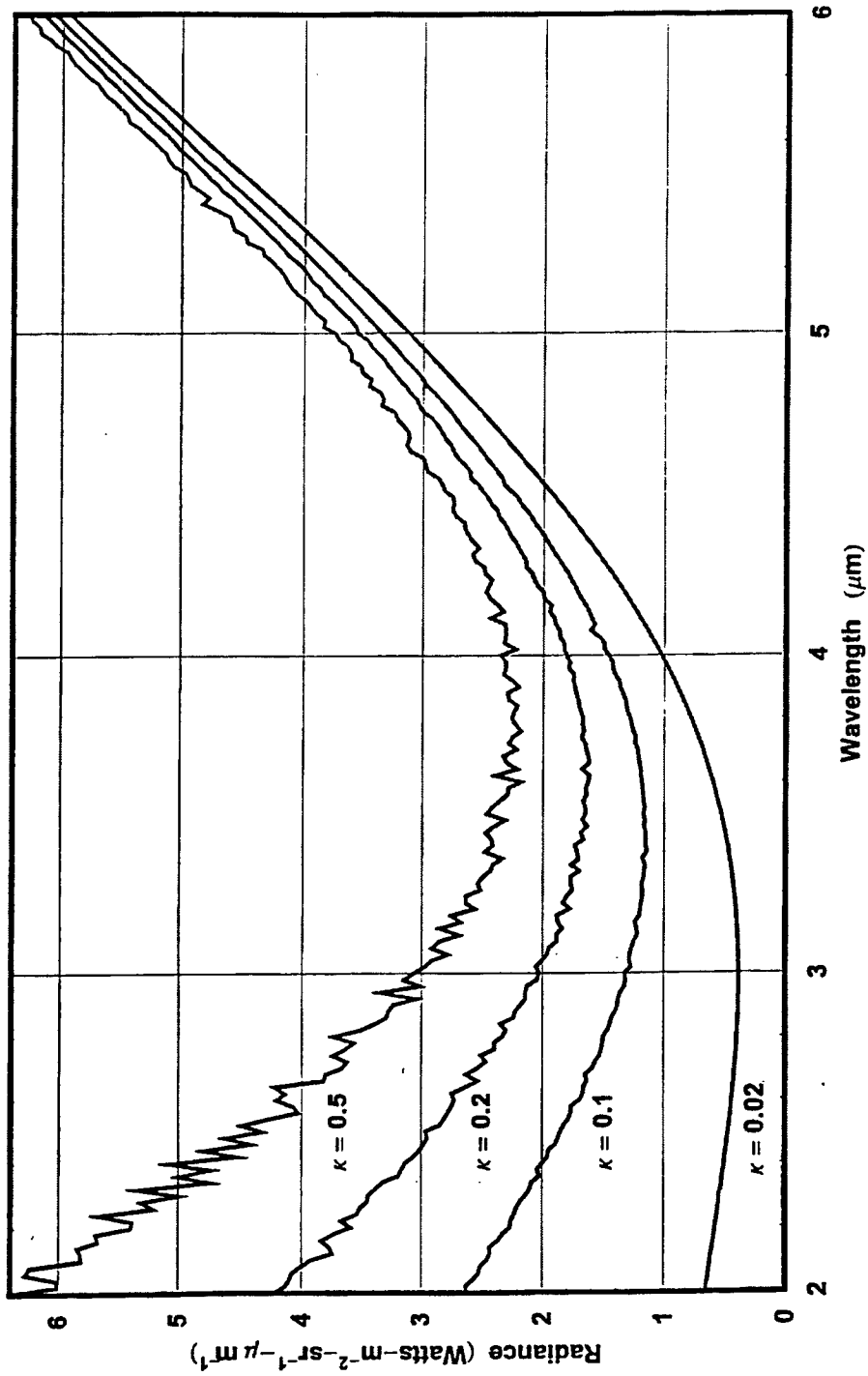
Figure 68. Variation in the Path Radiance as a Function of the Wavelength for a Single-Scattering Albedo = 1.0 for Four Volume Extinction Coefficients for 50 Photon Histories for 1000 Source Points in a Cube of Length 10 Meters. Total Source Power = 20,000 Watts, Asymmetry Parameter = 0.0, Flare Concentration = 1.0×10^{-8}.
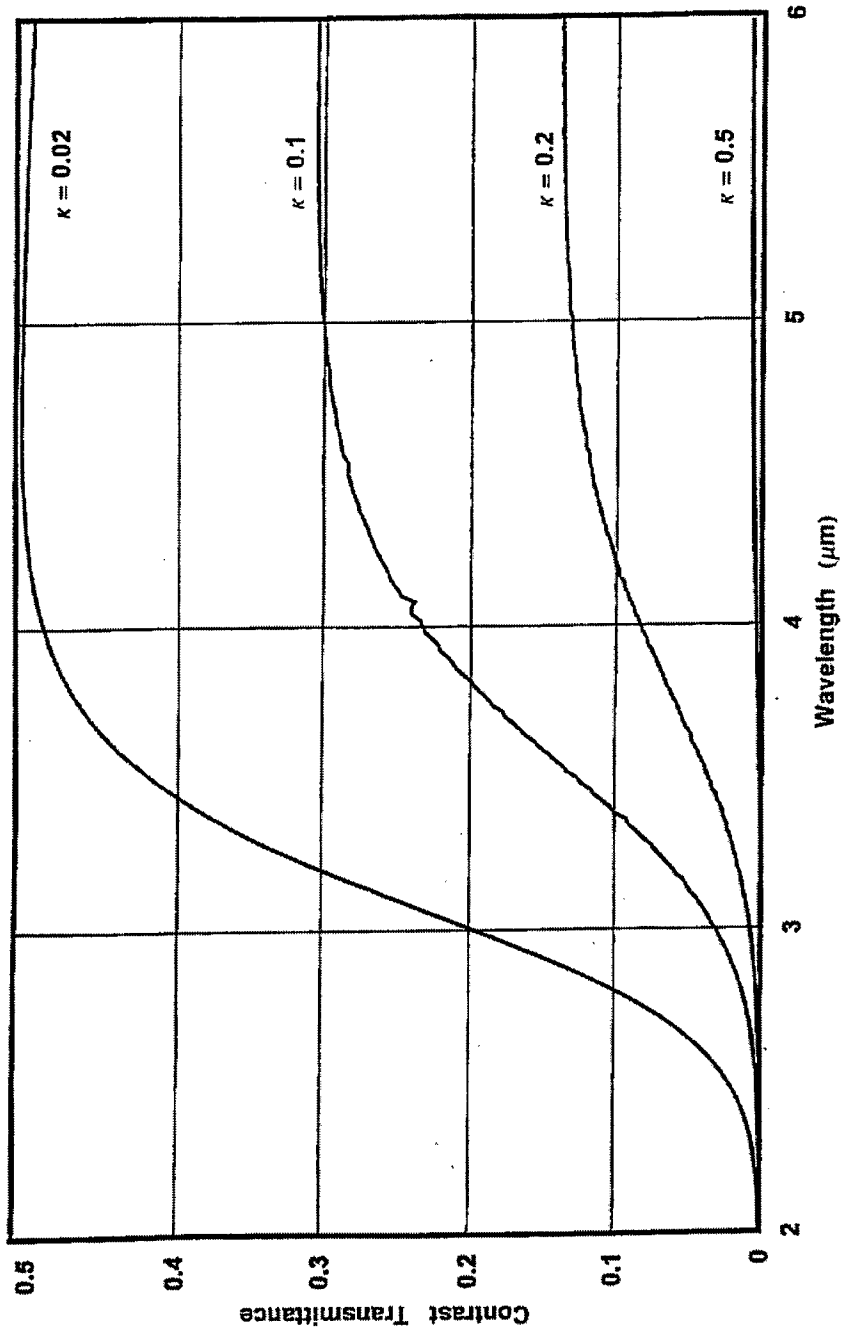
Figure 69. Variation in the Contrast Transmittance as a Function of the Wavelength for a Single-Scattering Albedo = 1.0 for Four Volume Extinction Coefficients for 50 Photon Histories for 1000 Source Points in a Cube of Length 10 Meters. Total Source Power = 20,000 Watts, Asymmetry Parameter = 0.0, Flare Concentration = 1.0×10^{-8}.

107
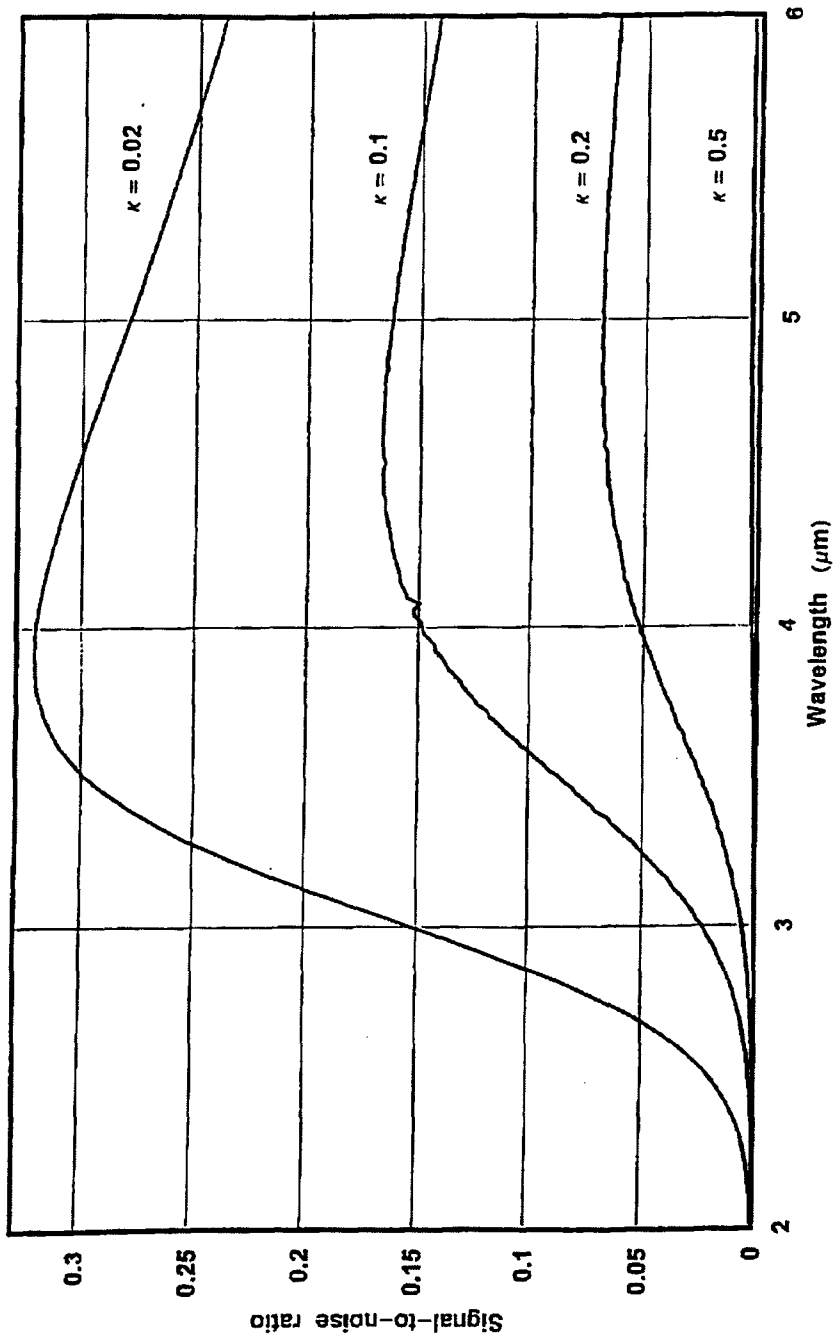
Figure 70. Variation in the Signal-to-Noise Ratio as a Function of the Wavelength for a Single-Scattering Albedo = 1.0 for Four Volume Extinction Coefficients for 50 Photon Histories for 1000 Source Points in a Cube of Length 10 Meters. Total Source Power = 20,000 Watts, Asymmetry Parameter = 0.0, Flare Concentration = 1.0×10^{-8}.
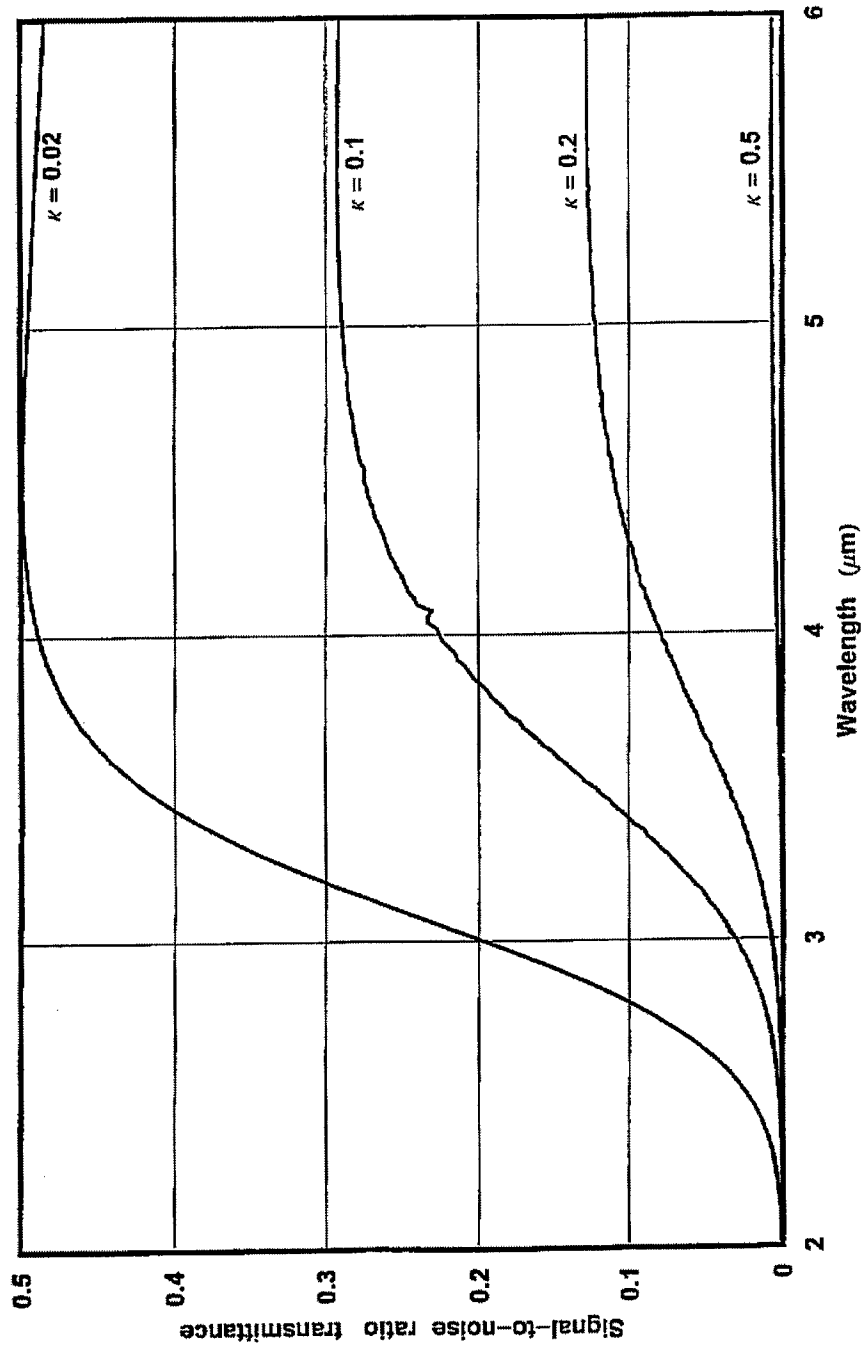
Figure 71. Variation in the Signal-to-Noise Ratio Transmittance as a Function of the Wavelength for a Single-Scattering Albedo = 1.0 for Four Volume Extinction Coefficients for 50 Photon Histories for 1000 Source Points in a Cube of Length 10 Meters. Total Source Power = 20,000 Watts, Asymmetry Parameter = 0.0, Flare Concentration = 1.0×10^{-8}.

emitted by the homogeneous gas and aerosol inside the cloud. In addition, we also considered radiation sources external to the medium such as those arising from the atmosphere, targets, and other background elements.

As indicated in this report we have examined in considerable detail the variation in selected sensor metrics as functions of the properties of the flares and the cloud constituents. The computer model computes many optical and thermal quantities and prints them into a specific output file for the user. Besides the path radiance the model also computes the contrast transmittance, the signal-to-noise ratio, and the signal-to-noise ratio transmittance with and without flares being present in the medium. All this is done spectrally for wavelengths from 0.1 μm to 1 meter! The model clearly demonstrates the effectiveness of the use of heated flares in a smoke cloud for the reduction in the contrast of a target. The flares produce so much additional path radiance that the contrast is, in many cases, greatly reduced for certain spectral ranges. Perhaps the most significant finding is that there is "competition" between the flare-produced radiance and that produced by the normal, warm smoke cloud itself. This was clearly shown in many figures in this report.

There is a wide range in the values of the parameters that describe the flares and the properties of the medium. Therefore, the user has many options to model a great variety of characteristics. Thus, one can model a large combination of the system parameters and simulate a variety of environmental conditions.

Finally, the model is easy to use. The investigator need only modify certain parameters in the input file and run the computer code. A detailed output file is automatically generated for each computer run. The computation time does depend on the magnitudes of certain key parameters in the model. The most important of these are the number of sources (flares) and the number of photon histories chosen for the Monte Carlo simulation. One should approach this model in a conservative manner, that is, use a relatively small number for these quantities until one learns the tradeoff between accuracy and computation time. We have found that in most cases it is not necessary to run the program for a large number of sources or for a large number of photon histories. On a simple desktop computer the run time is generally measured in seconds or a few minutes. It would be quite helpful if the user has a rudimentary background in thermal physics and some knowledge of basic computer formats. All of the quantities are defined in this report as well as in the input file. The units are clearly stated and must be adhered to, otherwise incorrect results may occur.

11.   RECOMMENDATIONS

We now have a model for the description of the radiation in and from emissive smoke clouds, that is, for clouds in which the sources of radiation consist of the internal thermal radiation from the ambient medium as well as from isolated flares, all characterized by the Planck function for their respective temperatures. The distribution of the flares in the cloud is in a regular, three-dimensional lattice with a uniform distribution throughout. It would be of interest to examine a spatially non-uniform distribution of flares as, for example, flares with a greater concentration in various parts of the cloud. Thus, one could have smoke clouds with a high concentration of flares near the top or the bottom of the cloud. This non-uniform distribution could result in quite a different radiance from that of a cloud with a uniform distribution of sources.

The present model uses a cubic geometry. A more advanced model can be designed to consider a regular parallelepiped geometry for the cloud with uniform and non-uniform distributions of flares. In addition, it is possible to account for the time dependence of the evolution of the cloud by considering the smoke density and flare source separations as functions of time. This would then produce a more realistic smoke cloud as the density of the smoke dissipates.

Finally, this model allows one to compute the sensor metrics for the multiply-scattered radiation in the cloud. One can also consider the directly attenuated radiation from the flares themselves for various sensor apertures. It would be interesting to compare the radiance from the flares with the scattered radiance as a function of the cloud optical thickness. For large optical thickness values we would expect a greater amount of scattered radiance but the directly attenuated radiance form the flare would be diminished. Interesting tradeoffs could result.

12. REFERENCES

1. B. Davison, "*Neutron Transport Theory*," Oxford at the Clarendon Press, 1957.

2. J. Embury, "Emissive versus Attenuation Smokes," Chemical Biological Center, U.S. Army Soldier and Biological Chemical Command, ECDC-TR-225, February 2002.